



HAL
open science

Identification and simulation of the motor command during the 3D non-constraints multi-articular movements

van Hoan Vu

► **To cite this version:**

van Hoan Vu. Identification and simulation of the motor command during the 3D non-constraints multi-articular movements. Neuroscience. Université Paris Saclay (COmUE), 2016. English. NNT : 2016SACLS509 . tel-01512591

HAL Id: tel-01512591

<https://theses.hal.science/tel-01512591>

Submitted on 24 Apr 2017

HAL is a multi-disciplinary open access archive for the deposit and dissemination of scientific research documents, whether they are published or not. The documents may come from teaching and research institutions in France or abroad, or from public or private research centers.

L'archive ouverte pluridisciplinaire **HAL**, est destinée au dépôt et à la diffusion de documents scientifiques de niveau recherche, publiés ou non, émanant des établissements d'enseignement et de recherche français ou étrangers, des laboratoires publics ou privés.

Université Paris-Sud et Paris-Saclay

Mouvement Humain, Adaptation et Performance Sportive

Laboratoire: Complexité, Innovation et Activités Motrices et Sportives

École doctorale No 566: Sciences du Sport, de la Motricité, du Mouvement Humain

THÈSE

Docteur en Sciences et Techniques des Activités

Physiques et Sportives

présentée et soutenue publiquement par

VAN HOAN VU

le 05 Decembre 2016

Thèse N°: NNT 2016SACLS509

Identification et simulation de la commande motrice des mouvements multi-articulés 3D non-contraints

Jury

Pr. Frédéric MARIN	Université de Technologie de Compiègne	Rapporteur
Dr. Nasser REZZOUG	Université de Toulon	Rapporteur
Dr. Jérémie GAVEAU	Université de Bourgogne	Examineur
Dr. Braffort ANNELIES	CNRS, Université Paris-Saclay	Examineur (Président)
Dr. Bastien BERRET	Univ. Paris-Sud, Université Paris-Saclay	Co-Directeur
Pr. Brice ISABLEU	Univ. Paris-Sud, Université Paris-Saclay	Directeur

Titre: Identification et simulation de la commande motrice des mouvements multi-articulés 3D non-contraints

Mots clés: mouvement 3D, contrôle moteur, contrôle optimal

Résumé: L'objectif de cette thèse vise à d'identifier les principes sous-tendant la planification des mouvements 3D du membre supérieur tout en tenant compte des différences inter-individuelles régulièrement observées dans de nombreuses études récentes. L'identification des principes généraux sous-tendant la planification des mouvements 3D du membre supérieur permet de valider la validité des approches computationnelles. Néanmoins, afin d'être complète toute théorie doit être en mesure de tenir compte à la fois des sources et du rôle des différences interindividuelles. À ce jour, les modèles computationnels du contrôle du mouvement humain ne tiennent pas compte de l'existence de typologies sensorimotrices (par ailleurs validée empiriquement), et sont encore moins capables de prédire les variables de contrôle qui leur sont associées. L'étude approfond et la modélisation des différences interindividuelles constituent donc un défi majeur pour la communauté scientifique afin de compléter les modèles computationnels actuels du contrôle des mouvements multiarticulés humains. Les travaux sur cette problématique permettront de mieux comprendre si les sources de différences interindividuelles sont d'origine centrale ou périphérique. Il s'agira de savoir par exemple si les paramètres anthropométriques (par exemple la masse corporelle, la longueur des membres) affectent les trajectoires de déplacement, et s'ils provoquent les différences entre les sujets, ou si au contraire les différences interindividuelles proviennent de processus supérieur exécuté en interne par le cerveau pendant la planification du mouvement. Dans cette optique, l'approche choisie dans le cadre de cette thèse combine des expériences originales (précisément des tâches de pointage laissant le choix du point final libre) avec des techniques de calcul avancées (ici des méthodes de contrôle optimal inverse numérique). Des mouvements de pointage du bras sans position finale précisément prescrite sont examinés dans différentes conditions de vitesse et/ou de masse afin de laisser émerger des stratégies motrices variées et d'évaluer les éventuels principes de planification motrice sous-jacents. L'idée centrale est de s'écarter du paradigme classique consistant à étudier des mouvements point-à-point (où la cible est généralement indiquée par un point dans l'espace, par exemple une cible lumineuse) et porte sur l'étude d'une tâche dans laquelle le choix du point final du mouvement est laissé libre aux participants afin de faire surgir les différences interindividuelles ainsi que le processus de sélection ou de décision motrice qui a conduit aux stratégies observées. Ce type de tâche permet de mieux décoder les caractéristiques du contrôleur moteur humain. Les résultats empiriques sont ensuite modélisés et interprétés grâce au contrôle optimal inverse dont l'hypothèse associée est que les trajectoires expérimentales découlent de la minimisation d'une certaine fonction de coût qui est éventuellement composite. Cette approche combinée vise à révéler les principes ou règles

qui gouvernent le processus de planification de ce type de mouvement des membres supérieurs et d'établir un lien entre les paramètres pertinents du geste, les fonctions de coûts et les caractéristiques individuelles.

Les résultats montrent que les sujets produisent des stratégies motrices différentes aux niveaux cinématique et dynamique en fonction de la façon dont ils s'adaptent aux changements de vitesse et/ou de masse. Dans l'ensemble, ces changements ont des effets significatifs sur les trajectoires de la main (par exemple l'emplacement des points finaux choisis par les sujets) et les commandes motrices (notamment sur l'utilisation des couples d'interaction). Pourtant, certains sujets présentaient des dépendances plus exacerbées que d'autres qui ne variaient que peu leur stratégie de pointage par rapport aux changements de vitesse ou de masse induits par la tâche. L'investigation par contrôle optimal inverse a montré que ces résultats pouvaient être expliqués par une optimisation d'un coût composite mélangeant essentiellement des variables cinématique et dynamique durant la phase de planification motrice. Un tel modèle composite surpassait les prédictions des modèles séparés soit cinématique soit dynamique dans la prédiction de l'évolution des caractéristiques importantes du mouvement et des différences interindividuelles. En outre, il a permis de réconcilier des résultats controversés débattus dans des études antérieures en montrant que des comportements adaptatifs divergents peuvent émerger en fonction du poids des fonctions de coût élémentaires qui composent la fonction de coût totale. Dans l'ensemble, nos résultats suggèrent que la planification motrice des mouvements 3D non-contraints du bras mêle nécessairement des variables cinématiques et cinétiques, et que ce compromis semble être idiosyncrasique et ainsi conduire à des différences interindividuelles subtiles.

Title: Identification and simulation of motor command of 3D non-constraint multi-articular movements

Keywords: 3D movement, motor control, optimal control

Abstract: The purpose of this thesis is to identify principles that could guide the planning of 3D upper-limb movements for different individuals. To this aim, the chosen approach combines novel experiments (namely, a “free reach-endpoint” motor task) with advanced computational techniques (here numerical inverse optimal control). Arm pointing movements without a prescribed final hand position are examined under different conditions of speed or load in order to let emerge various motor control strategies and assess the possible underlying motor planning principles. A core idea is to depart from classical point-to-point reaching paradigms (where the target is generally a dot, e.g. a spotlight target) to study a task in which the endpoint is left free to the participants in order to emphasize inter-individual differences as well as the selection process and motor decision that led to the observed strategies. This paradigm thus allows to better decipher the characteristics of the human motor controller. Empirical results are then modeled and interpreted in the inverse optimal control framework, hypothesizing that empirical arm trajectories derive from the minimization of a certain, possibly composite, cost function. This combined approach aims at revealing which principle or rule conceivably drives the planning process of these unrestrained upper-limb movements and to establish a link between relevant motion parameters, cost functions and inter-individual peculiarities.

The results show that subjects produced different motor strategies at both kinematic and dynamic levels depending on how they adapted to speed and/or load variations. Overall, significant motor adaptation of hand trajectories (e.g. location of reach endpoints) and motor commands (e.g. use of interaction torque) were found. Yet, some subjects exhibited stronger dependences than others who varied only little their reach strategies with respect to task-induced speed or load changes. When investigated from the optimal control viewpoint, these results could be accounted for by a composite cost essentially weighting kinematic and dynamic variables differentially at the motor planning stage. Such a composite model outperformed separate kinematic and dynamic ones in predicting the evolution of many important motion features and in explaining inter individual differences. Moreover, it allowed reconciling controversial findings of previous studies by showing that divergent adaptive behaviors can emerge depending on the weights of the elementary cost that may compose the total cost function. In sum, the present results suggest that motor planning of unrestrained 3D arm movements necessarily mixes kinematic and kinetic variables and that this trade-off may be idiosyncratic and lead to subtle inter individual differences.

Acknowledgements

I would like to express my gratitude to my supervisors, Pr. Brice Isableu and Dr. Bastien Berret. We had profitable scientific conversations during my Ph.D study and they were always ready and present to discuss the project and execution.

I would like to thank the committee members, Prof. Frédéric Marin and Dr. Nasser Rezzoug, who have provided their feedback in their function as Rapporteurs. Also I would like to thank Dr. Jérémie Gaveau and Dr. Braffort Annelies who accepted to be examiners at the defense of this dissertation.

My gratitude is also extended to all my colleagues. Thanks for the help to the secretaries and the technical staff. Being involved in such a multicultural environment, as the Faculty of Sport Science, has been a real enriching experience.

CONTENTS

Contents	i
1 Introduction	1
1.1 Problem statements	2
1.2 Thesis objectives	3
1.3 Thesis outline	4
2 Theoretical background	5
I Computational motor control theories	7
2.1 Internal models	9
2.2 Optimal control models	13
2.3 Direct optimal control	18
2.4 Inverse optimal control	21
II Biomechanical modelling	23
2.5 Anatomical background	25
2.6 Kinematic model of the arm	27
2.7 Dynamic model of the arm	36
2.8 Parameters of interest: rotation axis caculations	50
3 Thesis contribution	57
3.1 Introduction	58

3.2	On the nature of motor planning during arm pointing task	59
3.3	Compensation/Exploitation of interaction torque and its links to cost function	103
4	General discussion	143
4.1	Conclusions	144
4.2	Limitations	153
4.3	Perspectives	155
	List of Tables	157
	List of Figures	159
	Bibliography	167

CHAPTER



INTRODUCTION

1.1 Problem statements

Since a long time, researchers have been trying to answer the following fundamental question: how does the central nervous system (CNS) control voluntary limb movements? So far, it has remained impossible to fully answer this question and provide a generic model accounting for the large variety of possible human movements. Historically, researchers have started to study simple movements with few degrees of freedom, such as single-joint arm rotations or planar arm movements with elbow and shoulder rotations (Flash and Hogan, 1985; Gottlieb et al., 1988, 1989b,a). They tried to identify motor invariants that would remain similar across tasks or individuals with the aim to better understand how our movements are controlled. Researchers succeeded by showing for instance that hand trajectories were almost straight and velocity profiles systematically bell-shaped (JF Soechting, 1981; Soechting et al., 1995; Morasso, 1981; Flash and Hogan, 1985; Atkeson and Hollerbach, 1985; Ostry et al., 1987; Flanders et al., 1996). However, when studying unrestrained 3D motions with many more degrees of freedom, relatively large inter-individual differences can be observed (Berthoz, 1991; J, 1991; Isableu et al., 2003; Bernardin et al., 2005; Isableu and Vuillerme, 2006) and it has been proven that, in many tasks, subjects may diverge from the above "straight" or "bell-shaped" motion characteristics (Nagasaki, 1989; Papaxanthis et al., 1998, 2003). This is exemplified by the work of Isableu et al. (2009) which showed that humans tend to exploit the minimum inertia principal axis (denoted by e_3) in a subject-specific way during a 3D cyclical arm rotation task. The findings were interpreted as consequences of different strategies resulting from idiosyncratic sensorimotor preferences. In particular, the brain may coordinate the interaction torque with respect to the net torque and the muscle torque in various ways, which could be at the origin of such differences. The results are intriguing and motivate the demand for a deeper study of the role of e_3 or interaction torque in unrestrained arm movement as well as a clearer explanation of the nature of the observed inter-individual differences.

In order to model human movement planning, several motor control theories have been proposed (internal model theories vs equilibrium point theory). Lately, the optimal control theory seems to be the most promising and effective tool for investigating the above issues in a normative way (Wolpert et al., 1995b; Todorov, 2004). In optimal control theory, human movements are assumed to originate from a minimization principle just as the physical motion of objects results from a least action principle as expressed by Lagrangian

mechanics. Here, what would be the biological "Lagrangian" minimized by the CNS is what is sought for. The rationale of this approach is that the CNS is implicitly assumed to trigger trajectories that are (or tend to be) minimizers of a certain optimality criteria when planning limb movement. Put simply, the goal is to understand the variables the brain cares about when planning movements. In this vein, there have been controversial ideas among researchers: some argued for kinematic-based criteria (Hollerbach and Flash, 1982; Atkeson and Hollerbach, 1985; Sainburg et al., 1995; Bastian et al., 1996; Sainburg et al., 1999; Gribble and Ostry, 1999) while other supported dynamic/energetic-based ones (Dounskaia et al., 2002; Debicki et al., 2010, 2011; Hore et al., 2005, 2011). Therefore, whether the brain controls movement based on kinematic or dynamic/energetic variables still remains elusive despite considerable research efforts. If both views appear to be partly true and the answers may be task-dependent, it is then possible that the brain encodes both variables during the motor planning stage. This idea found supports in the works of Berret et al. (2011a,b) who showed that 2D vertical movements starting from different initial positions and executed at a relatively fast pace could be accounted for by a composite cost mixing the angle jerk (i.e. a kinematic variable) and the absolute work (i.e. an energetic variable). However, it remained unclear whether these results would extend to 3D motion and whether a single composite cost could explain movements executed at different speeds at once. Thus, it was necessary to investigate the composite cost hypothesis during 3D motion at different speeds of movement as well as to identify whether this composite cost could account for the exploitation of rotation around e3 axis, for the role of the interaction torque and for the inter-individual differences mentioned above. This thesis work merges those two previous experimental and computational approaches to improve our knowledge about how free 3D arm movements are planned.

1.2 Thesis objectives

The overall purpose of this thesis is to identify hypothetical principles that may guide movement planning of 3D multijoint unconstrained arm movements for different individuals. To this aim, the approach will combine novel experiments (free arm pointing task) with advanced computational techniques (numerical inverse optimal control). Free arm movements will be examined under different conditions of speed or load in order to let emerge various motor control strategies and assess their adaptiveness to new task conditions. A

core idea is to depart from classical point-to-point reaching paradigms (where the target is generally a dot, e.g. a spotlight target) to study a task in which the endpoint is left free to the participants. This increases the freedom and thus emphasizes inter-individual differences as well as the choice or decision of the underlying motor strategy, allowing better deciphering the characteristics of the motor controller. These empirical results will then be interpreted in the (inverse) optimal control framework, hypothesizing that the recorded arm trajectories derive from the minimization of a certain, possibly composite, cost function. This combined approach aims at revealing which principle/rule conceivably drives the planning process of unrestrained upper limb movements and to establish a link between relevant motion parameters and cost functions.

1.3 Thesis outline

The structure of this dissertation is organized to answer the essential questions mentioned above.

In chapter 2, the main objective is to provide the theoretical background that will serve as reference to the experiments and topics covered in the remaining chapters. This chapter is divided into 2 major parts as follows:

- Part 1: Computational motor control theories
- Part 2: Biomechanical modelling

In chapter 3, the original contribution of the present thesis will be introduced and divided into two sections, each of which will try to find the answer to the specific critical matters as follows:

- 1st section: we test the composite nature of the cost function during motor planning of 3D arm pointing movement and establish its link with rotation axis such as e_3 .
- 2nd section: we examine the role of interaction torque during a free 3D arm pointing task and related it to the composite nature of motor planning examined above.

In chapter 4, a general discussion about the present thesis results is given.

The reader can find the lists of tables and figures at the end of the thesis.

THEORETICAL BACKGROUND

Part I

Computational motor control theories

Motor control is a complex process by which humans use their brain to activate and coordinate the muscles and limbs to perform some purposive movements. This process involves the coordination of varieties of sensory and motor data which in general are highly redundant, nonlinear and noise-affected, making it quite challenging for the motor controller to accurately and reliably execute actions. In spite of those apparent difficulties, the central nervous system (CNS) is nonetheless able to find a relevant solution in a few hundred milliseconds to accomplish the motor task. In order to interpret what potentially takes place during such process and what motivates the resultant motor strategies, researchers have proposed several different motor control theories. Here, we will describe two influential and complementary theories: The first theory proposes a formalism to explain how motor commands and sensorimotor transformations are internally coordinated inside the brain in order to correct and generate a certain desired motion. The second theory is based on a assertion that our movements are actually optimal and that the selected movement among all the possible ones minimizes certain optimal criteria. We will thoroughly describe the latter theory on which all of our works have been based. It has to be noted that other theories exist such as equilibrium point or dynamical system theories, but they make quite distinct assumptions and therefore they will not be detailed here.

2.1 Internal models

Internal models are neural processes which play an important role in motor control as they allow the CNS to mimic the sensorimotor behaviours of the controlled system. Indeed, the concept of internal models seems appealing to develop a motor control theory but their concrete existence in the brain is still under debate in the neuroscience community. Whatever the neural representation they have, the formalisms associated with the internal models all come from the automatic and control theory and seem at least adequate to study the issue of planning and controlling human movement (for reviews, see [Wolpert and Ghahramani \(2000\)](#))

In general, the internal models could be classified into two different types: forward and inverse, each type of model serving a different purpose (Fig. 2.1). The forward internal models permit estimating the next state (e.g. position and velocity) or sensory feedback given the current state and the motor command whereas the inverse internal models allow determining the motor command required to achieve desired changes in the state.

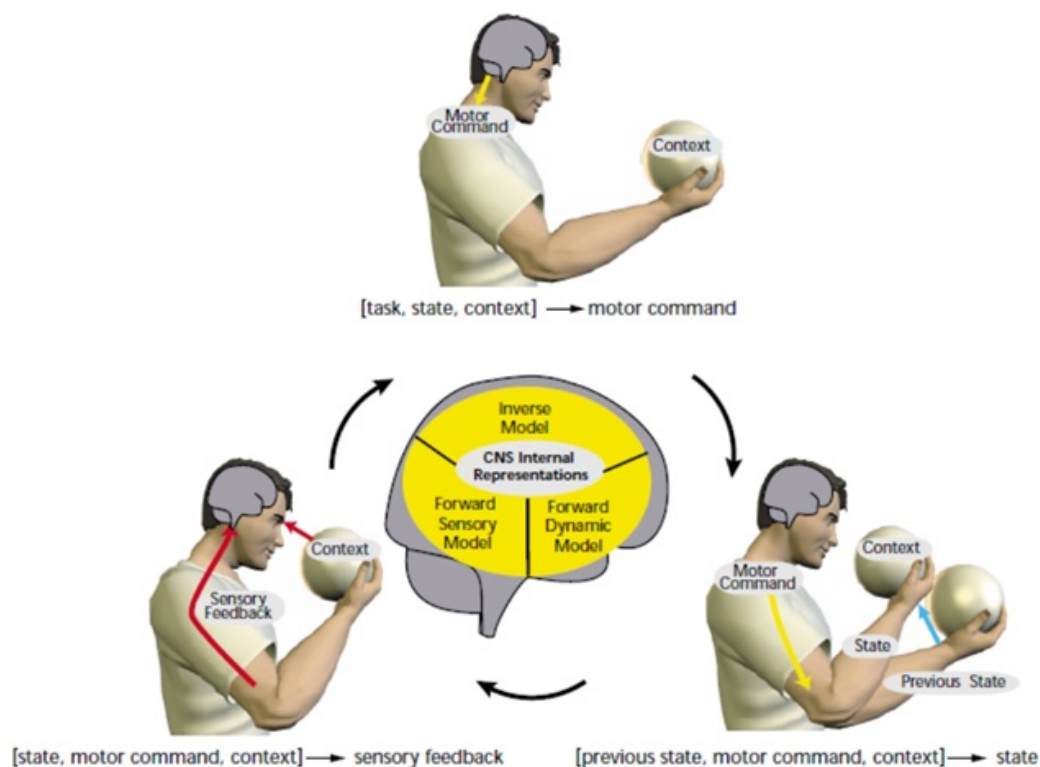


Figure 2.1. The sensorimotor loop can be divided into three stages. These three are represented in the CNS as the inverse model, the forward dynamic model and the forward sensory model, respectively [Wolpert and Ghahramani \(2000\)](#).

2.1.1 Forward internal models

Forward internal models of motor control are predictive internal models. They allow the motor control system to predict the outcome of a specific action by taking into account the available perceptual information and the motor command that causes the action. Specifically, they permit the brain to internally simulate the consequences of the planned action without the need to actually execute the motion. Those models are often described as a functional block within the brain to which the input data is the copy of the motor command signal from the CNS to the periphery (efference copy) and the output data is the estimated sensory feedback (called corollary discharge). This estimated sensory information is then compared with the actual sensory information coming from sensory receptors in the peripheral nervous system (afference). Their discrepancy informs the CNS the extent to which the the expected action agrees with the actual external action such that the CNS

can anticipate, update or cancel sensorimotor errors during a movement. In some cases, the forward internal models have been used to predict the next state of the arm dynamics given the input motor commands.

Evidence for the existence of forward internal models inside the brain mainly comes from studies of motor adaptation. For example, [Wolpert et al. \(1995b\)](#) studied a sensorimotor integration task in which subjects carried out arm movements involving the use of null, assistive and resistive force field in the dark after initially viewing their arm in light. At the end of the movements, the subjects were then asked to estimate the final position of their hand (which had been still hiding from view). The bias between the actual and estimated location was found consistently overestimated with respect to the moved distance. This result was then fully explained with the model of sensorimotor integration process which was actually a combination of two different processes (Fig. 2.2). The first one is a feed-forward process, using the motor command and the current state estimate, combining with the forward model of arm dynamics, to predict the next state. The second one is a feedback process, based on the difference between the predicted and the actual sensory feedback and the Kalman filter model to correct the estimated state obtained in the feed-forward step. This feed-forward-based process successfully accounted for the observed results, indicating the necessity of the internal model to estimate the final arm configuration.

The neurobiological concept of forward internal models has also been successfully applied to a large number of robot control problems. For instance, [Johannes Schrder-Schetelig \(2010\)](#) used the efference copy of motor commands and combined them with a forward internal model to predict the expected self-generated acceleration of a robot during walking. This predicted acceleration was compared with the actually measured one, and was then to update the controller such that walking stabilization was considerably improved.

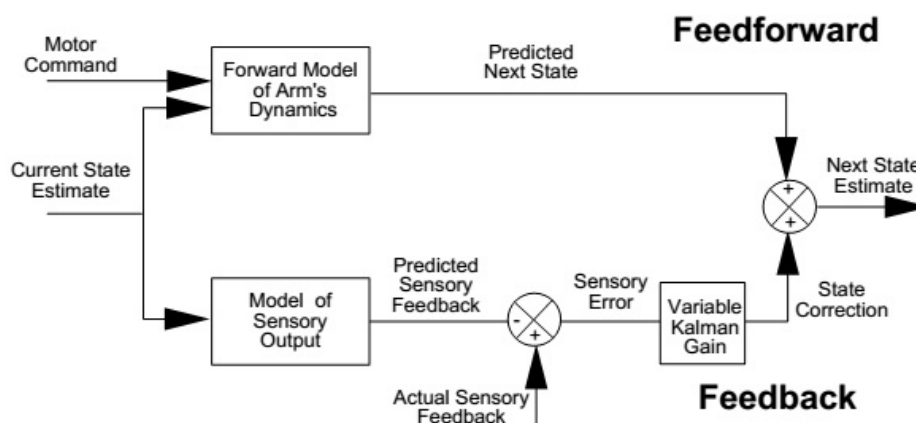


Figure 2.2. Internal sensorimotor integration model proposed by Wolpert et al. (1995b)

2.1.2 Inverse internal models

In contrast to the forward internal models, the inverse internal models enable the motor control system to predict necessary motor commands to achieve certain desired trajectories and sensory consequences. As such, the inverse internal models are important in motor control and often function as a basic module of open-loop control systems.

Again, motor adaptation studies have been used to prove the existence of inverse internal models. For example, by studying a goal-directed reaching movement perturbed by a force field, Shadmehr and Mussa-Ivaldi (1994) found that the participants gradually adapted their motor controller to compensate the dynamic perturbation in order to preserve some typical movement characteristics such as bell-shaped velocity profiles, straight line hand paths and smooth/continuous movements. However, when the perturbation was removed, the participants showed after-effects resulting in perturbed movement trajectories in a direction opposite to the one induced by the perturbation. This finding provided evidence for the existence of a predefined plan (an inverse model) that the motor control system might use to estimate the necessary motor commands to cancel or counteract the perturbation of the external forces and to preserve the characteristics of the normal movement. Moreover, the after-effect exhibited by the motor control system indicated that such inverse model could be modified through a training process (Fig 2.3).

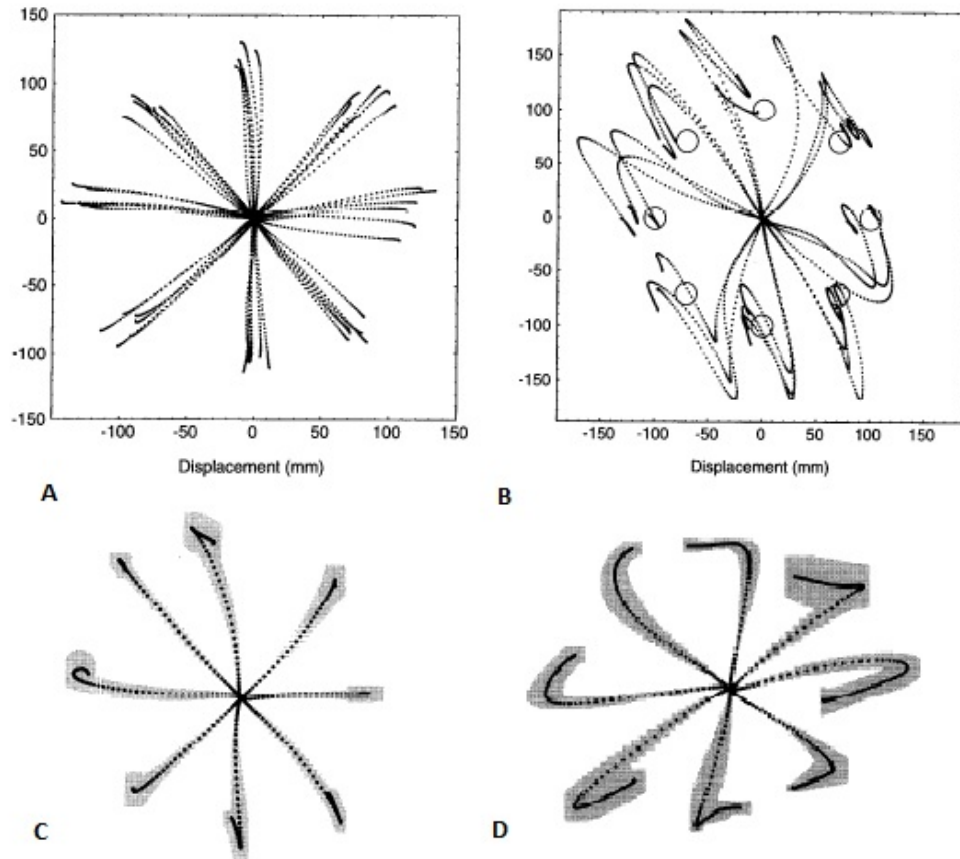


Figure 2.3. Experimental evidence for the existence of the internal inverse models. Panel A shows the trajectories without the perturbations; Panel B shows the initial perturbations that cause large movement variations; Panel C shows the trajectories with the perturbations after learning sessions and panel D shows the after effects of the trajectories when the perturbations are removed (Shadmehr and Mussa-Ivaldi, 1994).

2.2 Optimal control models

The optimal control approach hypothesizes that humans execute movements that are optimal with respect to certain optimal criteria. This approach is theoretically and practically appealing regarding to other classes of models (Todorov, 2004). (i) Theoretically, this approach is based on the natural observation that sensorimotor control is a process that is continuously repeated and updated to improve behavioural performance (across evolution and life time). Thus, even if a performance is not exactly optimal, it could be considered good enough with optimality as limit case. (ii) Practically, optimal control makes it pos-

sible to efficiently and easily solve the sensorimotor control problem without requirements of directly describing the kinematics and the dynamics of the motion as other alternative models may do. Indeed, the optimal control approach describes the motor system behaviour in terms of a global measure called a cost function. This global measure attributes a cost to a movement and the optimal movement is the one that minimises the cost. By specifying a cost, optimal control theory allows to predict an infinity of movements in a concise and elegant way.

In the literature, several cost functions have been proposed by different researchers and they could be classified into two different types: the objective and the subjective costs. The major difference between these costs relates to how they depend on the task specification. Indeed, objective costs are imposed by the task itself and could take various forms depending on the exact purpose of the task (e.g. maximize the precision or the accuracy of reaching, jump height, etc). In contrast, subjective costs usually reflect objectives of the sensorimotor control system itself and are mainly related to the physical structure of the body. These costs are fundamental to resolve all the task redundancy and select a preferred motor strategy. Throughout the thesis work, we focus on examining the subjective costs only as interesting findings regarding how the brain plans movement can be found here. In terms of subjective costs, we can list here several cost functions such as hand jerk (Flash and Hogan, 1985), angle jerk (Wada et al., 2001), angle acceleration (Ben-Itzhak and Karniel, 2008), torque change (Uno et al., 1989; Nakano et al., 1999), torque (Nelson, 1983), geodesic (Biess et al., 2007), energy (Nishii and Murakami, 2002; Berret et al., 2008), effort (Todorov and Jordan, 2002; Guigon et al., 2007). Each of them has been proved useful and relevant as it often replicates at least some experimental observations. In summary, they can be grouped into three main categories: kinematic, energetic and dynamic. Their detailed formulation will be described below.

2.2.1 Kinematic costs

Generally, kinematic costs are formulated based on the geometric variables of a sensorimotor system such as the hand (or finger) position in the Cartesian space or the angular displacement in the joint space and their respective time derivatives. As such, there existed several kinematic costs, each of which has been proved to successfully account for movements executed at a certain extent. Here, we will describe in detail the minimum jerk

cost as a representative element of this class. The idea of jerk cost originally comes from an observation that human movements have the fundamental characteristics of smoothness; i.e, small tremors (Flash and Hogan, 1985). Producing very low level of hand shaking, for instance, could be a target of the CNS to increase the accuracy at the level of the end-effector and/or to protect the joints and the tendons. Thus, the jerk cost aims at producing smooth movements in the Cartesian space. The mathematical formulation of this cost is hence described as follows:

$$C_{HandJerk} = \frac{1}{2} \int_0^T \left(\frac{d^3x}{dt^3} \right)^2 + \left(\frac{d^3y}{dt^3} \right)^2 dt \quad (2.1)$$

where T is the movement duration and (x, y) denotes the position of the end-effector (e.g. fingertip or hand) along the two respective coordinates at time t . Obviously, this equation is purely kinematical: it depends neither on the dynamic properties of the system nor on the environment.

The solution of the above equation is relatively simple. In Flash and Hogan (1985), the problem was directly solved by using the Euler-Lagrange equations and the trajectories minimizing the cost are as follows:

$$\begin{cases} x(t) = x_0 + (x_0 - x_f)(15t^4 - 6t^5 - 10t^3) \\ y(t) = y_0 + (y_0 - y_f)(15t^4 - 6t^5 - 10t^3) \end{cases} \quad (2.2)$$

where (x_0, y_0) and (x_f, y_f) are the initial and final coordinates of the end-effector, respectively. Note that this is the solution for movements starting and ending at zero speed and acceleration.

Here, the found solution has successfully predicted certain empirical observations (Flash and Hogan, 1985) showing that point-to-point reaching movements were approximately straight with bell-shaped tangential velocity profiles. This model thus suggested a kinematic planning of movement in the Cartesian space with some advantages because the end-effector trajectory could be easily found without specific knowledge of the arm dynamics. Moreover, the stipulation of the cost could easily be generalized into three spatial dimensions by simply taking the sum of squared jerk along each dimension which is equivalent to three independent minimizations. Consequently, the resulting trajectories all take the form of Equation 2.2 for each dimension and predict the straight movements for the end-effector in 3D with symmetric velocity profiles.

Besides advantages, the minimum jerk cost in Cartesian space, also known as hand jerk cost, has some limitations. The arguments for such limitations are twofolds: (i) The prediction of the hand jerk cost is mostly about the path movement of the end-effector; i.e. the highest level of the sensorimotor control system; thus it does not reveal any prediction about what could happen in the joint space or even at the lower level (muscle level) of the control system. (ii) When the subject's arm is hidden from his/her view, what the brain actually monitors is based on the sensory feedback/perception which is measured and sent to the brain by joint receptors. Therefore, the emerging idea is that the real aim of the CNS is probably to produce smooth movements in the joint space, and that the observation of smooth hand path in Cartesian space is just the consequence of what is planned in the joint space. [Wada et al. \(2001\)](#) thus extended the concept of hand jerk cost into the joint space by replacing the third derivatives of hand trajectories by those of joint angles. The equation of the minimum jerk in the joint space hence becomes:

$$C_{AngleJerk} = \int_0^T \sum_i \left(\frac{d^3\theta_i}{dt^3} \right)^2 dt \quad (2.3)$$

where i denotes the i^{th} joint angle. Their respective solutions all take the same form as in Equation [2.2](#).

The minimum-jerk model has been proved to play an important role in general. One example is to use the minimum jerk model to explain the two-thirds power law, which stipulates that the hand angular velocity during drawing or scribbling relates with the path curvature as a power of 2/3 ([Paolo Viviani, 1995](#)). Recently, by examining a novel bar reaching task from different initial arm postures ([Berret et al., 2011a](#)) these authors showed that the angle jerk cost contributed the most to the composite cost which replicated at best the experimental reaching behaviours.

2.2.2 Dynamic costs

Dynamic costs are formulated based on the dynamics of the sensorimotor control system where parameters of interest are often forces or torques acting on joints and their respective time-derivatives. Like the kinematic costs, the dynamic costs were also shown to account well for some empirical data. Here, it is useful to distinguish the dynamic costs from the kinematic costs. The critical difference between two costs is associated with the inverse dynamic process which is generally assumed to exist in the motor system. Indeed, kinematic

costs allow determining easily the optimal trajectories either in the intrinsic (joint) or the extrinsic (Cartesian) space without knowledge of the arm dynamics. Yet, in order to execute movements following the specified optimal trajectories, an inverse dynamics process is still required to estimate necessary torques/forces that would cause the desired trajectories. In contrast, dynamic cost functions do not require such inverse dynamics process. However, solving the optimal problem for the dynamic costs is often more challenging than for the kinematic costs and usually requires more complex numerical methods.

In the literature, several dynamic costs have been proposed by researchers. Their definition could be based on different dynamic variables such as torque, torque change, muscle tension or motor command, etc. Here, we will mainly describe the torque change cost and considered it as a representative element of the dynamic class of costs.

The torque change model has been first proposed by [Uno et al. \(1989\)](#), arguing that minimally changing the joint torque could protect the musculoskeletal system and produce smooth movements in torque space. The mathematical formulation of the cost is described as follows:

$$C_{TorqueChange} = \int_0^T \sum_i \left(\frac{d\tau_i}{dt} \right)^2 dt \quad (2.4)$$

where T is the duration movement, $d\tau_i/dt$ is the rate of change of torque at the i^{th} joint. Applying this criteria to horizontal movements of a bi-articular arm, [Uno et al. \(1989\)](#) found that the determined optimal trajectories accounted quite well for numerous empirical observations such as the curved hand path (observed as the subject moved his stretching arm from the side direction to the final position in front of the body) that the kinematic costs could not explain since the hand path predicted by the kinematic costs is always a straight line.

2.2.3 Energetic costs

At the interface between the kinematic and the dynamic costs are energetic costs which try to measure the actual energy expenditure of movements. Like the kinematic- and the dynamic-based models, several cost functions have been proposed in this category such as the absolute work ([Berret et al., 2008](#); [Gauthier et al., 2010](#)), the peak work ([Soechting et al., 1995](#)) and the geodesic ([Biess et al., 2007](#)). While it is usually hard to get an account of the metabolic energy consumed by different trajectories, the mechanical energy

expenditure can be well evaluated. Here, we will mostly consider the absolute work of muscle torques as a representative element of the energetic class of models.

The concept of the absolute work cost has been proposed by [Berret et al. \(2008\)](#) and supported by the inactivation principle emerging during the motor control process. According to this principle, minimizing a term similar to the absolute work predicts a brief simultaneous inactivation of agonistic and antagonistic muscles acting on each single joint near the time of peak velocity, for fast enough reaches. This cost function was also important to replicate other typical features of movements such as the hand trajectory, hand velocity profile or final arm postures. The mathematical formulation of the cost is described as follows:

$$C_{AbsoluteWork} = \int_0^T \sum_i |\dot{\theta}_i \tau_i| dt \quad (2.5)$$

where T is the movement duration, $\dot{\theta}_i$ is angle velocity and τ_i is the muscle torque acting on the joint i^{th} . Unlike the kinematic and the dynamic models, solving the optimal problem of absolute work cost is quite challenging because of its non-smoothness around zero due to the absolute function. In order to avoid this difficulty, in numerical analyses, a term similar to the absolute work was used and defined as

$$C_{AbsoluteWork} = \int_0^T \sum_i \tanh(\alpha |\dot{\theta}_i \tau_i|) |\dot{\theta}_i \tau_i| dt \quad (2.6)$$

where the parameter α quantifies discrepancy between the smooth approximation function and the real absolute work. The smaller the value of α , the higher the discrepancy. Through the thesis work, α was set equal to 10.

2.3 Direct optimal control

The goal of direct optimal control is to find a control variable and its corresponding controlled variables (e.g. a set of states such as positions and velocities) that minimize a given cost function while satisfying certain constraints. Conceptually, the direct optimal control can be stated as follows:

Direct optimal control will determine optimal state variables $x(t) \in R^{n_x}$, an optimal control $u(t) \in R^{n_u}$, possibly an initial time (t_0) and/or final time (t_f) and an optimal cost on that time interval that minimizes the following cost function:

$$\mathcal{L} = h(x(t_f), t_f) + \int_{t_0}^{t_f} g(x(t), u(t), t) dt$$

where h measures the cost value at the final time/states and g measures the infinitesimal cost value at any time t . The solution to this problem is subjected to the dynamic constraints:

$$\frac{dx}{dt} = f_d(x(t), u(t), t)$$

and the inequality/equality path constraints

$$p_{min} \leq f_p(x(t), u(t), t) \leq p_{max}$$

and some event constraints

$$e_{min} \leq f_e(x(t_0), t_0, x(t_f), t_f) \leq e_{max}$$

The function h , g , f_d , f_p , f_e are defined by the following mappings:

$$h : R^{n_x} \times R \rightarrow R,$$

$$g : R^{n_x} \times R^{n_u} \times R \rightarrow R,$$

$$f_d : R^{n_x} \times R^{n_u} \times R \rightarrow R^{n_x},$$

$$f_p : R^{n_x} \times R^{n_u} \times R \rightarrow R^{n_p},$$

$$f_e : R^{n_x} \times R \times R^{n_x} \times R \rightarrow R^{n_e},$$

The set of control variables which satisfies the control constraints during the time $[t_0, t_f]$ is called the set of admissible controls; whereas the set of state variables satisfying the state constraints is called the set of admissible states. Thus the purpose of the direct optimal control is to find among the admissible controls and states a control $u = \mathbf{u}^*$ and a corresponding state $x = \mathbf{x}^*$, connecting a source point \mathbf{x}_{t_0} to a final point \mathbf{x}_{t_f} on the time interval $[t_0, t_f]$ and yielding a minimal value of the cost \mathcal{L} .

The optimal control theory can be formulated in two different ways: the discrete time (where the time makes jumps according to a sampling frequency) and the continuous time formulations. Consequently, separate computation techniques have been proposed to solve the direct optimal control problem for each of these formulations.

In the discrete case, the first method developed in the 1950s in the United State is known under the name “dynamic programming” and is proposed by [Bellman \(1957\)](#). This

method is based on the following idea: the choice of optimal control in the future is independent of the choice of the optimal control in the past, which led to the present state. In the continuous case, the same principle can be generalized in the form of the equations of Hamilton-Jacobi-Bellman (HJB) which generally converts the optimal control problem to solving nonlinear partial differential equations of second-order. Meanwhile, in the Soviet Union and in line with the calculus of variations and the multiplier method of Lagrange, Lev Pontryagin and his colleagues developed the Maximum Principle (PMP) to give a powerful formalism for solving a wide range of problems. PMP provides necessary optimality conditions, while HJB equations give sufficient conditions of optimality. These methods are very powerful but their use is often limited to low-dimensional systems. Because of the curse of dimensionality or the difficulty of implementing shooting methods from PMP formalism, researchers often use more numerical approaches, especially when they deal with complex systems and non-quadratic cost functions. In practice, one common method to solve the continuous optimal control problem is called direct transcription. The rationale is that the continuous variables will be represented (or approximated) by discrete variables into N subintervals (denoted as $\{t_0, t_1, \dots, t_N\}$). Thus, continuous time variables are replaced by piece-wise constant functions. Eventually, this discretization allows one to convert the optimal control problem to a constrained non-linear programming problem, for which efficient numerical tools exist including for high-dimensional problems with thousands of variables.

Applying the direct optimal control to the study of neural movement control can be useful as it allows searching for the best theoretical trajectory for a specific criterion chosen a priori by the researcher. This simulated trajectory is then compared with the experimental data that allows verifying whether model or cost function replicates the real motor strategy. Thus, it permits assessing the possibility that the brain may use such criterion during motor planning stage. However, the limitation of direct optimal control is that the criterion must be always "guessed" by the researcher and even if a criterion is found to fit some data reasonably well, it does not prevent other criteria to perform equally well (or even better). Therefore, direct optimal control is useful to test the validity of criterion but does not resolve the question of why human trajectories have such a shape as other untested cost function might also reproduce the motion data. Understanding which variables are really critical for motor planning would require testing a bunch of cost functions. Recently, evidence showed that the brain possibly optimizes a combination of several different criteria

with different weights during the control of human movement. In order to determine these weights, we must employ another approach (generally considered as much more difficult) which is described hereafter.

2.4 Inverse optimal control

Unlike direct optimal control, the cost function is considered to be unknown and becomes what is sought for in case of inverse optimal control; instead, what we start from is the knowledge of presumed optimal state trajectories (via empirical motion data). This means that the optimal solution is known (also approximately) but the cost function underlying the resultant solution is unknown. Actually, inverse problems are commonly faced in the scientific fields, in particular in neural movement control where the principles according to which the brain may plan movement must be uncovered. In such cases, inverse optimal control allows automatically inferring the cost function by directly using the recorded data as one of its input information.

However inverse optimal control is an ill-posed problem in general, which means it may have no unique solution. To be more tractable, inverse optimal control usually assumes that the cost function takes the form of a combination of different criteria which are weighted differently. This combination is also called composite cost (denoted by $C(\alpha)$ here). Then, the purpose of inverse optimal control is to find the weights that make the simulated trajectories as close as possible to the real /measured ones. Let us denote the simulated and measured trajectories are \mathbf{X}_α^* and X^{meas} , respectively. Then the formulation of inverse optimal control can be stated as a “bi-level” problem with two loops (Mombaur et al., 2009; Berret et al., 2011a):

$$\begin{array}{ll}
 \textit{Outer loop} & \text{minimize}_{\alpha} \Phi(\mathbf{X}_\alpha^*, \mathbf{X}^{meas}), \\
 & \updownarrow \\
 \textit{Inner loop} & \textit{where } \mathbf{X}_\alpha^* \textit{ is the optimal solution corresponding to the value } \alpha \textit{ that} \\
 & \textit{yields a minimal value of composite cost } C(\alpha)
 \end{array} \tag{2.7}$$

The outer loop function Φ is a measure of the discrepancy between simulated and measured trajectories. Thus far, what metric we should use to compare simulated and real motion data is still under debate. It is likely that reproducing the geometry of the trajectory is required before looking at the velocities, accelerations or torques. Yet, different

functions could be used here. A conservative measure is for instance the maximal deviation from a simulated trajectory to the real path. The composite cost function $C(\alpha)$ is usually assumed to be composition of elementary costs C_i and takes the following form:

$$C(\alpha) = \sum_{i=1}^n \alpha_i C_i \quad (2.8)$$

The parameter $\alpha = (\alpha_i)_{1 \leq i \leq n}$ is referred to as the weighting vector whose elements are non-negative. Thus, the purpose of outer loop is to adjust $\alpha = (\alpha_i)_{1 \leq i \leq n}$ and finally find its optimal value $\alpha^* = (\alpha_i^*)_{1 \leq i \leq n}$ that has the simulated $X_{\alpha^*}^*$ respectively closest to the recorded X^{meas} .

Other difficulties are associated with numerical inverse optimal control such as time of the computations, robustness of the optimization steps etc. Inverse optimal control nevertheless allows testing an infinity of cost functions while only a couple are tested when doing direct optimal control. The possibility to test a great number of cost functions in an automated way is one of the most interesting property of inverse optimal control.

Part II

Biomechanical modelling

2.5 Anatomical background

2.5.1 Anatomical structures

The anatomical structure of the upper-limb composes of three segments: the upper arm, the forearm and the hand (Fig. 2.4). The upper arm is connected with the trunk through the shoulder girdle which consists of the clavicle and the scapula. Horizontally located on the anterior and upper part of the thorax, the clavicle is a long bone that serves as strut between the scapula and the sternum. Being flat, even and non-symmetrical triangular bone, the scapula locates on the upper and posterior part of the thorax leading to the glenohumeral joint. The glenohumeral joint is a ball and socket joint with three degrees of freedom involving the articulation between the scapula and the humeral head. The humerus itself is a long, non-symmetrical bone that connects the scapula and the forearm bones. The humerus is connected to the forearm through the synovial elbow hinge joint. The two long bones of the forearm, the radius and the ulna, form the radioulnar joint. The latter is on the lateral side and represents the mobile part (corresponding to pronation and supination) of the forearm whereas the former is on the medial side and is relatively fixed. The hand is divided in three parts, the carpus, the metacarpus and the phalanges. The carpus contains eight bones connecting the hand to the forearm that forms the radiocarpal joint or the wrist joint. The mobility of the individual carpal bones increases the freedom of movements of the wrist. The metacarpi are the bones of the palm. The phalanges consist of fourteen phalanx bones of the fingers, together with the metacarpi bones, forming the skeleton of the fingers.

2.5.2 Anatomical landmarks

Here, we use a set of anatomical landmarks which has been proposed by the International Society of Biomechanics (ISB) (Wu et al., 2005) and defined as follows (Table 2.1).

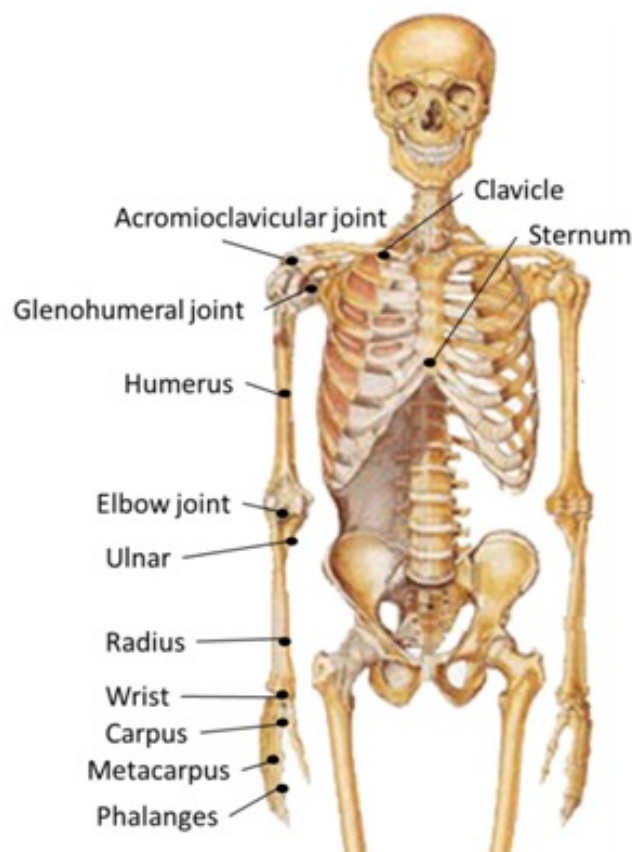


Figure 2.4. Anatomical model of the human upper body (Hansen, 2013).

Anatomical landmarks		
Thorax	C7	Processus Spinosus (spinous process) of the 7th cervical vertebra
	T10	Processus Spinosus (spinal process) of the 10th thoracic vertebra
	IJ	Deepest point of Incisura Jugularis (suprasternal notch)
	PX	Processus Xiphoideus (xiphoid process), most caudal point on the sternum
Clavicle	SC	Most ventral point on the sternoclavicular joint
	AC	Most dorsal point on the acromioclavicular joint (shared with the scapula)
Scapula	TS	Trigonum Spinae Scapulae (root of the spine), the midpoint of the triangular surface on the medial border of the scapula in line with the scapular spine
	AI	Angulus Inferior (inferior angle), most caudal point of the scapula
	AA	Angulus Acromial is (acromial angle), most laterodorsal point of the scapula
	PC	Most ventral point of processus coracoideus
Humerus	GH	Glenohumeral rotation center, estimated by regression or motion recordings
	EL	Most caudal point on lateral epicondyle
	EM	Most caudal point on medial epicondyle
Forearm	RS	Most caudal-lateral point on the radial styloid
	US	Most caudal-medial point on the ulnar styloid

Table 2.1. Anatomical landmarks

The real locations of these anatomical landmarks on the relative bones are virtually displayed in Figure 2.5.

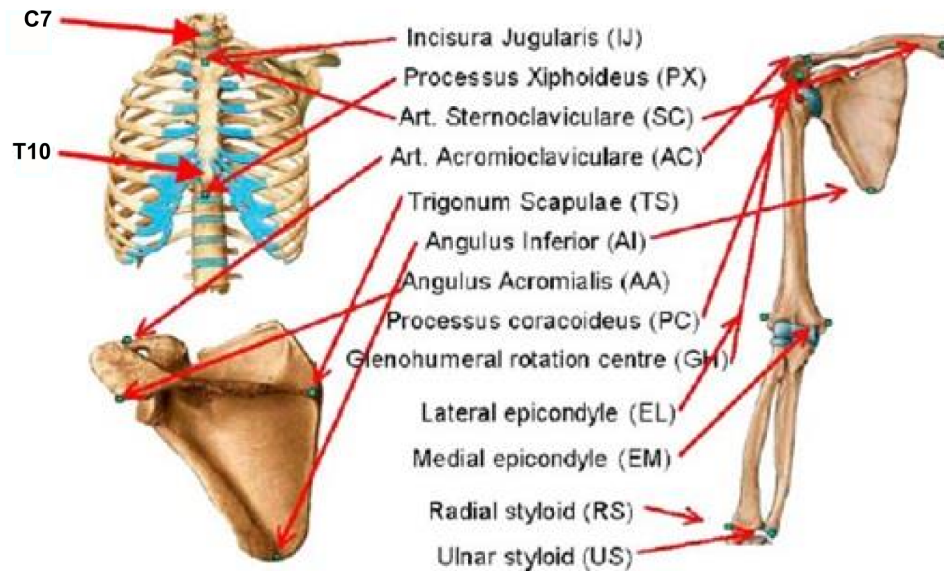


Figure 2.5. Body landmarks of the thorax, clavicle, scapula and humerus (Wu et al., 2005).

2.6 Kinematic model of the arm

2.6.1 Upper-body segment coordinate systems

The next section is dedicated to the definition of a segment coordinate systems (SCS) in accordance with the recommendations of the ISB for a human upper-body. More specifically, for each segment of interest, we will define a specific segmental coordinate (origin and three Euclidean axes) based on the anatomical landmarks that almost rigidly attach to and move along with the segment. The details will be described as follows.

Trunk coordinate system:

O_T	The origin coincident with the IJ
Y_T	The line connecting the midpoint of PX and T10 and the midpoint of IJ and C7, pointing upward.
Z_T	The line perpendicular to the plane formed by IJ, C7, and the midpoint of PX and T10, pointing to the right
X_T	The common line perpendicular to the Z_T and Y_T axis, pointing forwards

Table 2.2. Trunk coordinate definition

Humerus coordinate system:

O_A	The origin coincident with the GH
Y_A	The line connecting GH and the midpoint of EL and EM, pointing to GH
Z_A	The line perpendicular to the plane formed by Y_A and Y_F (see forearm coordinate definition just below) pointing to the right
X_A	The common line perpendicular to the Z_A and Y_A axis, pointing forward

Table 2.3. Humerus coordinate definition

Forearm coordinate system:

O_F	The origin coincident with the midpoint of EL and EM
Y_F	The line connecting the midpoint of US and RS and the midpoint of EL and EM, pointing to proximally
X_F	The line perpendicular to the plane through US, RS, and the midpoint of EL and EM, pointing forward
Z_F	The common line perpendicular to the X_F and Y_F axis, pointing to the right

Table 2.4. Forearm coordinate definition

Hand coordinate:

O_H	The origin is located at the midpoint of US and RS
Y_H	The line parallel to the long shaft of the ulna from O_H to intersect with the center of the dome of the ulnar head
X_H	The line perpendicular to the plane containing Y_H and the line connecting US to RS, pointing forward
Z_H	The common line perpendicular to the X_H and Y_H axis, to the right.

Table 2.5. Hand coordinate definition

Following these definitions, the segment coordinate systems of the upper right limb could be illustrated as in Figure 2.6.

2.6.2 Rotational model of upper-limb joints

Because we mainly study motions of the upper-limb while constraining motion of other parts, in the following paragraphs, we will only describe in details the rotational model of the upper-limb joints (i.e. shoulder, elbow and wrist joints).

Shoulder joint model. Although most of researchers agree that the motion of shoulder joint can be considered as consisting of three degrees of freedom (DoF), the specific rotational order of these DoFs is still under debate as different orders will lead to different estimated joint angle values. Indeed, many available rotational orders have been proposed such as the X-Y-Z order in Cardan angles or Y-X-Y order in Euler angles. Here we choose the Euler angle order as it permits the joint angles to remain as close as possible to the clinical definitions of joint and segmental motions. According to this choice and in accordance with the ISB recommendation (Wu et al., 2005), the first rotation will be executed around the Y_g axis of global coordinate (this global coordinate is actually coincident with the trunk coordinate in our consideration). The corresponding movement is the internal/external motion. It is also called “plane of elevation” because it indicates in which plane the subsequent movement called “elevation/depression” (corresponding to 2nd DoF) is executed. This latter motion is executed around the X_A axis of the humerus coordinate model rigidly attached to the humerus segment as mentioned above. Finally, the 3rd DoF corresponds to the humerus axial rotation (namely, ulnar/radial rotation) and is executed around the Y_A axis of the humerus coordinate. (See Fig. 2.6 for a visual illustration)

Elbow joint model. Less complex than the shoulder joint, the elbow joint has only two DoFs. Its first DoF corresponds to “flexion – extension” motion around the Z_A axis of the humerus coordinate model, followed by its 2nd DoF “pronation - supination” around the Y_F axis of the forearm coordinate model rigidly attached to the arm.

Wrist joint model. Finally, the wrist has two DoFs: “radio-ulnar deviation” around X_F axis of the forearm coordinate followed by “flexion-extension” around Z_H rigidly attached to the hand.

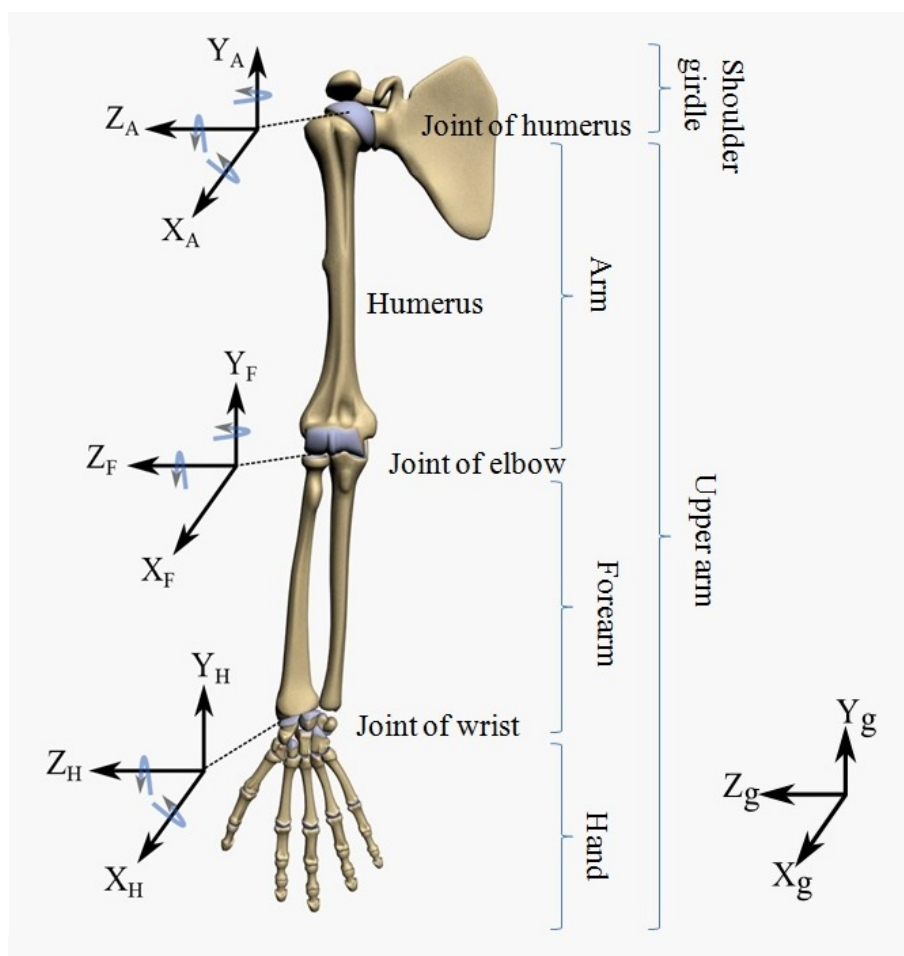


Figure 2.6. The segment coordinate model and the joint model of the upper right limb

2.6.3 Inverse kinematic calculation

2.6.3.1 Measuring human movements

Measuring human movements Over the last centuries, techniques allowing to measure human locomotion have been always developed and improved. At very early times, Weber brothers (1836) reported one of the first quantitative studies evaluating the temporal and distance parameters during human locomotion. Some years later, Marey (1873) and Muybridge (1878) were among the first to quantify patterns of human movement by using photographic techniques that turned out to successfully reveal a flight phase during the running stride in the horse gallop. More recently, instrumentation and computer technologies have provided new opportunities for the advancement of the study of human

locomotion including goniometers, accelerometers (Chung and Ng, 2012), inertia based and electromagnetic sensors (Lee and Park, 2011), active and passive optical motion capture systems (Maletsky et al., 2007; Richards, 1999) and even markerless optical motion capture devices (Ceseracciu et al., 2011), as well as ultrasound motion capture devices (Malmström et al., 2003). Nowadays, the most common method for accurately capturing three-dimensional human movement is to attach a set of markers, fixtures or sensors to the body segments, then use a number of high speed cameras to trace/record the movement of these attached points. The use of markers, for instance, is typical to infer the underlying relative position/orientation of two adjacent segments with the goal of precisely defining the movement of the joint. However, the accuracy of motion capture systems strongly depends on the number of camera, the size and quality of used marker, the distance from the camera to the marker, the quality of calibration, the calibration volume, the camera resolution and external infrared disturbances (Maletsky et al., 2007; Windolf et al., 2008; Chung and Ng, 2012; Richards, 1999). Furthermore, putting markers on the human body often leads to soft-tissue artifacts (STA) between skin-mounted markers and the underlying bones (Capozzo et al., 1996). Using bone pins may avoid the occurrence of STA (Reinschmidt et al., 1997; Benoit et al., 2006), but the feasibility of drilling pins in the bone of subjects to quantify joint and bone motions remains questionable.

Depending on the complexity and the detail of analyses, the choice of movement measurement device is important and usually dependent on the application and the budget. In our current study, we used an optical motion capture system consisting of eight-high-speed cameras (Vicon motion system Inc. Oxford, UK). The laboratory setup of the system is displayed as in Figure 2.7. The optoelectronic cameras are usually arranged along a circle around the subject.

Marker Set. In the current work, the set of ten anatomical markers described above was attached to the participants according to the following anatomical landmarks: 7th cervical vertebrae (C7), 10th thoracic vertebrae (T10), jugular notch where the clavicles meet the sternum (CLAV), xiphoid process of the sternum (STRN), right acromio-clavicular joint (RSHO, LSHO), lateral and medial epicondyle elbow (RELB, RELM), wrist bar thumb and wrist side and the hand (RWRA, RWRB) and the hand place on the dorsum of the hand just below the head of the second metacarpal (RFIN) and the tip of the index finger (FRI1).

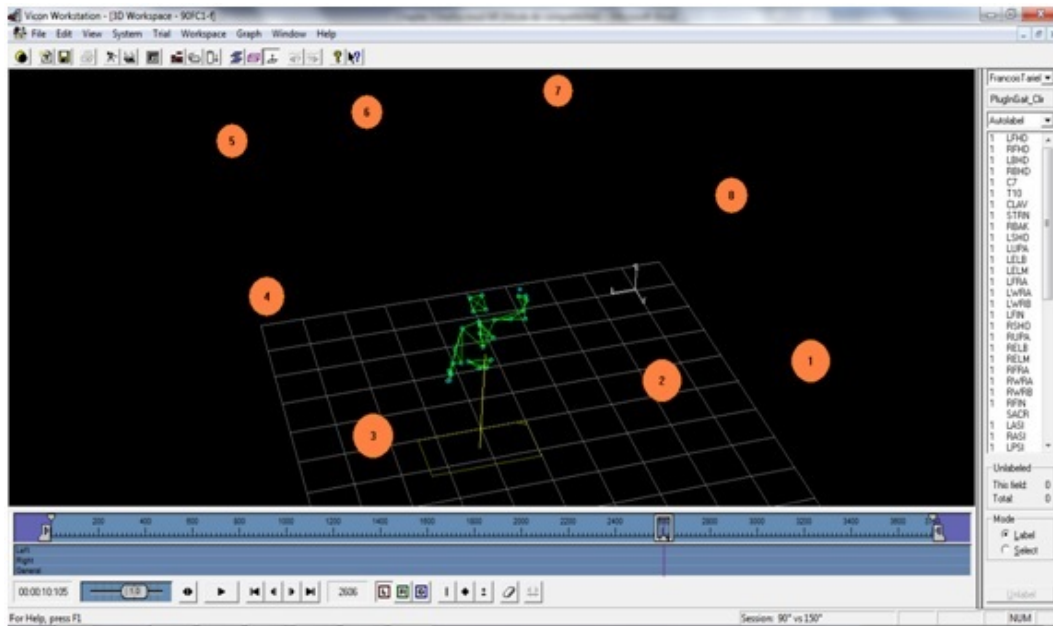


Figure 2.7. A motion capture system composing of eight cameras (Hansen, 2013).

Trunk

1. C7 = 7th Cervical vertebrae spinous process of the 7th cervical vertebrae
2. T10 = 10th thoracic vertebrae spinous process of the 10th thoracic vertebrae
3. CLAV = Clavicle jugular notch where the clavicles meet the sternum
4. STRN = Sternum xiphoid process of the Sternum
5. RSHO = right shoulder marker placed on the acromio-clavicular joint
6. LSHO = left shoulder marker placed on the acromio-clavicular joint

Upper-limb

7. RELB = right elbow placed on lateral epicondyle approximating elbow joint axis
8. RELM = right elbow placed on lateral epicondyle approximating elbow joint axis
9. RWRA = right wrist marker A right wrist bar thumb side
10. RWRB = right wrist marker B right wrist bar pinkie side
11. RFIN = right fingers actually placed on the dorsum of the hand just below head of the second metacarpal
12. RFI1 = on the tip of right index finger

Joint center

1. RHUP = right shoulder joint center
2. RHUO = right elbow joint center
3. RRAO = right wrist joint center

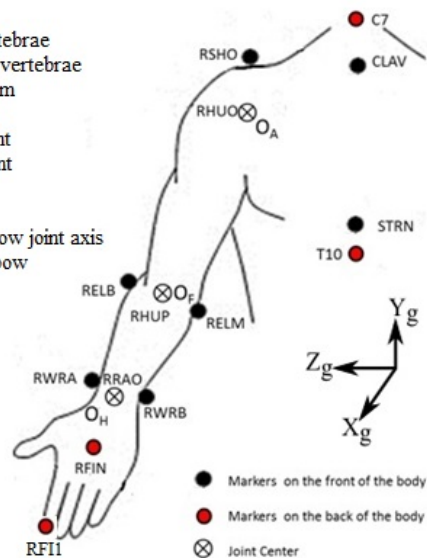


Figure 2.8. A set of marker used in the current work for the upper body (Hansen, 2013).

2.6.3.2 Joint angle calculations

Here we use an inverse kinematic approach to calculate the limb's joint angles with respect to specific limb posture. To this aim, we first link the limb's SCS as mentioned above with the set of markers that allows estimating such SCS based on the measured 3D position of markers. Depending on the determined coordinates, a set of rotation matrices standing for the rotational transformation from the global to the segmental coordinates is calculated in accordance with the chosen Euler rotational order. The obtained results are then used to infer another set of rotation matrices between two adjacent segments. This latter set of matrices in turn allows extracting the limb's relative joint angle displacements. The detail of process will be described as follows.

First, according to the biomechanical model of the upper-limb, the SCS and the order of rotational axes are summarized based on the marker set as described in Table 2.6.

Segment	Coordinate /Rotation definitions (based on markers)	Rotation Sequence
Trunk	Origin : CLAV	
	Y_t : midpoint of [STRN-T10] \rightarrow midpoint of [CLAV-C7]	
	X_t : midpoint of [STR-T10] \rightarrow CLAV \wedge midpoint of [STRN-T10] \rightarrow C7	
	$Z_t : X_t \wedge Y_t$	
Arm	Origin : Rotation Center of the Shoulder (RHUO)	Y-X-Y
	Y_a : midpoint of [RELM-RELB] \rightarrow Rotation Center of the shoulder	
	$Z_a : Y_a \wedge Y_f$	
	$X_a : Y_a \wedge Z_a$.	
	Rotation	
	a1 : Internal/external	
	a2 : Elevation/depression	
	a3: Axial rotation ulnar/radial	
Forearm	Origin : RHUP	Z-X-Y
	Y_f : RRAO \rightarrow midpoint of [RELB-RELM]	
	X_f : RRAO \rightarrow RELM \wedge RRAO \rightarrow RELB	
	$Z_f : X_f \wedge Y_f$	
	Rotation	
	a1 : Flexion/ extension	
a2: Pronation/ Supination		
Hand	Origin : RRAO.	Y-X-Z
	Y_h : RFIN \rightarrow midpoint of [RWRA-RWRB]	
	X_h : RFIN \rightarrow RWRA \wedge RFIN \rightarrow RWRB	
	$Z_h : X_h \wedge Y_h$	
	Rotation	
	a1 :Abduction / Adduction	
	a2 : Flexion/ Hyper-extension	

Table 2.6. The segment coordinate system based on the marker set and the order of rotational axes

Based on the above definition, we then calculate the coordinates for each segment with respect to the global coordinate system. We define the rotation matrices which represent the rotational transformation from the global to the segmental coordinates as follows:

$R_{01} = R_trunk$	From global coordinate to trunk coordinate
$R_{02} = R_upperarm$	From global coordinate to upper arm coordinate
$R_{03} = R_forearm$	From global coordinate to forearm coordinate
$R_{04} = R_hand$	From global coordinate to hand coordinate

We then define R_{12} , R_{23} , R_{34} as the rotation matrices describing the transformation from the trunk's coordinate to the upper arm's, from the upper arm's coordinate to the forearm's and finally from the forearm's coordinate to the hand's, respectively. Then, the rotation matrices from the global to the segmental coordinate could be rewritten as:

$$\begin{aligned} R_{02} &= R_{01}R_{12} \\ R_{03} &= R_{02}R_{23} \\ R_{04} &= R_{03}R_{34} \end{aligned} \quad (2.9)$$

by multiplying both left and right sides of these above equations with R_{01}^{-1} , R_{02}^{-1} , R_{03}^{-1} respectively. We obtain:

$$\begin{aligned} R_{12} &= R_{01}^{-1}R_{02} \\ R_{23} &= R_{02}^{-1}R_{03} \\ R_{34} &= R_{03}^{-1}R_{04} \end{aligned} \quad (2.10)$$

As such, the displacement of joint angles could be easily extracted by using the inverse Euler rotation transformation as follows :

- At shoulder : rotation order YXY

$$\begin{aligned} Angle_{S_x} &= -\arccos(R_{12}(2, 2)); \\ Angle_{S_{y1}} &= \arctan 2 \left(\frac{R_{12}(1,2)}{\sin(Angle_{S_x})}, \frac{R_{12}(3,2)}{\sin(Angle_{S_x})} \right) \\ Angle_{S_{y2}} &= \arctan 2 \left(\frac{R_{12}(2,1)}{\sin(Angle_{S_x})}, \frac{-R_{12}(2,3)}{\sin(Angle_{S_x})} \right) \end{aligned}$$

- At elbow : rotation order ZXY

$$\begin{aligned} Angle_{E_x} &= -\arcsin((R_{23}(3, 2))); \\ Angle_{E_y} &= \arctan 2 \left(\frac{-R_{23}(3,1)}{\cos(Angle_{E_x})}, \frac{R_{23}(3,3)}{\cos(Angle_{E_x})} \right) \\ Angle_{E_z} &= \arctan 2 \left(\frac{-R_{23}(1,2)}{\cos(Angle_{E_x})}, \frac{R_{23}(2,2)}{\cos(Angle_{E_x})} \right) \end{aligned}$$

- At wrist : rotation order YXZ

$$Angle_{W_x} = \frac{\pi}{2} \text{sign}(\arcsin(-R_{34}(2, 3))) + \arcsin(-R_{34}(2, 3))$$

$$Angle_{W_y} = \arctan 2(R_{34}(1, 3), R_{34}(3, 3))$$

$$Angle_{W_z} = \arctan 2(R_{34}(2, 1), R_{34}(2, 2))$$

It is noteworthy that there are only two real DoFs at elbow and wrist. Therefore, the $Angle_{E_x}$ and $Angle_{W_y}$ are actually equal to zero.

2.7 Dynamic model of the arm

Derivation of the dynamic model of human upper-limb plays an important role for the analysis of 3D movement and the interpretation of possible principles underlying sensorimotor control system. Having relatively accurate description of the arm's dynamics and efficient computational methods is especially important for the simulation processes as several cost functions (being tested in the current work) require intensive evaluation of the arm's dynamics. Moreover, the computation of forces and torques required for the execution of upper-limb motion provides insights about the properties of the motor command. The following paragraphs are thus dedicated to describe the dynamic model of the right upper-limb. We first introduce a method allowing to estimate the segment inertial parameters of the limb, then briefly describe some existing approaches permitting to calculate necessary forces/ torques associated with given kinematics.

2.7.1 Segment inertial parameter estimations

2.7.1.1 Moment of inertia/Inertia tensor

The term “moment of inertia” was first introduced by Leonhard Euler in his book titled “Theoria motus corporum solidorum seu rigidorum” in 1765. Just like mass (inertia) plays a role in the linear kinetics, moment of inertia plays a role in the rotational kinetics - both characterize the resistance of a body to changes in its motion. It is defined based on the mass elements of an object and the squared distance from these mass elements to the rotation axis. The moment of inertia thus depends on how mass is distributed around the axis of rotation and will vary depending on the chosen axis.

For a point-like mass, the moment of inertia about a certain axis is given by d^2m , where d is the distance to the axis, and m is the mass. For an extended body, the moment of inertia (or inertia matrix) is just the sum of all the small pieces of mass multiplied by the square of their distances from the axis. In general, in a 3D examination, the inertia matrix of a rigid body expressed in a Cartesian coordinate XYZ is of the form:

$$I = \begin{bmatrix} I_{xx} & -I_{yx} & -I_{zx} \\ -I_{xy} & I_{yy} & -I_{zy} \\ -I_{xz} & -I_{yz} & I_{zz} \end{bmatrix} \quad (2.11)$$

where the diagonal matrix elements I_{xx} , I_{yy} , I_{zz} are calculated by the following equation :

$$\begin{aligned} I_{xx} &= \iiint (y^2 + z^2) dm \\ I_{yy} &= \iiint (x^2 + z^2) dm \\ I_{zz} &= \iiint (x^2 + y^2) dm \end{aligned} \quad (2.12)$$

which subsequently represent the moment of inertia with respect to the X, Y and Z axes. The non-diagonal matrix elements, also called products of inertia, are calculated by the following relationship :

$$\begin{aligned} I_{xy} &= \iiint xy dm \\ I_{yz} &= \iiint yz dm \\ I_{zx} &= \iiint zx dm \end{aligned} \quad (2.13)$$

which reflect mutual impacts between the three major rotation axes (X, Y, Z). When the product elements obtain non-zero values, applying torques on a certain rotation axis (e.g. X axis) will cause rotational motions around the other axes (i.e. Y and Z axes).

The inertia matrix varies depending on the chosen rotation axes as well as the reference frame wherein it is calculated. It is shown that in a body-fixed frame (frame rigidly attached to the moving object), the inertia matrix is a constant real symmetric matrix. Thus, there exists an unique eigen decomposition into the product of a rotation matrix E and a diagonal matrix D, given by:

$$I = EDE^T \quad (2.14)$$

where,

$$D = \begin{bmatrix} I_1 & 0 & 0 \\ 0 & I_2 & 0 \\ 0 & 0 & I_3 \end{bmatrix}, \text{ and } E = \{e_1, e_2, e_3\}.$$

The unit eigenvectors e_1, e_2, e_3 define three principal (orthogonal) axes of the object while I_1, I_2, I_3 define the principal moment of inertia of the object around the three axes respectively (there are the eigen values of I). Interestingly, one of the characteristics of principal axes is that torques acting on these axes are independent of each other.

2.7.1.2 Human body segment inertial parameters (BSIP)

Calculating BSIP as mass, center of mass (denoted by CoM) and inertia tensor has been shown to be very important for clinical and biomechanical research (Rao et al., 2006; Pai, 2010). The measure of such parameters are obligedly required whenever researchers analyse the dynamical aspect of human motion. Thus, an efficient method that allows estimating accurately these parameters will considerably improve the accuracy of the dynamical analysis results (e.g. joint forces/ torques) which are often estimated through an inverse dynamic calculation (Pearsall and Costigan, 1999). In the literature, three main BSIP estimation methods exist which are the regression-based, the geometric and the dynamic estimation approach. The first method uses scaling functions based on numerous anthropometric measurements from cadaver studies (Dempster, 1955; Chandler et al., 1975). This method is limited by the measurement techniques and the sample population but quite convenient and timesaving as it allows estimating BSIP through total body mass and segment length (Dumas et al., 2007). The second method is based on either numerous anthropometric measurements Hanavan Jr. (1964) or body scanning methods (e.g. 3D scanner, IRM or Xray absorptionmetry). This method allows estimating personalized 3D BSIP (Cheng et al., 2000; Ganley and Powers, 2004; Mungiole and Martin, 1990) but consumes time and subjects must be exposed to radiation. The third method originates from the robotic field and it is based on human body mechanical models for which parameters are tuned to match kinematic and dynamic recorded data. The BSIP are identified based on the fact that the dynamics of the human system can be written using the Newton-Euler formalism (Venture et al., 2009b,a). This approach however is rather new, and the methods have yet not been validated against other methods.

Chosen BSIP estimation technique The estimation of the BSIP throughout the current work is based on the scaling functions proposed by [Dumas et al. \(2007\)](#). The scaling functions adjust the data of [McConville et al. \(1980\)](#) and of [Young et al. \(1983\)](#) and are expressed directly in the conventional SCS. This method is easy to apply and the subjects are not exposed to radiation kept for a long period time in the laboratory.

2.7.1.3 segment inertial estimation

Following Dumas's suggestion, one can estimate the upper-limb segmental mass of a specific participant, given the total weight of body and the appropriate scaling factors (Table. 2.7)

Segment	Gender	mass (%)
Upper arm	M	2.4
	F	2.2
Forearm	M	1.7
	F	1.3
Hand	M	0.6
	F	0.5

Table 2.7. Scaling factors for the weight of each segment of upper limb ([Dumas et al., 2007](#))

Again, one can estimate the CoM of each limb's segment with respect to its respective SCS (the coordinate is defined compatible with ISB recommendation as mentioned above), given the length of segments and the scaling factors (Table. 2.8)

Segment	Gender	X(%)	Y(%)	Z(%)
Arm	M	1.7	-45.2	-2.6
	F	-7.3	-45.4	-2.8
Forearm	M	1	-41.7	1.4
	F	2.1	-41.1	1.9
Hand	M	3.5	-35.7	3.2
	F	3.3	-32.7	2.1

Table 2.8. Scaling factors for the position of the CoM of each segment in percent of each segment's length, measured experimentally ([Dumas et al., 2007](#))

Thus, the segmental CoM can be defined by using the following equation :

$$CoM_i = L_i [X(\%) \ Y(\%) \ Z(\%)]^T$$

Segment	Gender	r_{xx} (%)	r_{yy} (%)	r_{zz} (%)	r_{xy} (%)	r_{xz} (%)	r_{yz} (%)
Arm	M	31	14	32	6	5	2
	F	33	17	33	3	5(i)	14
Forearm	M	28	11	27	3	2	8(i)
	F	26	14	25	10	4	13(i)
Hand	M	26	16	24	9	7	8(i)
	F	41	45	36	15(i)	0	0

Table 2.9. Scaling factors for the inertia tensor (Dumas et al., 2007) where i denotes negative product of inertia.

where L_i are the length of upper arm, forearm and hand, respectively.

In order to estimate the inertia tensor of each segment with respect to the SCS, the scaling factors (also called radii of gyration) are given in the Table 2.9.

Given these scalings, the inertia tensor of each segment can be estimated by the following equations :

$$I_{jk} = m_i(r_{jk}L_i)^2$$

where m_i is the mass of each segment, L_i is the length of each segment and r_{jk} is the scaling factors given in Table 2.9.

2.7.2 Torque calculations

2.7.2.1 Denavit-Hartenberg convention

Denavit-Hartenberg description In order to describe homogeneous transformations for a mechanical system consisting of serial links and joints, a systematic method is required to define the relative position and orientation of two consecutive links. In general, one can chose an arbitrary frame as long as it is attached to the link that it is referred to. However, it is more convenient to set up some rules (Denavit–Hartenberg convention) for definitions of the link frames. Let consider an example of two links as displayed in Figure 2.9.

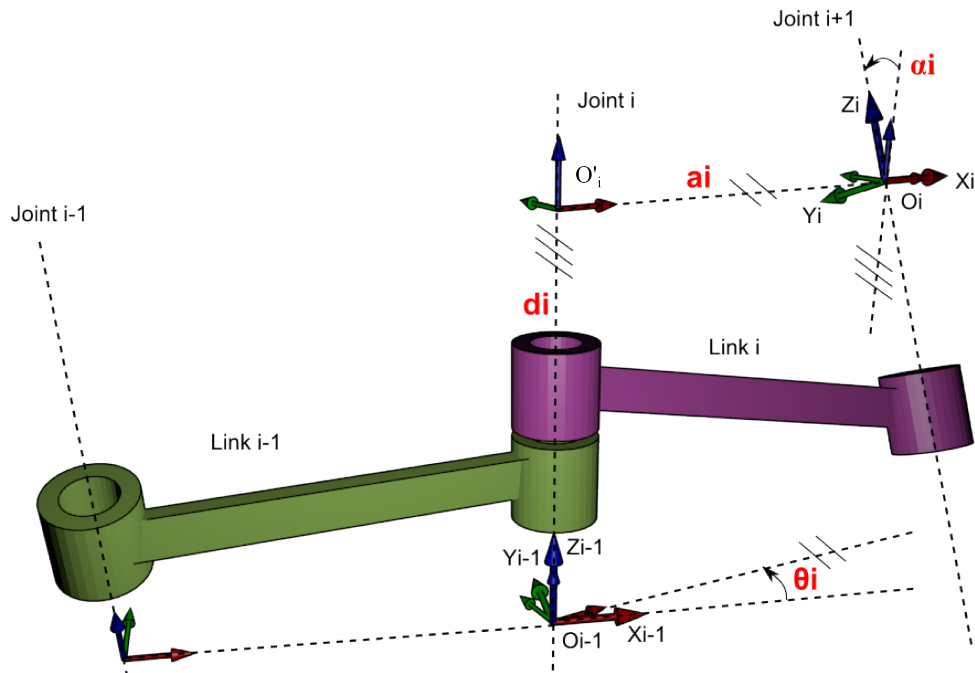


Figure 2.9. Illustration of Denavit-Hartenberg principle

Let axis z_{i-1} denotes the axis of the joint connecting Link $i-1$ to Link i ; the so-called Denavit-Hartenberg convention (DH) is adopted to define link Frame i as follows :

- Choose axis z_i along the axis of Joint $i+1$
- Locate the origin O_i at the intersection of axis z_i with the common normal to axes z_{i-1} and z_i . Also, locate O'_i at the intersection of the common normal with axis z_{i-1}
- Choose axis x_i along the common normal to axes z_{i-1} and z_i with direction from Joint i to Joint $i+1$
- Choose axis y_i so as to complete a right-handed frame.

Once the link frames have been established, the position and orientation of frame i with respect to frame $i-1$ are completely specified by the following parameters:

- a_i distance between O_i and O_{i-1}
- d_i coordinate of O_i along z_{i-1} ,
- α_i angle between axes z_{i-1} and z_i about axis x_i to be taken positive when rotation is made counter-clockwise,
- θ_i angle between axes x_{i-1} and x_i about axis z_{i-1} to be taken positive when rotation is made counter-clockwise.

Two of the four parameters (a_i and α_i) are always constant and depend only on the geometry of connection between consecutive joints established by Link i . At this point, it is possible to express the coordinate transformation between Frame i and Frame $i - 1$ according to the following steps:

- Choose a frame aligned with Frame $i - 1$.
- Rotate it by θ_i about axis z_{i-1} and translate the chosen frame by d_i along axis z_{i-1} ; this sequence aligns the current frame with Frame i and is described by the homogeneous transformation matrix

$$A_i^{i-1} = \begin{bmatrix} c_{\theta_i} & -s_{\theta_i} & 0 & 0 \\ s_{\theta_i} & c_{\theta_i} & 0 & 0 \\ 0 & 0 & 1 & d_i \\ 0 & 0 & 0 & 1 \end{bmatrix}$$

where c_{θ_i} stands for $\cos(\theta_i)$, s_{θ_i} stands for $\sin(\theta_i)$

- Translate the frame aligned with Frame i by a_i along axis x_i and rotate it by α_i about axis x_i ; this sequence aligns the current frame with Frame i and is described by the homogeneous transformation matrix

$$A_i^{i'} = \begin{bmatrix} 1 & 0 & 0 & a_i \\ 0 & c_{\alpha_i} & -s_{\alpha_i} & 0 \\ 0 & s_{\alpha_i} & c_{\alpha_i} & 0 \\ 0 & 0 & 0 & 1 \end{bmatrix}$$

The resulting coordinate transformation is obtained by post multiplication of the single transformations as

$$A_i^{i-1} = A_i^{i-1} A_i^{i'} = \begin{bmatrix} c_{\theta_i} & -s_{\theta_i}c_{\alpha_i} & s_{\theta_i}s_{\alpha_i} & a_i c_{\theta_i} \\ s_{\theta_i} & c_{\theta_i}c_{\alpha_i} & -c_{\theta_i}s_{\alpha_i} & a_i s_{\theta_i} \\ 0 & s_{\alpha_i} & c_{\alpha_i} & d_i \\ 0 & 0 & 0 & 1 \end{bmatrix} \quad (2.15)$$

D-H table of the upper-limb. Following the D-H convention, the CSC of the upper-limb is re-described as a manipulator of 7 DoFs connected to each other by consecutive links. Here, a special consideration is taken regarding the length of these links. Indeed, for two DoFs located at the same joint (e.g. three DoFs coupled at the shoulder), the length

of the link will be set equal to zero. However, when it connects two DoFs located at two different joints (e.g. the link connects the 3rd DoF at shoulder to 1st DoF at elbow), the length of the link is estimated equal to the length of the associated segment.

The order of rotation sequences directly influences the results of the joint angle calculation (Senk and Chèze, 2006). To remain consistent with previous work, we chose to configure the limb model following the recommendations of the ISB (Wu et al., 2005).

As such, the coordinate defined for each DoF with respect to its link and rotation axis is illustrated in Figure 2.10

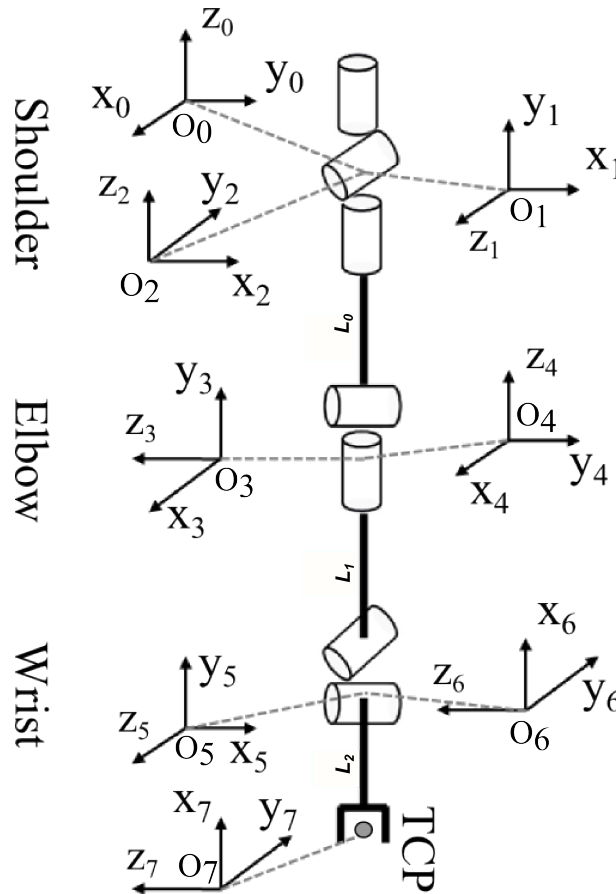


Figure 2.10. Coordinate systems of the upper arm based on D-H description

The respective D-H parameters are then listed in Table 2.10 as follows:

Segment	Rotation sequence	Angles	θ	d	a	α	Offset
Arm	YXY	Internal/External	θ_1	0	0	$\pi/2$	$\pi/2$
		Elevation/Depression	θ_2	0	0	$-\pi/2$	0
		Axial/Rotation	θ_3	$-L_0$	0	$\pi/2$	$-\pi/2$
Forearm	ZXY	Flexion/Extension	θ_4	0	0	$-\pi/2$	0
		Pronation/Supination	θ_5	$-L_1$	0	$\pi/2$	$\pi/2$
Hand	YXZ	Abduction/Adduction	θ_6	0	0	$-\pi/2$	$\pi/2$
		Flexion/Extension	θ_7	0	$-L_2$	0	0

Table 2.10. Denavit-Hartenberg parameters associated with each DOF of the model

The column parameters θ values correspond to each of the joint angles expressed in radians. L_0 , L_1 , L_2 are the length of upper arm, forearm and hand, respectively. The column “Offsets” has been added in the biomechanical model to indicate what is the arm posture when all angles are equal to zero and are corresponding to the anatomical reference position for which the ISB coordinates are also defined. Thus it is noteworthy that it is always possible to convert the angles expressed in the D-H to the ISB (or vice versa) by simply adding (or subtracting) the Offset to the angles.

2.7.2.2 Euler-Lagrange formulation

Euler-Lagrange formulation allows deriving the dynamic model of a manipulator based on determining its kinetic energy and potential energy (Bruno Siciliano, 2009). With Euler-Lagrange formulation, the dynamical equation of motion can be derived in a systematic way independently of the reference coordinate frame. Once a set of variables (in the case of human upper-limb are θ_i , $i=1,\dots,7$), also termed generalized coordinates, are chosen, which effectively describe the configuration of a 7-DoF manipulator, the Lagrangian of the mechanical system can be defined as a function of the generalized coordinates:

$$\mathcal{L} = \mathcal{T} - \mathcal{U}$$

where \mathcal{T} and \mathcal{U} denote the total kinetic energy and potential energy of the system, respectively.

The Euler-Lagrange equation is then expressed by:

$$\frac{d}{dt} \left(\frac{\delta \mathcal{L}}{\delta \dot{\theta}} \right)^T - \left(\frac{\delta \mathcal{L}}{\delta \theta} \right)^T = \xi \quad (2.16)$$

where $\theta = [\theta_1, \dots, \theta_7]$, ξ is a vector of the generalized forces associated with the vector of the generalized coordinates θ .

it is relatively easy to determine the total kinetic and potential energy of the system. We can thus solve the Euler-Lagrange equation (Eq. 2.16) and it is well-known that the solution is of the following form:

$$\tau = M(\theta)\ddot{\theta} + C(\theta, \dot{\theta})\dot{\theta} + g(\theta) + R(\theta, \dot{\theta}) \quad (2.17)$$

where τ is the actuation torques; $M(\theta)$ is the mass matrix; $C(\theta, \dot{\theta})\dot{\theta}$ stands for the Coriolis torque elements; $g(\theta)$ denotes the gravity torque; R reflects frictional and viscous or elastic torques created by all soft tissues. For most of studies, the term R is neglected and assumed to be negligible compared to the other torques. A dot above a variable stands for its time derivative.

2.7.2.3 Newton-Euler formulation

Unlike Lagrange formulation, Newton-Euler formulation is based on a balance of all the forces acting on the link of the manipulator. This leads to a set of equations whose structure allows a recursive type of solution, a forward recursion relative to the propagation of velocities and accelerations and a backward recursion for the propagation of forces and moments along the structure. The Newton-Euler formulation can be briefly described as follows (its details could be found in (Bruno Siciliano, 2009)).

Let consider the link i of a n -DoFs manipulator connected to its adjacent link by joint i and joint $i+1$ as displayed in Figure 2.11. We define the following parameters :

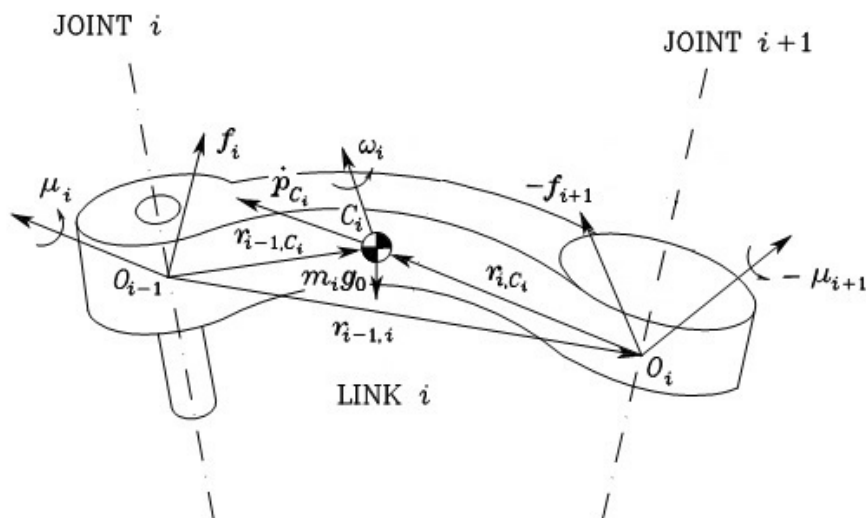


Figure 2.11. Characterization of Link i for Newton-Euler formulation (Bruno Siciliano, 2009)

- m_i : mass of augmented link,
- I_i : inertia tensor of augmented link with respect to center of mass,
- r_{i-1,C_i} : vector from origin O_{i-1} of Frame $i^{th} - 1$ to centre of mass C_i ,
- r_{i,C_i} : vector from origin O_i of Frame i^{th} to centre of mass C_i ,
- $r_{i-1,i}$: vector from origin O_{i-1} of Frame $i^{th} - 1$ to origin O_i of Frame i^{th} ,
- \dot{p}_{C_i} : linear velocity of center of mass C_i ,
- \dot{p}_i : linear velocity of origin of Frame i^{th} ,
- ω_i : angular velocity of link,
- \ddot{p}_{C_i} : linear acceleration of center of mass C_i ,
- \ddot{p}_i : linear acceleration of origin O_i of Frame i^{th} ,
- $\dot{\omega}_i$: angular acceleration of link,
- g_0 : gravity acceleration.

For forces and torques:

- f_i : force exerted by Link $i^{th} - 1$ on Link i^{th} ,
- $-f_{i+1}$: force exerted by Link $i^{th} + 1$ on Link i^{th} ,
- μ_i : moment exerted by Link $i^{th} - 1$ on Link i^{th} with respect to origin of Frame $i^{th} - 1$,
- $-\mu_{i+1}$: moment exerted by Link $i^{th} + 1$ on Link i^{th} with respect to origin of Frame i^{th} .

Then, the Newton equation for the translational motion of the center of mass can be written as :

$$f_i - f_{i+1} + m_i g_0 = m_i \ddot{p}_{C_i}$$

The Euler equation for the rotational motion of the link (referring moments to the center of mass) can be written as :

$$\mu_i + f_i \times r_{i-1, C_i} - \mu_{i+1} - f_{i+1} \times r_{i, C_i} = \frac{d}{dt} (I_i \omega_i)$$

Solving the two equations gives us the two recursive solutions, one is for link acceleration calculation and another is for torque/force calculation. Their concrete equations are of the following form :

- For forward recursion calculation

$$\omega_i^i = R_i^{i-1T} (\omega_{i-1}^{i-1} + \dot{\theta}_i z_0)$$

where $z_0 = \begin{bmatrix} 0 & 0 & 1 \end{bmatrix}^T$ and R_i^{i-1} is the rotation matrix from frame i-1 to frame i, ω_i^i is the angular velocity of link i (the lower subscript) expressed in frame i (the upper subscript). The meaning of lower and upper subscripts are similar for the following equations.

$$\dot{\omega}_i^i = R_i^{i-1T} (\dot{\omega}_{i-1}^{i-1} + \ddot{\theta}_i z_0 + \dot{\theta}_i \omega_{i-1}^{i-1} \times z_0)$$

$$\ddot{p}_{C_i}^i = R_i^{i-1T} \ddot{p}_{i-1}^{i-1} + \dot{\omega}_i^i \times r_{i-1, i}^i + \omega_i^i \times (\omega_i^i \times r_{i-1, i}^i)$$

$$\ddot{p}_{C_i}^i = \ddot{p}_i^i + \dot{\omega}_i^i \times r_{i, C_i}^i + \omega_i^i \times (\omega_i^i \times r_{i, C_i}^i)$$

- For inverse recursion calculation

$$f_i^i = R_{i+1}^i f_{i+1}^{i+1}$$

$$\mu_i^i = -f_i^i \times (r_{i-1, i}^i + r_{i, C_i}^i) + R_{i+1}^i \mu_{i+1}^{i+1} + R_{i+1}^i f_{i+1}^{i+1} \times r_{i, C_i}^i + I_i \dot{\omega}_i^i + \omega_i^i \times (I_i \omega_i^i) + \omega_i^i \times (I_i \dot{\omega}_i^i)$$

$$\tau_i = \mu_i^{iT} R_i^{i-1T} z_0 + F_{vi} \dot{\theta}_i + F_{si} \text{sgn}(\dot{\theta}_i)$$

where τ_i denotes the generalized forces/torques resulting at the joint i^{th} referred to the current Frame i^{th} on Link i^{th}

The calculation process of Newton-Euler formulation can be illustrated in Figure 2.12

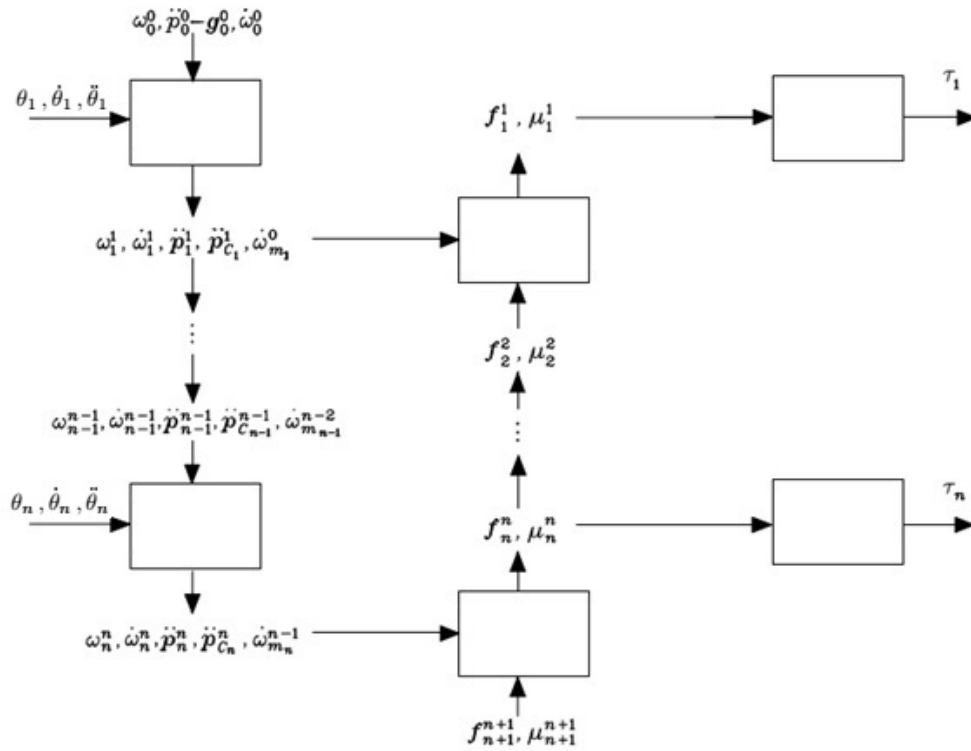


Figure 2.12. Algorithm of Newton-Euler method(Bruno Siciliano, 2009)

for which there exist two different phases:

- Phase 1 : The angle velocity, angle acceleration of a certain link are calculated based on the values of angle velocity, angle acceleration of the previous link. This calculation process begins at the link zeros (usually referred as a base) and go on up to link n (in the case of present human upper-limb model, n=7)

- Phase 2 : Based on the angle velocity, angle acceleration calculated in Phase 1, the torques/forces are calculated inversely from the end-effector to the link 1. In the graph, the f_{n+1}/ u_{n+1} represents the interaction force/torque between the end-effector and the environment. For the free movement of end-effector, this force/torque is equal to zero

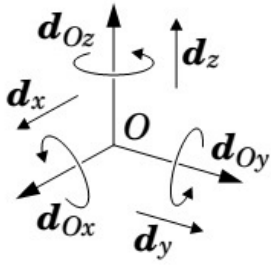
2.7.2.4 Roy Featherstone's formulation

In the Newton-Euler formulation mentioned above, the dynamics of a rigid body is calculated based on 3D vectors. Consequently, two separate processes (namely equations) are demanded to formulate its dynamics (Eq. 2.18)

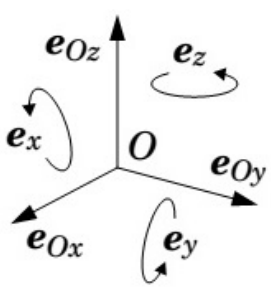
$$f = ma_c \text{ and } \tau_C = I\dot{\omega} + \omega \times I\omega \quad (2.18)$$

The first expresses the relationship between the force applied to the body and the linear acceleration of its center of mass. The second expresses the relationship between the torque applied to the body, referred to its center of mass, and the rate of change of angular momentum.

In order to improve the performance of this conventional formulation, Roy Featherstone (Featherstone and Orin, 2000) has proposed the ideas of using 6D vector instead of two separate 3D vectors. As such, the three DoFs of linear sliding motion with the three DoFs of rotational motion are combined to form a spatial velocity vector of six dimensions

	$\mathcal{D}_O = \{d_{Ox}, d_{Oy}, d_{Oz}, d_x, d_y, d_z\} \subset M^6$ $\hat{\underline{v}}_O = \begin{bmatrix} \omega_x \\ \omega_y \\ \omega_z \\ \vartheta_{Ox} \\ \vartheta_{Oy} \\ \vartheta_{Oz} \end{bmatrix} = \begin{bmatrix} \underline{\omega} \\ \underline{\vartheta}_O \end{bmatrix}$ $\hat{\underline{v}}_O = \omega_x d_{Ox} + \omega_y d_{Oy} + \omega_z d_{Oz} + \vartheta_{Ox} d_x + \vartheta_{Oy} d_y + \vartheta_{Oz} d_z$
---	---

and force and torque are combined to form a spatial force vector.

	$\xi_O = \{e_x, e_y, e_z, e_{Ox}, e_{Oy}, e_{Oz}\} \subset F^6$ $\hat{\underline{f}}_O = \begin{bmatrix} \tau_{Ox} \\ \tau_{Oy} \\ \tau_{Oz} \\ f_x \\ f_y \\ f_z \end{bmatrix} = \begin{bmatrix} \underline{\tau}_O \\ \underline{f} \end{bmatrix}$ $\hat{\underline{f}}_O = \tau_{Ox}e_x + \tau_{Oy}e_y + \tau_{Oz}e_z + f_xe_x + f_ye_y + f_ze_z$
---	--

Consequently, at the same time, we can simultaneously compute the linear and rotational acceleration during the kinematics process or simultaneously compute the force and torque during the dynamics process. Indeed, the performance of Roy Featherstone formulation is actually compared with that of conventional Newton-Euler formulation when calculating the necessary forces/torques given the linear/rotational acceleration. The result showed that both methods give the same result but the former is nearly 10 times faster than the latter in our case.

2.8 Parameters of interest: rotation axis calculations

2.8.1 Shoulder-Elbow rotation axis (SE)

The shoulder-elbow axis is geometrically defined as a vector connecting the shoulder joint to the elbow joint. This vector varies with the movement and can be calculated based on the homogeneous transformation. The rationale is that: because the base (namely, global) coordinate (i.e. O_0xyz) is rigidly attached to the center of the shoulder joint position while the coordinate O_3xyz is rigidly attached to the center of the elbow joint (Fig 2.10), the shoulder-elbow axis could be determined by Cartesian position of the origin O_3 in the O_0xyz coordinate. In addition, to be compatible with the subsequent analyses when being compared with other rotation axes, the O_3 's coordinates are eventually normalized by the length of Euclidean line O_0O_3 . As such the shoulder-elbow rotation axis is quantified as an unit vector (bi-point) whose origin locates at O_0 (i.e. shoulder joint) and direction passes through the origin point O_3 (i.e. elbow joint). Supposed that the homogeneous transformation from O_0xyz to O_3xyz is of the following form:

$$H_{O_0O_3} = H_{O_0O_1}H_{O_1O_2}H_{O_2O_3} = \begin{bmatrix} R_{O_0O_3} & P_{O_0O_3} \\ 0 & 1 \end{bmatrix}$$

Then SE axis corresponds to $\frac{P_{O_0O_3}}{|P_{O_0O_3}|}$

2.8.2 Minimum principal rotation axis (e3)

It is noteworthy that at every time step of the movement, the limb (composing of three elements: upper arm, forearm and hand) can be treated as a rigid body. Consequently, there always exists three perpendicular axes, so-called principal rotation axes, around which the inertia tensor is a constant real diagonal matrix. Among these three axes, the minimal principal axis (e3) is defined as the one for which the moment of inertia obtains the smallest value. Practically, to determine this axis, several steps involving the limb inertia computation need to be implemented.

Based on Dumas's proposal, one could estimate the inertia tensor of each segment (i.e. upper arm, forearm, hand) with respect to *CoM* in the relative SCS (ISB-based coordinate) (Fig 2.6), given the segment length and the total weight of subjects. However, in order to sum up them as the inertia tensor of the whole upper-limb, these segment inertia matrices all need to be evaluated into the same frame, namely reference frame. To this goal, there are two different approaches that could be employed. First, one could continue relying on the ISB frames and use the respective Euler rotation matrixes to compute all necessary transformation with respect to the reference frame as being described in [Isableu et al. \(2009\)](#). However, in order to be consistent with our simulation work wherein the kinematics and the dynamics of upper limb both are calculated through the D-H convention, we prefer another approach that will initially convert the segment inertia tensors in ISB frames to D-H ones and then use the homogeneous transformations to convert the inertia matrix between frames. In this method, the base frame O_0xyz of the DH-based coordinate system (Fig. 2.10) is chosen as the reference frame. The detail of this process is described in what follows.

2.8.2.1 Inertia tensors and CoMs: From ISB- to DH-based frames

Inertia tensors in DH-based frames. We first convert the segment inertia tensors of upper arm, forearm and hand in the ISB-based frames to the DH-based frames. To this

aim, we suppose that the inertia tensors of upper arm, forearm and hand estimated in the ISB-based frames referred to the CoM would be ${}^{CoM}I_a^{ISB}$, ${}^{CoM}I_f^{ISB}$ and ${}^{CoM}I_h^{ISB}$ and that the rotation matrices transforming the ISB-based frames to the DH-based frames (O_3xyz , O_5xyz and O_7xyz) are R_{aO_3} , R_{fO_5} and R_{hO_7} , respectively. Then the inertia tensors referred to the CoM expressed in the O_3xyz , O_5xyz and O_7xyz will be of the following forms:

$${}^{CoM}I_a^{O_3} = R_{aO_3}^T {}^{CoM}I_a^{ISB} R_{aO_3}$$

$${}^{CoM}I_f^{O_5} = R_{fO_5}^T {}^{CoM}I_f^{ISB} R_{fO_5}$$

$${}^{CoM}I_h^{O_7} = R_{hO_7}^T {}^{CoM}I_h^{ISB} R_{hO_7}$$

where the rotational matrices are determined as below:

$$R_{aO_3} = \begin{bmatrix} 1 & 0 & 0 \\ 0 & 1 & 0 \\ 0 & 0 & 1 \end{bmatrix}$$

$$R_{fO_5} = \begin{bmatrix} 0 & 0 & 1 \\ 0 & 1 & 0 \\ -1 & 0 & 0 \end{bmatrix}$$

$$R_{hO_7} = \begin{bmatrix} 0 & -1 & 0 \\ 1 & 0 & 0 \\ 0 & 0 & 1 \end{bmatrix}$$

CoMs in DH-based frames. Similarly to inertia tensor conversion, the $CoMs$ of limb segments defined in the ISB-based frames need to be converted to the DH-based frames. We suppose that the $CoMs$ of upper arm, forearm and hand in the ISB-based frames would be ${}^{CoM}M_a^{ISB}$, ${}^{CoM}M_f^{ISB}$, ${}^{CoM}M_h^{ISB}$, respectively. Then the $CoMs$ expressed in the O_3xyz , O_5xyz and O_7xyz will be of the following forms:

$$\begin{bmatrix} {}^{CoM}M_a^{O_3} \\ 1 \end{bmatrix} = H_{aO_3} \begin{bmatrix} {}^{CoM}M_a^{ISB} \\ 1 \end{bmatrix}$$

$$\begin{bmatrix} CoM_f^{O_5} \\ 1 \end{bmatrix} = H_{fO_5} \begin{bmatrix} CoM_f^{ISB} \\ 1 \end{bmatrix}$$

$$\begin{bmatrix} CoM_h^{O_7} \\ 1 \end{bmatrix} = H_{hO_7} \begin{bmatrix} CoM_h^{ISB} \\ 1 \end{bmatrix}$$

where,

$$H_{aO_3} = \begin{bmatrix} R_{aO_3} & 0 \\ 0 & 1 \end{bmatrix} T_{aO_3} \text{ and } T_{aO_3} = \begin{bmatrix} 1 & 0 & 0 & 0 \\ 0 & 1 & 0 & L_0 \\ 0 & 0 & 1 & 0 \\ 0 & 0 & 0 & 1 \end{bmatrix}$$

$$H_{fO_5} = \begin{bmatrix} R_{fO_5} & 0 \\ 0 & 1 \end{bmatrix} T_{fO_5} \text{ and } T_{fO_5} = \begin{bmatrix} 1 & 0 & 0 & 0 \\ 0 & 1 & 0 & L_1 \\ 0 & 0 & 1 & 0 \\ 0 & 0 & 0 & 1 \end{bmatrix}$$

$$H_{hO_7} = \begin{bmatrix} R_{fO_7} & 0 \\ 0 & 1 \end{bmatrix} T_{fO_7} \text{ and } T_{fO_7} = \begin{bmatrix} 1 & 0 & 0 & L_2 \\ 0 & 1 & 0 & 0 \\ 0 & 0 & 1 & 0 \\ 0 & 0 & 0 & 1 \end{bmatrix}$$

2.8.2.2 Inertia tensors and CoMs in the base frame

Based on the previous calculation, we obtain the *CoMs* and inertia tensors of limb segments expressed in their respective DH-based local frames (i.e. O_3xyz , O_5xyz , O_7xyz). These local *CoMs* and inertia tensors all still need to be converted to the base frame (i.e. O_0xyz), and then using the Huygens-Steiner theorem to evaluate the resulting tensors with respect to the shoulder joint center (i.e. O_0).

CoMs in the base frame. We suppose that the homogeneous transformation between O_0 to O_i ($i = 1..7$) will be of the form :

$$H_{O_0O_i} = \begin{bmatrix} R_{O_0O_i} & P_{O_0O_i} \\ 0 & 1 \end{bmatrix}$$

Then, the *CoMs* of limb segments (i.e. upper arm, forearm, hand) can be expressed in the base frame by the following equations (the superscript G on the right side of a vector denotes the fact that the vector is expressed in the base frame):

$$\begin{bmatrix} CoM_a^G \\ 1 \end{bmatrix} = H_{O_0O_3} \begin{bmatrix} CoM_a^{O_3} \\ 1 \end{bmatrix}$$

$$\begin{bmatrix} CoM_f^G \\ 1 \end{bmatrix} = H_{O_0O_5} \begin{bmatrix} CoM_f^{O_5} \\ 1 \end{bmatrix}$$

$$\begin{bmatrix} CoM_h^G \\ 1 \end{bmatrix} = H_{O_0O_7} \begin{bmatrix} CoM_h^{O_7} \\ 1 \end{bmatrix}$$

Inertia tensors expressed in the base frame with respect to CoM. Again, the local inertia tensors of upper arm, forearm and hand with respect to *CoM* could be expressed in the base frame by multiplying them with the respective rotational matrix as follows:

$${}^{CoM}I_a^G = R_{O_0O_3} {}^{CoM}I_a^{O_3} R_{O_0O_3}^T$$

$${}^{CoM}I_f^G = R_{O_0O_5} {}^{CoM}I_f^{O_5} R_{O_0O_5}^T$$

$${}^{CoM}I_h^G = R_{O_0O_7} {}^{CoM}I_h^{O_7} R_{O_0O_7}^T$$

The resulting matrices represent the inertia tensors of upper arm, forearm and hand with respect to their CoM expressed in the base frame.

Inertia tensors with respect to the shoulder joint center expressed in the base frame. Using the generalized Huygens theorem, the segment inertia matrices are evaluated at the shoulder joint center. To do this, the following equation is used for each segment:

$${}^{SH}I_i^G = {}^{CoM}I_i^G + \begin{bmatrix} m_i({}^GCoM_{i_y}^2 + {}^GCoM_{i_z}^2) & -m_i {}^GCoM_{i_x} {}^GCoM_{i_y} & -m_i {}^GCoM_{i_z} {}^GCoM_{i_x} \\ -m_i {}^GCoM_{i_x} {}^GCoM_{i_y} & m_i({}^GCoM_{i_x}^2 + {}^GCoM_{i_z}^2) & -m_i {}^GCoM_{i_y} {}^GCoM_{i_z} \\ -m_i {}^GCoM_{i_z} {}^GCoM_{i_x} & -m_i {}^GCoM_{i_y} {}^GCoM_{i_z} & m_i({}^GCoM_{i_x}^2 + {}^GCoM_{i_y}^2) \end{bmatrix}$$

where,

${}^{SH}I_i^G$ is the inertia tensor of segment i with respect to the shoulder expressed in the base frame.

${}^{CoM}I_i^G$ is the inertia tensor of segment i with respect to CoM expressed in the base frame.

m_i is mass of segment i

$[{}^GCoM_{i_x} \ {}^GCoM_{i_y} \ {}^GCoM_{i_z}]^T$ are the coordinates of CoM_i^G expressed in the base frame
 i stands for a, f, h corresponding to upper arm, forearm and hand.

Then, the inertia tensor of whole limb expressed in the base frame with respect the shoulder joint center is of the following form:

$${}^{SH}I_{limb}^G = {}^{SH}I_a^G + {}^{SH}I_f^G + {}^{SH}I_h^G$$

Here, we carry out the eigen decomposition of ${}^{SH}I_{Limb}^G$ into the product of a rotation matrix R and a diagonal matrix D such that:

$${}^{SH}I_{Limb}^G = RDR^T$$

where,

$D = \begin{bmatrix} I_1 & 0 & 0 \\ 0 & I_2 & 0 \\ 0 & 0 & I_3 \end{bmatrix}$, and $R = \{e_1, e_2, e_3\}$. Supposed that $I_1 > I_2 > I_3$, then the eigenvector e_3 is the minimum principal rotation axis that we are interested in.

THESIS CONTRIBUTION

3.1 Introduction

This chapter will present the original contribution of the thesis. The results are divided into two sections, each of which aims at solving a specific goal of thesis as follows:

- We first examine the nature of variables underlying the planning of unrestrained 3D arm reaching. To this aim, we consider a discrete arm reaching task performed at three different speeds starting from an “L-shaped” initial arm posture. Within the optimal control framework, we uncover which optimality criterion explains at best the empirical data. We test whether a weighted combination of kinematic, energetic and dynamic cost functions is necessary to account for all the critical features of experimental results.
- The second section aims at investigating the mechanisms that the brain might use to control the dynamical interaction generated during the limb’s motion. More specifically, we question whether the brain exploits or compensates interaction torque to assist/resist the movement. To this aim, we examine the effects of speed/load variations upon the chosen arm trajectories during free arm movements. The findings are then examined in the framework of optimal control. We test whether the compensation versus exploitation controversy might be tightly linked with the optimization of a trade-off between kinematic and dynamic cost functions.

3.2 On the nature of motor planning during arm pointing task

On the nature of motor planning variables during arm pointing movement: compositeness and speed dependence

Van Hoan Vu, Brice Isableu, Bastien Berret

This article is published in Neuroscience 328, April 2016

Abstract

The purpose of this study was to investigate the nature of the variables and rules underlying the planning of unrestrained 3D arm reaching. To identify whether the brain uses kinematic, dynamic and energetic values in an isolated manner or combines them in a flexible way, we examined the effects of speed variations upon the chosen arm trajectories during free arm movements. Within the optimal control framework, we uncovered which (possibly composite) optimality criterion underlay at best the empirical data. Fifteen participants were asked to perform free-endpoint reaching movements from a specific arm configuration at slow, normal and fast speeds. Experimental results revealed that prominent features of observed motor behaviors were significantly speed-dependent, such as the chosen reach endpoint and the final arm posture. Nevertheless, participants exhibited different arm trajectories and various degrees of speed dependence of their reaching behavior. These inter-individual differences were addressed using a numerical inverse optimal control methodology. Simulation results revealed that a weighted combination of kinematic, energetic and dynamic cost functions was required to account for all the critical features of the participants' behavior. Furthermore, no evidence for the existence of a speed-dependent tuning of these weights was found, thereby suggesting subject-specific but speed-invariant

weightings of kinematic, energetic and dynamic variables during the motor planning process of free arm movements. This suggested that the inter-individual difference of arm trajectories and speed dependence was not only due to anthropometric singularities but also to critical differences in the composition of the subjective cost function.

Introduction

Understanding how the brain controls 3D arm movement is a long standing issue in motor neuroscience. The complexity of the musculoskeletal system is such that the accurate achievement of athletic tasks but also of the most basic daily life activity constitutes a challenging problem. In particular, the anisotropic distribution of mass, gravity, and interaction torques acting on all degrees of freedom make the upper-limb dynamics highly nonlinear but the brain seemingly overcomes those difficulties effortlessly. Coping with such a complexity requires efficient control strategies and, therefore, the central nervous system (CNS) might internally represent or monitor some critical variables to implicitly value skilled movements such as baseball pitching, overarm throwing or just placing a cup of coffee on a table. What is the exact nature of these variables and computational rules underlying the selection of one trajectory among the infinity of possible trajectories, and whether cells in the motor cortex encode dynamic, kinematic separately or a combination rule of such variables during movement planning remain questionable even though the issue was extensively investigated in neurophysiological studies ([Georgopoulos et al., 1982](#); [Kalaska et al., 1989](#); [Mussa-Ivaldi, 1988](#)). In general, tackling this problem is tricky because kinematic and kinetic quantities are tightly linked by the equations of motion and many sensorimotor transformations, through internal models ([Wolpert et al., 1995b](#); [Kawato et al., 1987](#)), may occur within the CNS before a goal-directed movement is eventually triggered. This question was nonetheless addressed in many behavioral and computational studies, but whether the control of upper-limb motion relies more upon geometrical properties pertaining to the position of body segments and joint angles (i.e. kinematic variables) or upon mechanical properties pertaining to the mass distribution and torques (i.e. dynamic variables) is still a matter of debate ([Darling and Hondzinski, 1999](#); [Pagano and Turvey, 1995](#); [Wolpert et al., 1995a](#); [Soechting and Flanders, 1998](#)). [Isableu et al. \(2009\)](#) showed that, during a cyclical upper-limb rotation task with a flexed arm

(“L-shaped”), subjects exhibited spontaneous changes of rotation axis, switching from a geometrical one (Shoulder-Elbow axis, SE, a kinematic-related parameter) to an inertial one (minimum principal inertia axis, e3, a dynamic-related parameter) when executing the task at a larger speed. Hence, this suggested that the variables represented by the brain to control unrestrained 3D arm movement might combine both kinematic and dynamic parameters and that, importantly, their interplay may depend on speed.

Interestingly, the optimal control framework precisely makes hypotheses about the variables potentially represented by the brain during motor control (Todorov, 2004). Therefore, the question of which variables are the subject of motor planning can be rephrased in a normative way as follows: what is the nature of the optimality criterion underlying trajectory formation? (see Soechting and Flanders, 1998). In this context, some researchers have argued for kinematic-oriented motor planning (in either extrinsic or intrinsic space) where the nonlinearities of the motion dynamics are just compensated for or suppressed by the brain to preserve limb’s stability (Hollerbach and Flash, 1982; Atkeson and Hollerbach, 1985; Bastian et al., 1996; Sainburg et al., 1995, 1999; Gribble and Ostry, 1999). The main advantage of using a kinematic-based motor control would be to simplify control and allow the brain (re)using a common motor pattern to perform movements at various speeds (i.e. “scaling law”). This approach found some experimental support in the literature (Gribble et al., 1998; Atkeson and Hollerbach, 1985). According to this view, speed-independent arm trajectories should be observed (and were actually observed to some extent in several arm reaching studies, e.g. Atkeson and Hollerbach, 1985; Gribble et al., 1998). Other authors have instead argued for dynamic-oriented motor planning where the mechanical limb properties are taken into account and exploited to the greatest extent possible (Dounskaia et al., 2002; Debicki et al., 2010, 2011; Hore et al., 2005, 2011). The advantage would be to utilize all the non-muscular torques originating from the nonlinearities of the limb’s dynamics for producing least effort movements and somehow reducing the overall amount of muscle torque (or its mechanical work) to a minimum (Sainburg and Kalakanis, 2000; Galloway and Koshland, 2002; Dounskaia et al., 2002; Berret et al., 2008; Hirashima et al., 2007; Gaveau et al., 2011b, 2014). In Wolpert et al. (1995a), the authors directly addressed the issue about whether the brain controls movement in kinematic or dynamic coordinates for visually-guided movements. They showed that the planning of constrained planar arm reaches was associated with the optimization of a kinematic cost function (i.e. Cartesian jerk) in order to perceive straight endpoint displacements on a screen. However it is known

that unrestrained or 3D movements may have very different characteristics (Desmurget et al., 1997; Gielen, 2009) and whether the control of free arm movements also relies more upon kinematic rather than upon dynamic variables remained unclear. For 3D arm movements, evidence was found for a dynamic level of planning as the final arm posture was shown to depend on the initial arm posture in a way that could not be accounted for by any kinematic optimality criterion (Soechting et al., 1995). However, the effect of speed onto the final posture selection, which is a crucial assessment to distinguish between kinematic and dynamic strategies, has not been addressed in that study but experimental studies later revealed an invariance of the final whole-arm configuration with respect to motion velocity (Nishikawa et al., 1999) despite the fact that dynamic motor planning may potentially involve trajectory modifications with respect to speed because of the complex velocity and acceleration dependent musculoskeletal dynamics.

To reconcile all these findings, the idea of composite cost functions relying upon kinematic, energetic and dynamic variables emerged as a possible avenue. Using inverse optimal control techniques for unveiling optimality criteria and/or rule from experimental trajectories (Mombaur et al., 2009; Berret et al., 2011a) and the free reach-endpoint paradigm for better discriminating between candidate cost functions (Berret et al., 2011b,a, 2014), it was shown that vertical movements starting from different initial positions and executed at a relatively fast pace could be accounted for by a composite cost mixing the angle jerk (i.e. a kinematic variable) and the absolute work (i.e. an energetic variable). However, it remained unclear whether these results would extend to 3D motion and whether a single composite cost could explain movements executed at different speeds. This question is also critical in regards to the understanding of self-paced movements where a cost of time may also combine with trajectory costs and the extent to which the latter varies according to speed instructions is a related open question (see Shadmehr et al., 2010; Shadmehr, 2010; Berret and Jean, 2016).

Here we combined a specific motor task with an inverse optimal control methodology to address the above questions. First, we considered free 3D arm movements without a prescribed reach endpoint (the hand could freely move in 3D), which differs from classical point-to-point reaching paradigms; namely we considered a planar target. Thus, participants were free to choose any final finger position on the target plane while only caring about the vertical error (i.e. the task goal). Considering a 4-dof arm, the subjects were thus left with three angles to choose at the movement end. A real life example of this

laboratory experiment would be that of placing a cup on an empty table or pushing a door for opening it. Furthermore, we varied the instructed speed to emphasize differences between kinematic versus dynamic control strategies or combination of them and used inverse optimal control techniques to identify the elementary components of the cost function among kinematic, energetic and dynamic quantities as well as their relative weights and speed dependence.

Experimental Procedures

Experimental task

Participants

Fifteen healthy subjects (7 women and 8 men) voluntarily agreed to participate in the experiment. Written informed consent was obtained from each participant in the study as required by the Helsinki declaration and the EA 4042 local Ethics Committee. All of them were right-handed, free of sensory, perceptual and motor disorder, aged 27 ± 4 years, weighted 66 ± 8 kg and 167 ± 6 cm tall. All the participants were naive to the purpose of the experiment.

Free endpoint motor task

The motor task is illustrated in Figure 3.9. A small solid stick serving as a reference position for the initial fingertip position was attached to a vertical slider bar, allowing the experimenter to adjust appropriately the height of this reference point relative to the arm's length of each participant. A uniform horizontal surface, made of a thin and soft block of foam, served as a target throughout this experiment. It was positioned on a table just below the participant's chest. On the wall in front of the participants, a yellow marker was positioned to fix gaze in a predefined direction (looking straight ahead). Gaze was constrained in order to reduce the influence of visuomotor processing during arm movement control and to limit possible inter-trial and inter-individual fluctuations due to eye motion and eye-head-hand coordination. Participants sat comfortably on a chair with their back tighten upright against the chair's splash to freeze motion of other body parts during the execution of arm movement. The initial arm configuration was setup such that the shoulder-elbow axis was approximately abducted to the horizontal while the flexion-extension elbow angle was actively held at 90 degrees and the fingertip was kept strictly to the reference position. Participants were free to rotate their shoulder and elbow in 3D space during the motion, but their wrist rotation was constrained by two lightweight bars attached to the distal part of the forearm and the proximal part of hand. One of the two bars also froze the movement of the index finger. Such constraints allowed to approximate the forearm and the hand as a single rigid body and to simplify the whole-arm model by reducing the actual arm's degrees-of-freedom (DoF) from seven to five (three at shoulder and two at elbow). In practice, only the first four DoFs were relevant

because the elbow pronation/supination rotation showed negligible displacements in this study and was irrelevant to the pointing task under consideration (fingertip end-effector). We therefore considered a 4-DoF arm model in this study. Note that with a 4-DoF arm and a planar target, the task is redundant: for a given admissible fingertip position of the target plane (which is chosen by the subject himself), three joint angles can be freely adjusted. If we had use a dot as a target, only one angle could have been selected for the prescribed reach endpoint. Hence the main originality of the present protocol is to let subjects solve the “where to go” problem as well as the “how to go there” problem at once, which is a common situation (e.g. putting a cup of coffee on an empty table is an analog of such a laboratory experiment).

During the experiment, participants were instructed to move their fingertip from the initial configuration to the destination (i.e. a uniform planar target, with no prescribed reach endpoint) by performing a smooth, one-shot movement while looking at the eyes reference marker. They were required to point to the planar surface with their fingertip and stop their motion right onto the surface but without hitting it. No instruction was given to the participants regarding the final position of the fingertip on the planar surface. As such, all reach endpoints were equi-efficient regarding task achievement but conceivably not equi-efficient regarding the subjective values associated with the actual arm trajectory leading to the chosen reach endpoint (see also [Berret et al., 2011b,a, 2014](#) for related studies). Here and throughout the paper, subjective costs (i.e. costs not imposed by the task but related to the subject or body) will be contrasted with objective costs that are imposed by the task itself (e.g. pointing error) ([Knill et al., 2011](#); [Berret et al., 2011b](#)).

For the purpose of this study, three different speeds were examined: slow (S), comfortable/natural (N) and fast (F). Before each trial, participants were verbally instructed to move at one specific speed. Speed instruction was randomized across trials in order to prevent habituation and memorization effects (especially regarding the endpoint reached in the previous trial). Velocity constraints were hypothesized to reveal the nature of the planning variables used in such 3D movements, and the free reach-endpoint paradigm was used to emphasize the possible differences of arm trajectories as a function of the instructed speed.

Prior to the experiment, participants were trained to become familiar with the task. They were told to move their arm toward the target while the experimenter verified that all the task instructions had been well understood. The training process consisted of 20

trials on average and at the end all the participants had the capability of executing their movement while satisfying the experimental instructions, which were as follows: (i) place consistently the fingertip at the initial reference position while keeping the same initial “L-shaped” arm posture, (ii) try to stop the movement right onto the horizontal target surface, by minimizing errors along the vertical axis, (iii) look at the reference marker during the whole movement execution and (iv) mark a clear difference of motion speed based upon the verbal instruction given by the experimenter at the beginning of trial.

For each participant, 15 trials were recorded per speed. Thus, a total number of 675 trials (15 trials x 3 speeds x 15 participants) were recorded and used for subsequent analyzes in the study. During the experiment, participants were allowed to rest in order to minimize fatigue effects. The duration of the experiment was approximately 45 minutes per participant.

Data collection and processing

Materials

An optical motion capture system consisting of eight high-speed cameras was used to record the arm motion at a frequency of 250Hz (Vicon motion system Inc. Oxford, UK). A set of plug-in-gait markers was attached to the participant body. Precisely, thirteen markers were placed at well-defined anatomical locations on the dominant arm and the other parts of the body, namely: seventh cervical vertebrae, 10th thoracic vertebrae, clavicle, sternum, right and left acromion, lateral and medial humeral epicondyles, ulnar and radial styloids, 2nd and 5th metacarpal heads and 1st fingertip.

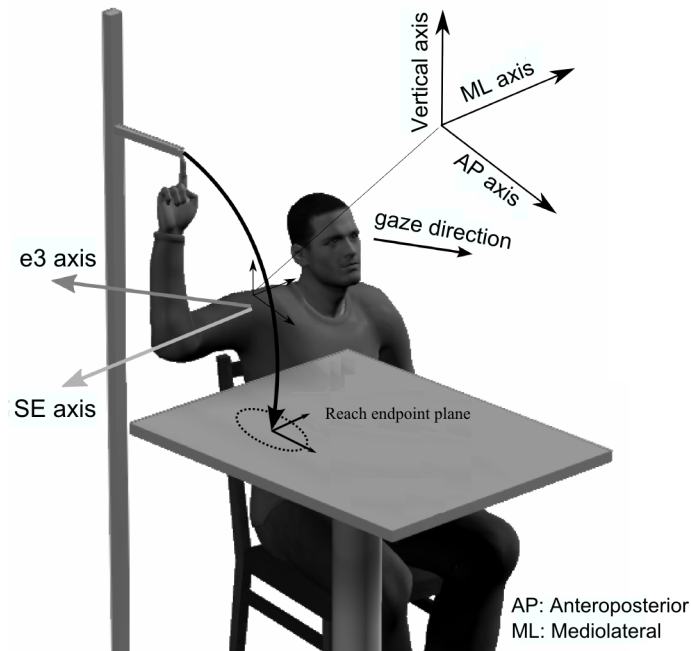


Figure 3.1. Illustration of the experimental paradigm. Fixed initial arm position and horizontal target plane were tested, thereby defining a free reach-endpoint motor task. The reach endpoint was one prominent movement parameter. Two other relevant movement parameters (rotation axis displacements, SE and e3) are depicted. Gaze direction was controlled during the movement as indicated by the arrow. Note that any possible path leading to any location onto the surface was possible regarding task achievement. The task was thus redundant (3 free joint angles for most endpoint locations) and 3D as the arm could freely move in 3D space without any constraint, except that of reaching the target plane at various instructed speeds (slow, normal and fast, denoted by S, N and F respectively).

Motion analysis

All the analyzes were performed with custom software written in Matlab (Mathworks, Natick, MA) from the recorded three-dimensional position of the markers. The recorded positional data were first smoothed using a 2nd-order Butterworth low-pass filter with cut-off frequency at 10Hz and then processed to compute other kinematic and dynamic parameters, as described hereafter.

Kinematic-level analysis *Hand kinematics.* For every recorded trial, the position of the fingertip marker was numerically differentiated to obtain the corresponding velocity profile. Based on this velocity profile, the movement duration (MD) was estimated by

the time window where the velocity magnitude was above 5% of the peak velocity. Other kinematic parameters relevant to the purpose of the present study were then computed and analyzed to check for differences in hand kinematics with respect to the instructed speed, as follows: the reach endpoint location in 3D (RE, described by its Cartesian coordinates X, Y and Z with respect to a frame whose origin is located at the shoulder joint), the peak velocity (PV), accuracy and precision along the vertical axis (denoted by Za and Zp, respectively). In practice, Za was defined based on the distance from the final finger position to the planar target and Zp was defined as the standard deviation of the vertical RE coordinates. They were used to verify constant and variable errors along the vertical axis. Note that, in the present task, Xa and Ya were undefined as the task did not impose any final fingertip position in the plane. Finally, Xp and Yp were analyzed via 95% confidence ellipses showing the distributions of RE within the target plane.

Joint kinematics. The 4-DoF arm configuration was computed from the recorded motion data. To this aim, we employed the method previously described in [Isableu et al. \(2009\)](#). Briefly, this method considered the 3D arm as an articulated chain of rigid bodies connected by joints. Then, a local segment coordinate system was calculated based on the measured 3D position of the markers in a way that was consistent with the International Society of Biomechanics (ISB) recommendation ([Wu et al., 2005](#)). From the resulting coordinates, rotation matrices converting a specific coordinate to its parent coordinate were computed in accordance with the rotation orders, which allowed angles to remain as close as possible to the clinical definition of joint and segment motion. Based on these calculated rotation matrices, the values of (Euler) rotation angles (internal/external, elevation/depression, ulnar/radial at shoulder and extension/flexion at elbow) were easily inferred. Again, the joint velocities and accelerations were obtained by numerically time-series differentiating the angular displacements.

Dynamic-level analysis Inverse dynamic analysis was used to estimate the muscle torques underlying the observed motion kinematics. A dynamical model of the arm was required to infer these movement parameters. As mentioned above, the arm was viewed as the combination of rigid bodies connected by series of revolute joints. If such a model can be easily established for planar systems (e.g. [Berret et al., 2011a](#)), the task is more tedious in 3D especially when computational efficiency really matters. Thus, special considerations were taken into account. Firstly, the series of arm rotation axes as well as

the segment coordinates in Wu's model (Wu et al., 2005) were re-approached within the standard robotic point of view wherein the four rotation axes were re-described using Denavit-Hartenberg parameters. The same description could be found for instance in Asfour and Dillmann (2003), where the robotic model of a humanoid arm was described. From this formalism, many of the advanced tools developed in robotics could be applied to calculate both forward or inverse kinematic and dynamic parameters. Secondly, another crucial piece was the anthropometric parameters. The parameters reported in Dumas et al. (2007) were used, providing us with an approximation of anthropometric values such as mass, center of mass position and inertia matrix for each segment. These parameters were adjusted for each participant given his/her total mass and the lengths of the body segments (measured via motion capture).

From a classical application of Lagrange mechanics, the arm skeleton dynamics can be expressed as follows:

$$\boldsymbol{\tau} = \mathcal{M}(\boldsymbol{\theta})\ddot{\boldsymbol{\theta}} + \mathcal{C}(\boldsymbol{\theta}, \dot{\boldsymbol{\theta}}) + \mathcal{G}(\boldsymbol{\theta}) + \mathcal{R}(\boldsymbol{\theta}, \dot{\boldsymbol{\theta}}), \quad (3.1)$$

where $\boldsymbol{\tau}$ is the muscle torque, \mathcal{M} is the mass matrix (4x4 size here), \mathcal{C} is the Coriolis and centripetal torque, \mathcal{G} is the gravitational torque. Note that computed in this way, the muscle torque is actually affected by some term $\mathcal{R}(\boldsymbol{\theta}, \dot{\boldsymbol{\theta}})$ reflecting frictional and viscous or elastic torques created by all soft tissues. In the current work, the latter term \mathcal{R} was neglected and assumed to be negligible compared to the other torques. The vector $\boldsymbol{\theta} = (\theta_1, \dots, \theta_4)$ denotes the four angles describing the arm's configuration and a dot above a variable stands for its time derivative.

We may subsequently define the muscle, net, interaction and gravitational torques as follows:

$$\begin{aligned} \tau_{mus} &= \boldsymbol{\tau}, \\ \tau_{net} &= \text{diag}(\mathcal{M}(\boldsymbol{\theta}))\ddot{\boldsymbol{\theta}}, \\ \tau_{int} &= - \left[(\mathcal{M}(\boldsymbol{\theta}) - \text{diag}(\mathcal{M}(\boldsymbol{\theta}))) \ddot{\boldsymbol{\theta}} + \mathcal{C}(\boldsymbol{\theta}, \dot{\boldsymbol{\theta}}) \right], \\ \tau_{gra} &= -\mathcal{G}(\boldsymbol{\theta}). \end{aligned}$$

where $\text{diag}(\mathcal{M}(\boldsymbol{\theta}))$ represents the diagonal matrix built from the diagonal terms of the mass matrix. Then, equation 3.9 can be rewritten as follows:

$$\tau_{net} = \tau_{mus} + \tau_{int} + \tau_{gra}, \quad (3.2)$$

which is similar to the description given in [Yamasaki et al. \(2008\)](#) and [Sande de Souza et al. \(2009\)](#). In particular, this shows that the net torque at each joint is produced by a combination of muscle torque, interaction torque and gravitational torque.

In practice, the above analytic formulas are quite long to evaluate explicitly and using them is therefore computationally inefficient for intensive simulations. Hence we used a recursive Newton-Euler algorithm to compute the arm dynamics in our simulations. State-of-the-art algorithms for rigid body dynamics can be found in [Featherstone and Orin \(2000\)](#). Actually, by replacing 3D vectors by 6D spatial vectors in the classical Newton-Euler recursive algorithm, efficiency of the arm’s dynamics calculation could be largely improved (for both direct and inverse dynamics). Computational efficiency was especially crucial in the present study because optimal control methods involve very intensive computations and numerous evaluations of the arm’s dynamics (see below). We actually checked that both methods to calculate the dynamics (either based on Lagrangian or Newton-Euler formalisms) gave the same result but the latter was about 10 times faster than the former in our settings (note that a compiled version of the code provided by [Featherstone and Orin \(2000\)](#) was eventually used for better efficiency).

Global motion parameters In this study, three indexes summarizing different aspects of the overall arm motion were analyzed. Most of them were discussed in previous papers ([Isableu et al., 2009](#); [Pagano and Turvey, 1995](#); [Sainburg and Kalakanis, 2000](#); [Riley and Turvey, 2001](#)), which is the reason why our analysis will rely upon them. The first parameter is the reach endpoint index (RE index); the second and third indexes respectively the average deviation of the shoulder-elbow axis (SE index, i.e. kinematic parameters) and the average deviation of the minimum inertia axis (e3 index, i.e. a kinetic parameter).

Antero-posterior reach endpoint position (RE index). The RE index was defined as the final fingertip position on the planar target along the AP axis (X_{AP}) normalized by the maximal distance that the participant could reach to without moving bending the trunk (D_{max} , corresponding to a fully-extended arm such that the fingertip was on the target plane).

$$RE\ index = \frac{X_{AP}}{D_{max}} \times 100. \quad (3.3)$$

Minimum principal inertia axis deviation (e3 index). This dynamic parameter is based on the minimum principal inertia axis (referred to as e3 in previous studies). A method

to calculate the instantaneous e3 axis during a 4-DoF arm movement was described in [Isableu et al. \(2009\)](#). Importantly, it is worth noting that e3 definition only relies on the instantaneous whole-arm configuration and its anthropometric characteristics. At each time step, the angle between the current e3 axis direction and its initial ($t = 0$) one, $a_{e3}(t)$, was computed and the e3 index was calculated as in Eq. 3.4.

$$e3\ index = \frac{1}{T} \int_0^T |a_{e3}(t)| dt. \quad (3.4)$$

A strict rotation around e3 axis would thus indicate a strategy exploiting the inertial properties of the arm (when viewed as a single “L-shaped” rigid body). Indeed, the task could be performed by strictly rotating the arm around e3 axis, with no forearm flexion/extension. Intuitively, such a strategy could facilitate the production of large angular accelerations at equivalent muscle torque magnitude. For instance, rotating the arm around the maximum principal inertia axis would lead to smaller acceleration for similar muscle torque, which is just the result of the intrinsic inertial properties of an arm in such a L-shape configuration. Moreover, rotating around e3 may be advantageous because the angular momentum then becomes parallel to the angular velocity vector of the rigid body and therefore a muscle torque around e3 only produces angular acceleration around e3 without inducing accelerations around other axis (i.e. interaction torques).

Shoulder-elbow deviation index (SE index). The SE index was defined as the mean integral of the absolute shoulder-elbow axis deviation. At each time step, the angle between the current shoulder-elbow axis direction and its initial (at $t = 0$) one, $a_{SE}(t)$, was computed and the SE index was calculated as reported in Eq. 3.5:

$$SE\ index = \frac{1}{T} \int_0^T |a_{SE}(t)| dt \quad (3.5)$$

where T was the total movement duration (obtained experimentally for each trial). A strict rotation around this axis when performing the task was possible, yielding a SE index equal to zero. In turn, this would indicate the use of a kinematic control strategy possibly aiming at stabilizing the upper arm segment during the whole motion ([Isableu et al., 2009](#)).

Optimal control modeling and inverse optimal control method

In this section, we describe the optimal control methods and the numerical inverse optimal control approach that we used. The method follows the works of [Mombaur et al. \(2009\)](#)

and Berret et al. (2011a), and aims at accounting for the 3D arm motion from an optimal control standpoint by finding the subjective costs underlying the experimental trajectories. The control dynamics, denoted by noted (Σ), is formed of the skeletal dynamics given in Eq. 3.9 and some basic muscle dynamics. Muscle dynamics was added here to account for the smoothness of velocity and acceleration signals and was not assumed to be an accurate model of the muscle-tendon complex. Therefore, we used a simple model accounting for the low-pass filter property of muscles, as it is quite common in optimal control studies (e.g. Uno et al., 1989; Guigon et al., 2007; Berret et al., 2011a). Precisely, we assumed that the motor command (i.e. control signal) was simply the derivative of the muscle torque, as follows:

$$\dot{\tau} = \mu \tag{3.6}$$

where the control μ can be thought as the overall motor input given to the muscle.

Solving an optimal control problem with non-linear dynamics and non-quadratic cost functions is generally a difficult problem especially for problems with large dimensions (here the state vector had 12 dimensions and the control vector had 4 dimensions). One could however observe that the limb and muscle dynamics together form a fully-actuated control system that is feedback linearizable. Therefore, it was possible to effectively change the nonlinear control problem into a linear control problem by directly controlling the derivative of the angular acceleration vector instead of the derivative of the muscle torque. This mathematical change of control variable allowed us to replace Eq. 3.6 with the following one:

$$\ddot{\theta} = \mu \tag{3.7}$$

The muscle torque (and its derivative) could then be recovered via inverse dynamics (see above). Even though we could control μ directly, we generally observed that such approach yielded faster and more robust convergence during the numerical resolution of the optimal control problems under consideration. The numerical difficulties were then left to the possible non-quadraticity of the cost function.

In the literature, several cost functions were proposed by different authors. It is useful to distinguish subjective and objective cost functions. Subjective costs differ from objective ones in that the former reflect a subject's decision/choice while the latter are imposed by the task (e.g. accuracy). Here we focus on the identification of subjective costs only. Various subjective cost functions were proven useful and relevant as it often replicated at

least some experimental observations. Briefly, previously proposed cost functions may be grouped into three main categories: kinematic, energetic and dynamic. All classes with one relevant representative cost are listed in Table 3.4. Here we considered the minimum angle jerk (Wada et al., 2001) to represent the kinematic cost family (we could have used a minimum acceleration criterion (Ben-Itzhak and Karniel, 2008) but the predictions of the two models only differed slightly). For the dynamic class, we considered the minimum torque change model (Uno et al., 1989). We also tested the minimum torque model (Nelson, 1983) but we found that the torque change model was more relevant for the present motor task. At last, at the interface between kinematic and dynamic variables are energetic costs that measure actual energy expenditures associated with the movements. We chose the minimum absolute work of muscle torques here (Berret et al., 2008; Gauthier et al., 2010; Gaveau et al., 2014). The geodesic (Biess et al., 2007) or the minimum peak work model (Soechting et al., 1995) are other models that could have been considered within this class but their exact formulation is less easily integrable within a generic optimal control scheme, which may be problematic for running inverse optimal control (see below).

Class	Criterion	Cost function	References
Kinematic	<i>Angle jerk</i>	$C_{Kine} = \int_0^T \sum_{i=1}^4 \ddot{\theta}_i^2 dt$	Wada et al. (2001)
Energetic	<i>Absolute work</i>	$C_{Ener} = \int_0^T \sum_{i=1}^4 \dot{\theta}_i \tau_i dt$	Nishii and Murakami (2002); Berret et al. (2008)
Dynamic	<i>Torque change</i>	$C_{Dyna} = \int_0^T \sum_{i=1}^4 \dot{\tau}_i^2 dt$	Uno et al. (1989); Nakano et al. (1999)

Table 3.1. Cost functions considered in this article. Their overall class (kinematic, energetic or dynamic), the chosen representative element of each class with its classical name, the mathematical definition of the cost and the references which proposed them.

Although each of the above cost function was proved to be effective under specific conditions, it is actually very difficult and likely impossible to identify a unique and generic cost function that will account well for all possible human arm movements. It may thus seem reasonable to widen the optimal control hypothesis and investigate the idea of composite cost functions. In this vein, recent work (Berret et al., 2011a) showed that free arm pointing movement could not be explained by any single cost among a variety of 7 possible candidates but by the combination of mainly two of them, namely angle jerk and absolute work optimality criteria. Based on these prior findings and because of the computational load and complexity of the present 4-DoF arm model we restricted our analysis to the combination of the three cost functions listed in Table 3.4, which we shortly refer to as

kinematic (Kine), energetic (Ener) and dynamic (Dyna) throughout the study. Thus, the composite cost function may be written as:

$$C(\boldsymbol{\alpha}) = C_{Kine} + \alpha_1 C_{Ener} + \alpha_2 C_{Dyna} \quad (3.8)$$

The triplet $\boldsymbol{\alpha} = (1, \alpha_1, \alpha_2)$ uniquely determines the composite cost function. We will refer to $\boldsymbol{\alpha}$ as the weighting vector (whose elements are non-negative). The factor 1 in the first component of the triplet is due to the fact that the composite cost can be normalized (see Mombaur et al., 2009; Berret et al., 2011a). Our investigations showed that the kinematic cost was relevant and necessarily present to account for the subject’s behavior. Considering 3 costs (and thus having only 2 free parameters) also enabled convenient visualization possibilities (see Results).

It is noteworthy that for each participant three different speeds (S, N, F) were studied in the current work. In order to find the composite cost functions that best replicated the recorded data, two solutions were available. Firstly, one could try to find a composite cost corresponding for each speed, thereby assuming that task instructions could affect the weights of the subjective cost. We thus termed this type of cost “speed-dependent composite costs” and denoted it by SDComp. Alternatively, one could also try to find a single composite cost accounting for all speeds at once. We termed this type of cost “speed-independent composite cost” and denoted it by SIComp. These two possible hypotheses make divergent assumptions regarding the flexibility of subjective costs with respect to task instructions. The results of both SDComp and SIComp costs will be compared to determine which one is the more plausible following Occam’s razor principle (for similar accuracy, the most parsimonious model should be retained).

Optimal control problem (OCP). The OCP corresponding to the cost $C(\boldsymbol{\alpha})$ can be stated as follows: *Find an optimal control $\mathbf{u}_{\boldsymbol{\alpha}}^*$ and its corresponding optimal trajectory $\mathbf{q}_{\boldsymbol{\alpha}}^{*\top} = (\boldsymbol{\theta}^\top, \dot{\boldsymbol{\theta}}^\top, \ddot{\boldsymbol{\theta}}^\top)$ of system (Σ) , connecting a source point \mathbf{q}_s to a final point on the target plane in time T and yielding a minimal value of the cost $C(\boldsymbol{\alpha})$ (then denoted by $C^*(\boldsymbol{\alpha})$).*

To solve this problem, the Matlab software GPOPS (Rao et al., 2010) was used. This method employs an orthogonal collocation technique to convert the continuous time OCP into a nonlinear programming problem (NLP) with constraints. The well-established numerical software SNOPT was used to solve the NLP problem. For each simulation, the angular velocity and acceleration at initial and final times were set to zero since the participants were required to start and stop their motion with a static state. The other

parameters such as the initial angular configuration θ_0 and the motion duration T were directly estimated from the recorded data. The anthropometric parameters such as inertia, mass, center of mass, segment length were customized for each participant, thereby accounting for physical inter-individual differences.

Inverse optimal control (IOC). Inverse optimal control problem was stated as a bi-level problem with an outer loop seeking for the α best fitting the recorded trajectories, and an inner loop that finds the optimal trajectory for the current α (see also [Mombaur et al., 2009](#); [Berret et al., 2011a](#) for details).

Importantly, a function (or metric, denoted by Φ) to compare simulated and recorded arm trajectories is needed. Here, we sought for a vector α allowing to replicate at best the recorded four angles in the joint space. At the initial time, the simulated and recorded angles (respectively denoted by \mathbf{q}_α^* and \mathbf{q}^{meas}) coincided perfectly, but differences typically appeared during the course of motion. The function used to measure this discrepancy was defined as the maximal deviation of the simulated angular displacements from the reference ones (simply taken as the average experimental values observed for each speed condition). Note that this metric was quite conservative as it involved the maximal deviation and not the averaged one. Eventually, four deviations corresponding to the four joint angles were obtained, which were averaged to get a single overall error in joint space, denoted by $E_{Joint}(\alpha)$. Different values of E_{Joint} were obtained for different values of α_1 and α_2 , hence this error could be visualized using 3D plots (see Results).

Therefore, by definition, $\Phi(\mathbf{q}_\alpha^*, \mathbf{q}^{meas}) = E_{Joint}(\alpha)$ for the SDComp case. For the SIComp case, the metric was modified to minimize the error for all 3 speeds together (the average was simply used). The purpose of the outer loop is to minimize this error (Φ) by finding the best α , that is, the best-fitting cost combination for replicating the experimental data (for each speed separately for SDComp and for all speeds simultaneously for SIComp).

To solve this part of the problem, a method called CONDOR standing for Constrained, Non linear, Direct, parallel optimization was used. A re-scaling method described in [Berret et al. \(2011a\)](#) was also needed in the present work to improve the efficiency of the algorithm (due to the different units and order of magnitudes of the costs). In addition, the value of α or $\bar{\alpha}$ was initialized with random non-negative values and 10 random restarts were considered for each inverse optimal control problem and for each participant in order to limit the issue of being stuck at a local minimum. The best α were eventually chosen as the ones that made the function Φ as small as possible. In total applying this procedure

to all the participants required solving 450 IOC problems (10 restarts \times 3 speeds \times 15 participants) for the SDComp case and 150 IOC problems (10 restarts \times 15 participants) for the SIComp case.

Cost contribution calculation. We used the formula originally described by Berret et al. (2011a) to evaluate the contribution of each cost function to the total cost. Investigating cost contributions was interesting because the components of the vector α could not be straightforward to interpret: the largest α_i could potentially be of minor importance with respect to trajectory fitting depending on the units or order of magnitudes of each elementary cost.

Comparison between simulated and experimental trajectories Simulated and experimental trajectories were compared in two ways: first, absolute errors were computed and, second, relative errors linked to speed variations were estimated to assess how each cost could predict the speed dependence of motor strategies.

Cartesian error of the finger trajectory. In order to estimate the accuracy of trajectory reconstructions also in Cartesian space, we computed the maximal deviation between experimental and simulated 3D finger trajectories and this Cartesian error was denoted by E_{Cart} .

Reach endpoint index error (E_{RE}). The reach endpoint error measured the distance between the recorded RE index (RE_{exp}) (simply taken as the average experimental values observed for each speed condition) and the simulated one (RE_{sim}) generated by either SDComp or SIComp or each of the three elementary costs. The E_{RE} values were computed for each speed and each subject.

e3 index error (E_{e3}). Similarly to the E_{RE} , the e3 index error measured the distance between the recorded e3 index ($e3_{exp}$) and the simulated one ($e3_{sim}$).

RE or e3 slope errors ($E_{\bar{K}_{RE}}$ or $E_{\bar{K}_{e3}}$). In order to evaluate whether simulated results were able to replicate hypothetical speed-dependences of RE and e3 for each subject, we also compared the experimental and simulated slopes resulting from a linear regression of each parameter with respect to the instructed speed. To normalize slope values across subjects, we did not use the value of K resulting from a regression against the real speeds of subjects because it could differ substantially across them. Instead, we used the value \bar{K} obtained when regressing against the instructed speed, i.e. S, N, and F labels. We then defined the speed-dependence error as the absolute difference between \bar{K}_{exp} and \bar{K}_{sim} . The analysis

was done for both RE and e3 parameters, thus leading to the definition of $E_{\bar{K}_{RE}}$ and $E_{\bar{K}_{e3}}$ for parameters RE and e3 respectively.

Statistical analyses

Repeated-measures one-way ANOVAs were performed to assess the effect of speed on relevant movement parameters. The ANOVA's sphericity assumption (using Mauchly test) was checked, and p-values and degrees of freedom were corrected using estimates of sphericity (Greenhouse-Geisser/Huynh-Feldt). Post-hoc tests were conducted with Bonferroni corrections when appropriate (the chosen threshold was 0.05 and analyzes were conducted using SPSS). We used quantile-quantile plots to visually check whether the data were normally distributed (qqplot Matlab function). Shapiro-Wilk's test was used to quantify these observations for the relevant parameters.

Results

Experimental observations

Inter-individual analysis *Peak velocity and Movement duration.* Repeated-measures ANOVAs were used to statistically check that subjects yielded significant differences with respect to the instructed speed. Recorded peak velocities were significantly different across S, N and F speed conditions ($F(2,28) = 74.8$, $p < 0.001$). This confirmed that the verbal instruction of speed was effective. Post-hoc analyses showed that all speeds were significantly distinct. Quantitative values are given in Table 3.5. The mean and standard deviation across subjects for the S, N, and F conditions were 1.0 ± 0.3 m/s, 2.1 ± 0.4 m/s and 3.4 ± 0.7 m/s respectively. A similar statistical analysis performed on movement duration showed similar results ($F(2,28) = 21.1$, $p < 0.001$).

	S	N	F
MD (s)	0.90±0.20	0.54±0.12	0.30±0.06
PV (m/s)	1.0±0.3	2.1±0.4	3.4±0.7
$Sh_{internal/external}$ (°)	10.4±7.9	11.9±8.8	12.6±8.5
$Sh_{elevation/depression}$ (°)	10.1±6.4	10.4±6.0	10.4±6.2
$Sh_{ulnar/radial}$ (°)	92.6±15.8	94.8±15.8	96.2±15.2
$El_{extension/flexion}$ (°)	27.2±8.3	25.7±9.1	24.1±9.0
RE index (%)	83.1±9.1	81.2±9.6	79.8±8.7
e3 index (°)	19.3±5.1	18.2±5.2	17.6±5.8
SE index (°)	7.6±3.9	8.1±3.5	8.3±3.3
Z_a (cm)	0.6±0.4	0.7±0.4	0.6±0.5
Z_p (cm)	0.4±0.3	0.3±0.2	0.4±0.3

Table 3.2. Experimental movement parameters (mean±std across subjects).

Reach accuracy and precision. Although the task did not impose any particular point to reach to, the subjects had to control the constant error along the vertical axis. One objective of the task was thus to position the fingertip onto the target surface. Constant errors along the vertical (Z_a) were relatively small and independent of the speed, indicating that the final position constraint was fulfilled by all the participants. Regarding the variable error along the Z_p axis, they were of comparable magnitude with no speed effect. For X_p and Y_p , giving the distributions of reach endpoint in the target plane, analyses via confidence ellipses were conducted (see below for the RE index).

Angular excursions. The four angle excursions (shoulder's internal/external, elevation/depression, ulnar/radial, elbow's extension/flexion), averaged across subjects, are given in Table 3.5. The magnitude of angular displacements tended to depend on the instructed speed. Precisely, when speed increased, the shoulder angles (internal/external angle, elevation/depression angle, ulnar/radial angle) tended to increase while the elbow's extension/flexion angle tended to decrease. Repeated-measures ANOVAs did not show any significant effect of speed for the two first shoulder angles ($F(2,28)=2.3$, $p=0.139$; $F(2,28)=0.08$, $p=0.92$) but a significant effect was observed for the third shoulder and the elbow angles ($F(2,28)=4.5$, $p<0.05$; $F(2,28)=16.3$, $p<0.001$, respectively). Regarding the magnitude of angular excursions, it is interesting to note that although subjects could accomplish the task by simply rotating their arm only about the shoulder ulnar/radial axis, all subjects actually chose more complex joint displacements. Actually, while the movement was mainly achieved by rotating around the shoulder ulnar/radial axis (considered as a major axis), we also measured

quite large displacements of elbow extension/flexion (about 1/3 of shoulder ulnar/radial excursion), and non-negligible amounts of shoulder internal/external, elevation/depression angular rotations. Therefore, the movement chosen by the subjects generally involved the coordinated displacement of several joints in different proportions.

SE, e3 and RE indexes. The above observations were further analyzed in terms of the global movement parameters described in the Materials and Methods. The mean \pm std values of SE/e3/RE indexes across all the subject were reported in Table 3.5. In agreement with the joint excursions, the SE index was relatively small for all speed conditions ($7.6 \pm 3.9^\circ$ for S; $8.1 \pm 3.5^\circ$ for N; $8.3 \pm 3.3^\circ$ for F), although it tended to slightly increase with respect to speed. Repeated-measures ANOVAs did not reveal any significant differences for this global movement parameter index ($p=0.23$). In contrast, both e3 and RE indexes tended to decrease with respect to speed and obtained the values of $19.3 \pm 5.1^\circ$, $18.2 \pm 5.2^\circ$, $17.6 \pm 5.8^\circ$ and $83.1 \pm 9.1\%$, $81.2 \pm 9.6\%$, $79.8 \pm 8.7\%$ for S, N, F respectively. For those parameters, repeated-measures ANOVAs revealed significant changes with respect to speed ($F(1.4,20.1)=7.4$, $p<0.01$; $F(2,28)=14.8$, $p<0.001$ for e3 and RE indexes respectively). A finer examination of RE and e3 indexes showed that some subjects exhibited more speed dependencies than others, which is analyzed below.

Intra-individual analysis *Reach endpoints.* The distribution of reach endpoints projected onto the transverse plane is illustrated in Figure 3.2. The data of two representative subjects were reported (S5 and S14 represent speed-sensitive subjects and speed-insensitive subjects, respectively). A qualitative inspection revealed an effect of speed for S5 but not in S14. Precisely, for S5, increase of speed was accompanied by reach endpoints that tended to get closer to the shoulder location in the AP direction. Correlation analyzes performed for the RE index confirmed these observations (Fig 3.3). Indeed, while the RE index for S5 showed a significant negative correlation with respect to speed ($R=-0.76$, $p<0.001$), the correlation for S14 was not significant ($p=0.48$). The data of individual subjects are reported in Table 3.3 (R values, p values and K slopes are given).

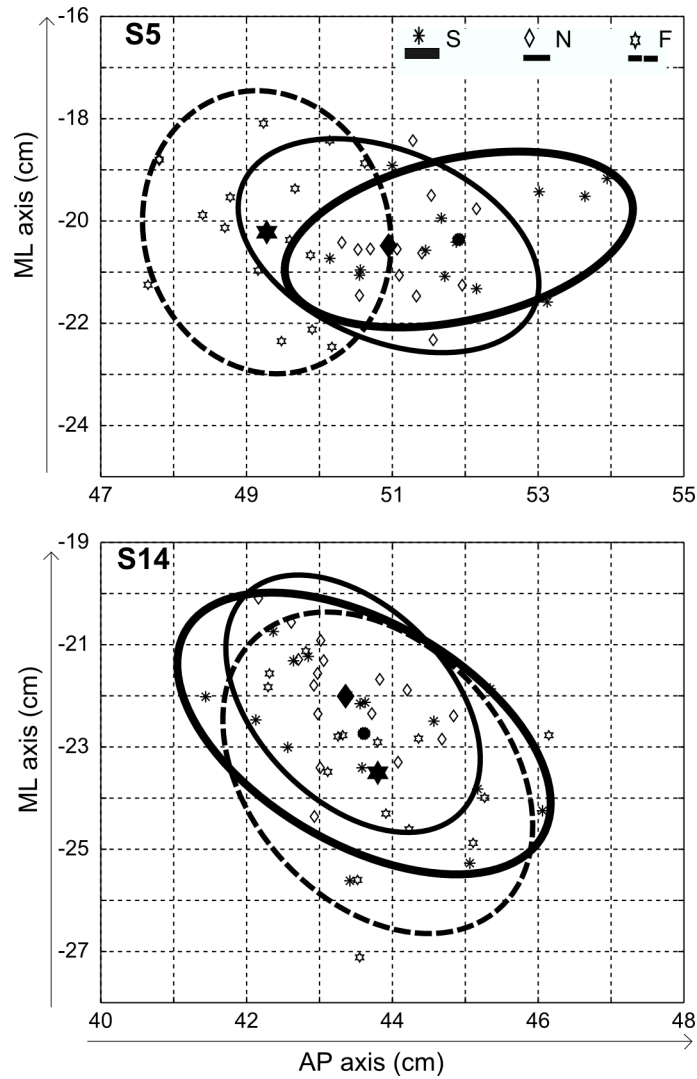


Figure 3.2. Reach endpoint positions of two subjects (S5 and S14) for the three different speeds (S, N and F). The 95% confidence ellipses of reach endpoints in the S, N and F speed conditions are drawn in thick, thin and dotted lines, respectively. Note that along the antero-posterior (AP) axis, the distributions of finger positions of S14 remain relatively constant regardless of movement speed while those of S5 tend to decrease when movement speed increases.

e3 and *SE* indexes. The variations of *e3* with respect to the movement speed for the two typical subjects (S5 and S14) are shown in Figure 3.3 (bottom panel). Similarly to RE indexes, it is visible that the *e3* index was independent of speed for S14 ($p=0.50$) while it clearly decreased with speed increments for S5 ($R=-0.85$, $p<0.001$). Regarding *SE* index (not depicted), it was increasing according to speed for S5 while speed invariant for S14

(values). The data of individual subjects are again reported in Table 3.3 (R values, p values and K slopes are given).

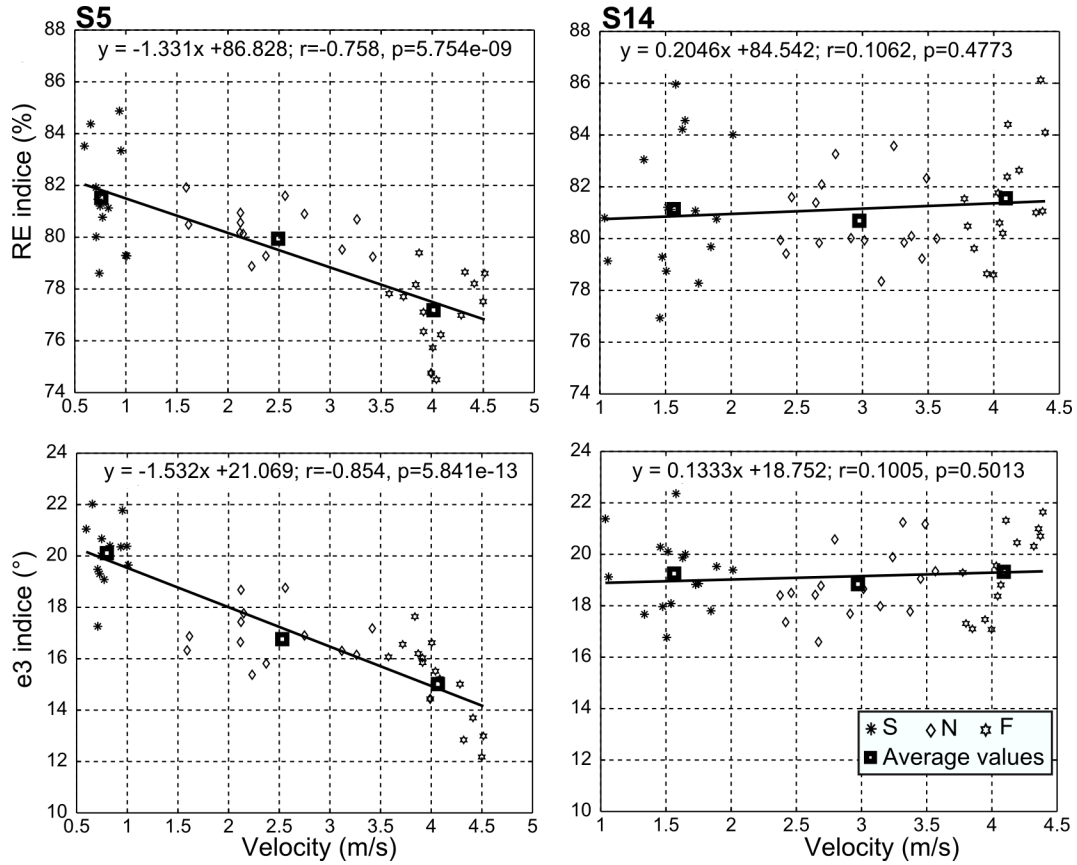


Figure 3.3. Dependence of RE and e3 indexes on movement speed for the two subjects S5 (*left*) and S14 (*right*). For each examined index, linear correlation and regression lines (thin black lines) were computed based on all recorded data (each dot of the graphs corresponds to a single trial). For S14, RE and e3 indexes appear to be nearly independent of speed variations while those of S5 decrease clearly when movement speed increases.

In summary, the above investigations revealed idiosyncratic behavioral strategies, with some participants using speed-dependent reach endpoints and joint trajectories while others conserved the same arm trajectories irrespective of speed instructions. Note that the use of a pointing task with unconstrained reach endpoints was essential to uncover the existence of speed-dependent strategies in some subjects. Next, to account for these experimental observations, an inverse optimal control approach is presented, which aimed at identifying the costs underlying the arm trajectories of each individual for every speed. This will prove to be useful to explain the inter-individual divergences within a unique normative

framework.

	S1	S2	S3	S4	S5	S6	S7	S8	S9	S10	S11	S12	S13	S14	S15
R	-0.63	-0.17	-0.12	-0.50	-0.76	-0.17	-0.26	-0.76	-0.62	-0.10	-0.43	-0.14	-0.05	0.10	0.06
RE	p<0.001	0.17	0.46	p<0.001	p<0.001	0.19	p<0.05	p<0.001	p<0.001	0.49	p<0.01	0.32	0.70	0.48	0.62
K_{RE}	-1.93	-0.82	-0.38	-2.60	-1.33	-0.51	-0.59	-1.98	-1.21	-1.61	-1.98	-0.69	-0.17	0.20	0.38
R	-0.61	-0.15	-0.46	-0.39	-0.85	0.02	0.14	-0.68	-0.88	-0.35	-0.48	-0.06	-0.21	0.10	0.20
e3	p<0.001	0.24	p<0.01	p<0.01	p<0.001	0.82	0.27	p<0.001	p<0.001	p<0.05	p<0.001	0.65	0.11	0.50	0.12
K_{e3}	-1.21	-0.32	-0.80	-1.18	-1.53	0.08	0.22	-0.80	-1.3	-0.97	-0.87	-0.19	-0.41	0.13	0.93

Table 3.3. Correlation analyses for RE and e3 indexes for all the participants. Correlation coefficients R, statistical significance p and slopes of linear regression (K) for two examined parameters (RE, e3) with respect to the peak of velocity (in m/s) are reported for each of the 15 subjects. Correlation coefficients significantly different from 0 are emphasized in bold.

Optimal control results

Reach endpoint location and rotation axis displacement as predicted by kinematic, energetic and dynamic elementary cost functions In order to provide preliminary insights about the predictions of each elementary cost function for the present pointing task, optimal control simulation results for a subject (here S5) are shown in Figure 3.4. The dependence of each single cost with respect to the required speed is also emphasized. The left panel depicts the finger's simulated movement paths while the right panel displays the variation of two global parameters (RE and e3) with respect to three speeds (S, N, F). It is noteworthy that the initialized parameters (such as the initial configuration of arm, movement durations, position of planar target) were imported directly from recorded data and kept fixed during the simulation processes. Importantly, the simulated results showed that each cost function produced different movement paths to the planar target, leading to different RE locations. For a specific movement speed (e.g. N), the kinematic cost would generate the farthest movement (i.e. more distant RE location with respect to the vertical projection of shoulder position on the planar target). Between the energetic/dynamic costs, the dynamic cost tended to produce the less distant RE index. Furthermore, in terms of speed dependencies, the three costs made distinct predictions: the kinematic cost did not depend on speed at all, in agreement with its theoretical foundation. However, energetic and dynamic costs exhibited some dependence on speed in both hand path curvatures and RE location. Visually, when the speed increased from S to F, the energetic cost generated quite distinguishable movement paths (smallest RE location at F speed) while the dynamic cost generated slightly different movements between speeds (but the curvature noticeably decreased with respect to speed increments). A quantitative analysis showed that the kinematic cost always produced constant RE/e3 indexes across movement speed while the energetic/dynamic costs reduced RE or e3 indexes at high or low rates when movements sped up. A finer examination of arm posture showed that the movements generated by kinematic cost mainly involved rotation about the shoulder ulnar/radial axis and negligible displacements about the other axes regardless of speed, accounting for the low values of SE index for this cost. On the contrary, the energetic/dynamic costs generated the movements that associated with all the rotational axes, yielding quite large displacements around the shoulder internal/external, elevation/depression, elbow extension/flexion axes. Thus, one could conclude that the optimization of movement based

on the sole kinematic cost could only account for speed-insensitive strategies while the optimization of pure energetic/dynamic costs should produce speed-dependent arm trajectories.

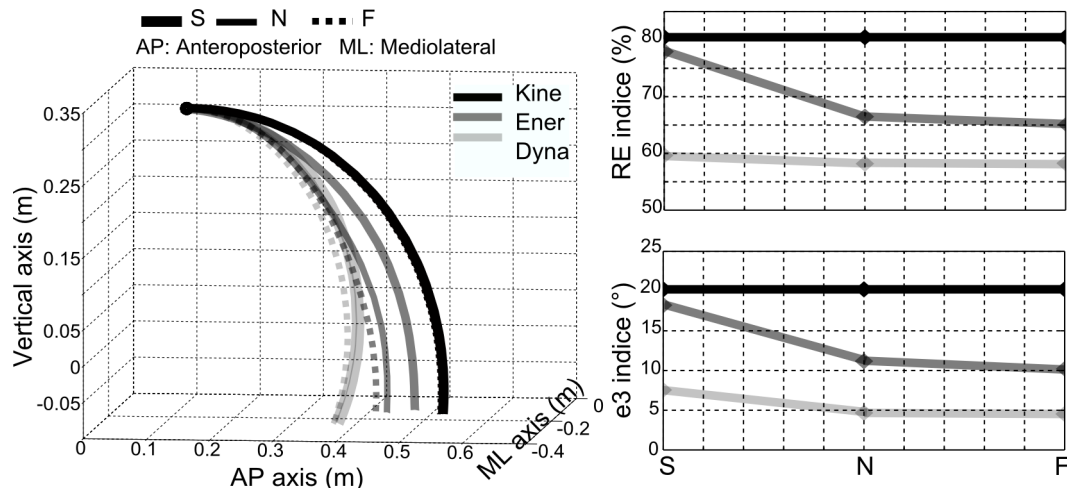


Figure 3.4. Movement parameters predicted by each elementary cost (kinematic, energetic and dynamic) during the plane-reaching task at three different speeds (S, N and F). *Left.* Movement paths of the fingertip start from the same position (black circle) but end at different reach endpoints on the target surface. *Right.* Variation of RE and e3 indexes with respect to speed. The kinematic cost generated speed-invariant trajectories (constant movement path as well as RE and e3 indexes), whereas the dynamic and energetic costs generated relatively small and large speed-dependent trajectories respectively. RE and e3 indexes varied accordingly for the two latter costs. These two costs exhibited some degree of speed dependence because they both involved dynamic variables such as muscle torques and the musculoskeletal dynamics was highly nonlinear.

Composite cost identification *Overall fitting errors.* Composite costs were fitted to the data of each subject in order to uncover the optimality criteria underlying their experimental behaviors. In order to evaluate the performance of composite costs, their performance was systematically compared to what would be obtained using the three elementary costs separately (Kine, Ener and Dyna). For composite costs, two competing hypotheses were tested: speed-dependent vs. speed-independent composite costs (SDComp vs. SIComp, respectively). The joint space and Cartesian space fitting errors (E_{Joint}/E_{Cart} , mean \pm std values across subjects) are reported in Figure 3.5. As expected, errors obtained from the best-fitting composite costs were constantly smaller than for each of the elementary costs. In joint space, the maximal angular deviations between simulated and experimental displacements were $5.5 \pm 3.2^\circ$ and $6.6 \pm 2.9^\circ$ for SDComp and SIComp, re-

spectively. Those values were nearly half smaller than those of Kine cost and much smaller than those of Ener/Dyna costs. Repeated-measures ANOVAs indicated the significant differences in E_{Joint} between costs ($F(2.6,116.5)=112.1, p<0.001$). Post-hoc analysis revealed that the E_{Joint} of SDComp/SIComp were significantly smaller than those of three elementary costs but between the two composite costs there was no significant difference. Similar results were observed for E_{Cart} . The maximal deviations of simulated 3D finger paths from experimental ones were 5.1 ± 3.4 cm and 5.0 ± 3.2 cm for SDComp and SIComp respectively, while those of the three elementary costs were 8.9 ± 6.5 cm, 17.6 ± 9.2 , and 20.4 ± 4.5 cm for Kine, Ener and Dyna, respectively. Repeated-measures ANOVAs and Post-hoc analysis also showed significant differences in E_{Cart} between SDComp/SIComp and the three elementary costs but no significant differences between SDComp and SIComp. The chosen error was quite conservative given that it was based on maximal deviations. For the sake of comparison, the average deviation for the SIComp cost was 2.6 ± 2.0 cm, suggesting that average deviations were about half E_{Cart} in general. As such, this confirmed that the composite costs were significantly better to improve the goodness of fit by producing arm trajectories that matched quite accurately the recorded ones. Here, in order to visualize how well the simulated trajectories fit the empirical data, real and simulated arm trajectories using the uncovered speed-independent composite cost are plotted in Figure 3.6.

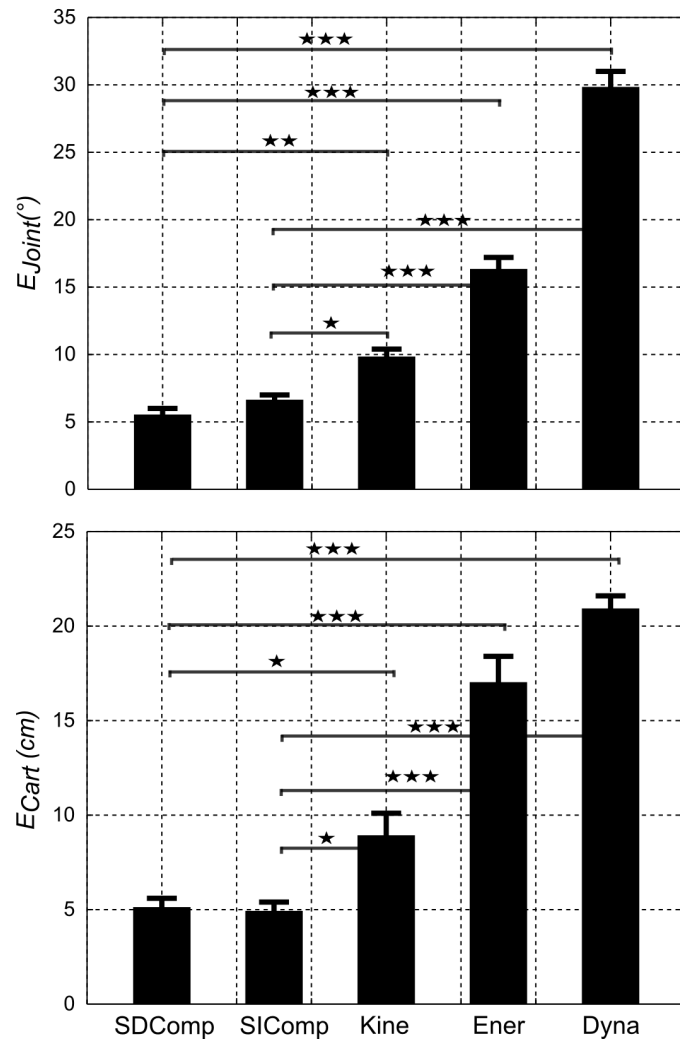


Figure 3.5. Reconstruction errors in joint space (E_{Joint}) and Cartesian space (E_{Cart}) for the best-fitting speed-dependent composite cost (SDComp) and speed-independent composite cost (SIComp) as well as each of the three cost elements taken separately, for the different speeds (S, N and F). Error values were averaged across subjects (with standard errors indicated by error bars). Noticeably, in terms of both joint and Cartesian errors, the composite costs (SDComp and SIComp) performed better than each elementary cost taken alone (Kine, Ener and Dyna). Horizontal bars with stars indicate the results of post-hoc analysis. One, two and three stars stand for $p < 0.05$, $p < 0.01$ and $p < 0.001$ respectively.

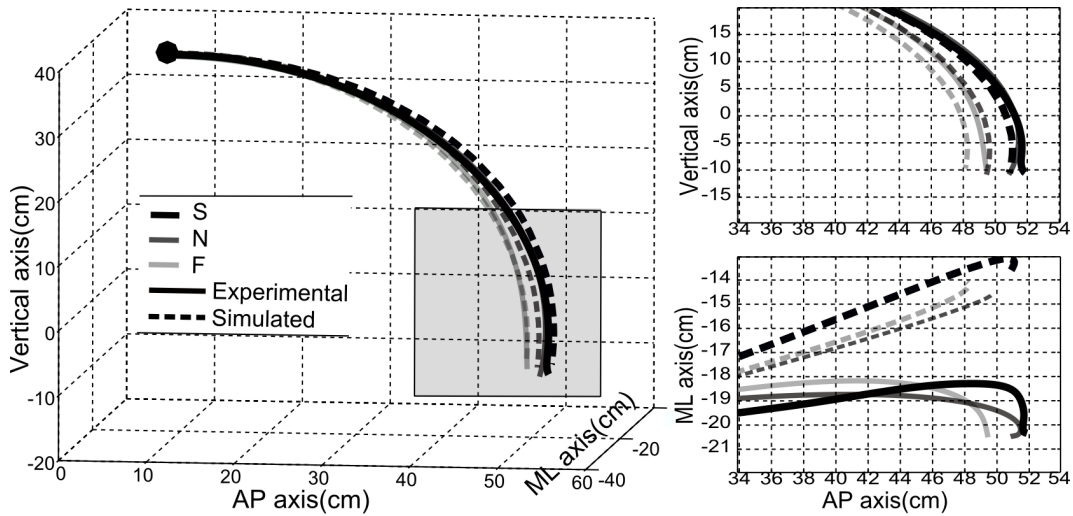


Figure 3.6. Simulated finger paths predicted from the best-fitting composite cost (SIComp) and average experimental finger paths for subject S5. *Left.* 3D finger paths for the three speeds for experimental (plain traces) and simulated (dotted lines) data. *Right.* The zoomed-in projections of finger paths on the sagittal plane (*top*) and the transverse plane (*bottom*) for the last part of the movement, in order to emphasize differences. In general, fitting errors mainly arose from the discrepancy of trajectories along the ML axis while along the AP axis (main axis of interest here), the simulated trajectories better matched the recorded ones and clearly exhibited a speed dependence.

Absolute and relative predictions of RE and e3 indexes across speeds. We quantified whether the identified composite costs could also replicate the movement parameters investigated above better than the elementary costs. The absolute reconstruction errors E_{RE} and E_{e3} for all examined costs are depicted in Figure 3.7. In terms of E_{RE} (top left panel), a visual inspection revealed a quite large difference between the value of Dyna cost with respect to the others, thus implying that the reach endpoints predicted by such a dynamical criteria were quite far from the recorded ones regardless of the speed. For the other costs, the two composite costs SDComp/SIComp obtained relatively smaller values than Kine/Ener costs. Indeed, those values of these two costs were approximately three times smaller than those of Kine cost and five times smaller than those of Ener cost. Repeated-measures ANOVAs and Post-hoc analysis confirmed significant differences of E_{RE} between the two composite costs (SDComp/SIComp) and the three elementary costs (Kine/Ener/Dyna) ($F(2.8,121.5)=81.3$, $p<0.001$), but no significant difference between SDComp and SIComp ($p=1.0$).

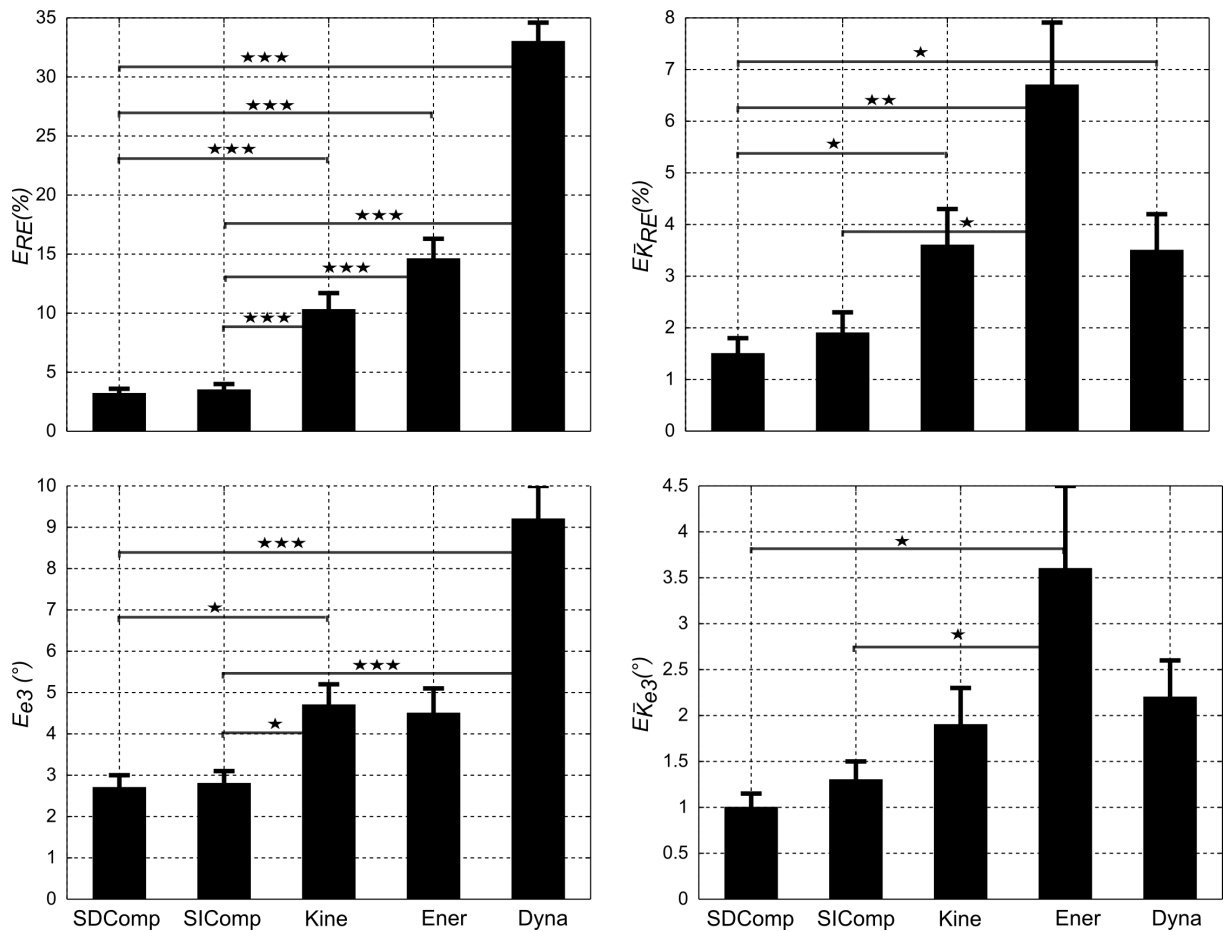


Figure 3.7. Reconstruction errors for some relevant movement parameters (E_{e3} , E_{RE} , $E_{\bar{K}e3}$, $E_{\bar{K}RE}$) for the SDComp, SIComp costs and the three cost elements taken separately. Error values were first averaged across speeds and then across subjects (with standard errors indicated by error bars). Visual inspection reveals that in terms of both E_{RE} and E_{e3} the dynamic cost performs quite poorly compared to the other costs. In terms of $E_{\bar{K}RE}$ and $E_{\bar{K}e3}$, the energy cost overestimates the speed dependence of RE and e3 parameters. Overall, the kinematic cost performs relatively well but the composite costs perform significantly better than the latter. Importantly, the kinematic cost is also unable to account for any speed-dependence as it predicts constant movement parameters for all speeds. Finally, no significant difference was found between the SDComp and SIComp.

A similar analysis was carried out for e3 index (Figure 3.7, bottom left panel). In agreement with the above results, a large difference for E_{e3} between Dyna cost and the others were still observed. Between composite costs (SDComp/SIComp) and the two elementary costs (Kine/Ener), the E_{e3} differences were smaller (approximately two third of the values for Kine/Ener costs). However, repeated-measures ANOVAs and Post-hoc analyzes still

indicated significant differences for E_{e3} between SDComp/SIComp and the three elementary costs ($F(2.2,95.9)=17.7$, $p<0.001$). Between the two composite costs, no significant difference was observed ($p=1.0$).

In order to assess whether costs could reproduce the speed-dependence (or independence) exhibited by each subject for e3 and RE indexes, the prediction of slopes given in Table 3.3 was investigated. The right panels in Figure 3.7 shows the errors $E_{\bar{K}_{RE}}$ and $E_{\bar{K}_{e3}}$. In terms of RE index, it appeared that the Ener cost were quite large (about 2 times larger than Kine/Dyna and 3times larger than SDComp/SIComp), thus implying that the Ener cost tended to overestimate the speed-dependence of arm trajectories across subjects. Among the other costs tested, the Kine and Dyna costs obtained quite similar slope errors but these values were larger than those of SDComp/SIComp. Repeated-measures ANOVAs and Post-hoc analysis showed significant differences between the $E_{\bar{K}_{RE}}$ of SDComp and Kine/Ener/Dyna ($F(2.4,33.8)=4.7$, $p<0.05$) but no significant difference between SDComp and SIComp ($p=1.0$). Similar observations were obtained for $E_{\bar{K}_{e3}}$. Repeated-measures ANOVAs and Post-hoc analysis showed a significant difference between SDComp/SIComp and Ener cost ($p<0.05$). However, between SDComp/SIComp and Kine/Dyna, we did not observe any significant distinctions. Between SDComp and SIComp, again no significant difference was observed.

In summary, our results showed that only composite costs could reproduce both the absolute and speed-relative behaviors of the 15 participants. Furthermore, no significant gain was found when tuning the weights of the composite cost according motion speed compared to the assumption of a speed-independent composite cost. But if each subject relies upon an idiosyncratic composite cost function, a question remains about how to explain the emergence of speed-dependent and speed-independent arm trajectories. This issue is addressed hereafter.

Idiosyncrasy of composite costs On average, composite costs were $\alpha_1 = 4.84 \times 10^3 \pm 3.15 \times 10^3$ and $\alpha_2 = 0.46 \times 10^2 \pm 0.43 \times 10^2$, but these weights varied across participants and appeared to be crucial to account for the arm trajectories across speeds. For instance, the coefficients characterizing the best-fitting composite cost for S5 was $\alpha=[1, 4.23 \times 10^3, 0.43 \times 10^2]$ and was $\alpha=[1, 2.71 \times 10^3, 0 \times 10^2]$ for S14. To get a more representative account of these costs, the contribution of each element was computed (see Materials and Methods). This analysis revealed that the Kine cost contributed on average across speeds and subjects

to $80\pm 15\%$ of the total cost while the Ener and Dyna costs were about $6\pm 5\%$ and $13\pm 12\%$ respectively. Although small, the previous analyses suggested that these contributions of energetic and dynamical costs were crucial to replicate the speed-dependences observed several subjects. Yet, although they used a composite cost, some other subjects did not exhibit speed-dependent behaviors.

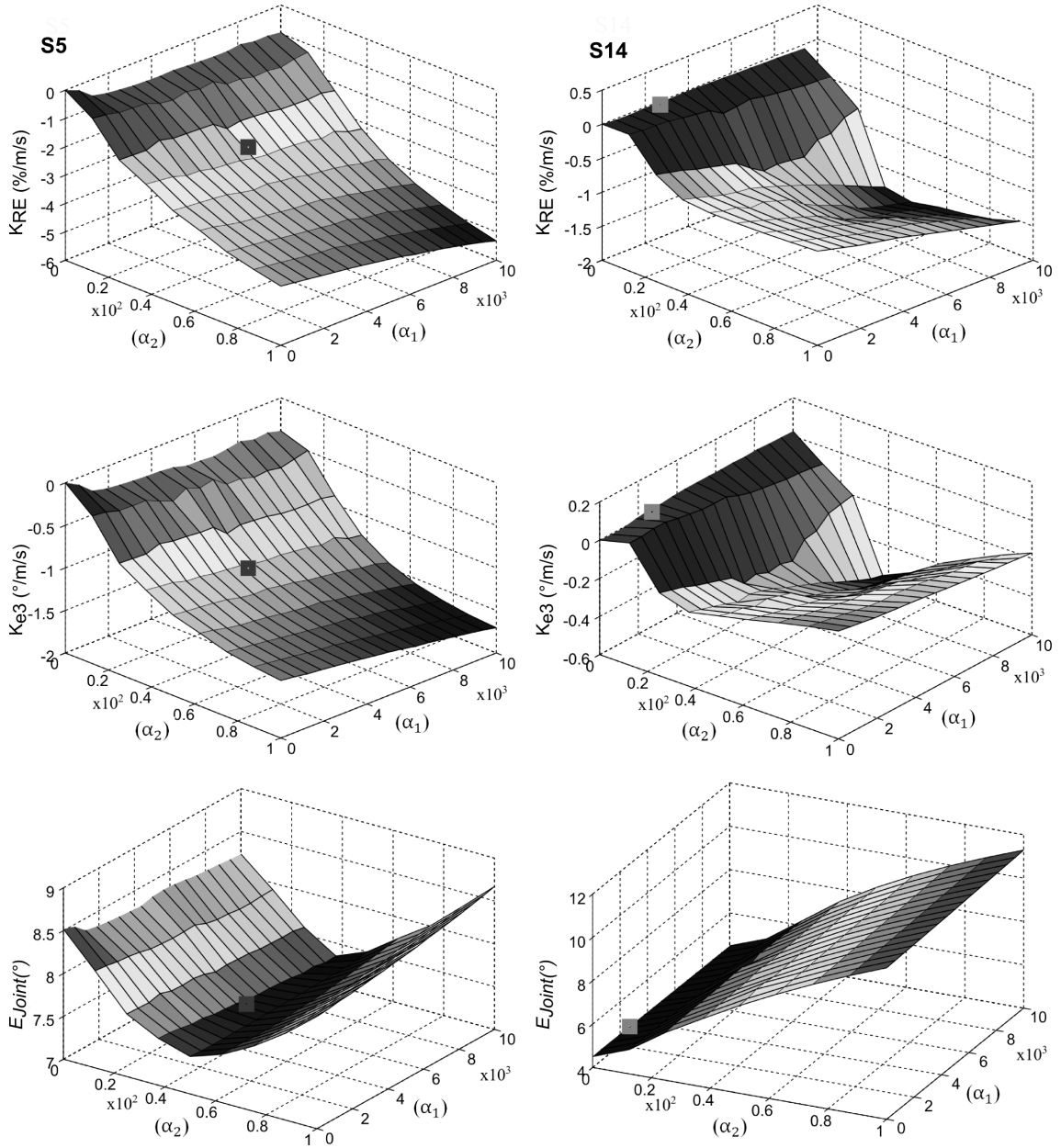


Figure 3.8. 3D plots of K_{RE} , K_{e3} and E_{Joint} for the two typical subjects S5 (*left*) and S14 (*right*) as a function of the weights of the composite cost $C(\alpha)$. In these graphs, α_1 and α_2 were varied to visualize how the speed dependence as well as the error minimized during inverse optimal control varied according to the chosen weights. Remind that $C(\alpha) = C_{Kine} + \alpha_1 C_{Ener} + \alpha_2 C_{Dyna}$. The squares indicated on each 3D plot show the position of the best-fitting speed-independent composite cost (SIComp) found during inverse optimal control. S5 and S14 have different anthropometric characteristics. Interestingly, by choosing appropriate α_1 and α_2 weights, subjects could exhibit different degree of speed dependence (almost zero K_{RE}/K_{e3} or negative K_{RE}/K_{e3}). For example, S14 could have been speed dependent if he/she chose a different cost combination (but this was not uncovered here because his/her trajectories were not compatible with such a cost function).

To better understand the role of the weights onto the speed-dependence of arm trajectories for each subject, we varied the energetic (α_1) and dynamic (α_2) coefficients of the composite cost ($C(\alpha) = C_{Kine} + \alpha_1 C_{Ener} + \alpha_2 C_{Dyna}$) and evaluated the speed-dependence of trajectories predicted from forward optimal control simulations. The resulting slopes K_{RE} , K_{e3} and joint space fitting error E_{Joint} (the minimized quantity during inverse optimal control) for the two subjects S5 (*left*) and S14 (*right*) were computed and depicted in Figure 3.8. It is noteworthy that these two subjects had different anthropometric parameters, thus allowing to test whether anthropometric discrepancies could explain differences in speed sensitivity at fixed composite cost. For both subjects, the patterns of K_{RE} and K_{e3} were relatively similar but the speed-dependence of S5 appeared to be much larger in terms of magnitudes. This implied that if both subjects had use the same composite cost, S5 would intrinsically appear to be more speed-dependent than S14 just because of anthropometric peculiarities. On the other hand, by changing the weights of the composite cost, subject S5 had the possibility to be more or less speed-dependent. Similarly, subject S14 could be speed-dependent if increasing the weights of the energy and dynamic coefficients. Nevertheless, this would have changed their arm trajectories (and the minimum in E_{joint} graphs) and this is why it was not found by the inverse optimal control algorithm in the present data.

In summary, these 3D plots show that anthropometry partly explains why a given composite costs may lead to differences in terms of speed dependence of behaviors. However, the composition of composite costs was clearly idiosyncratic, thereby implying that different arm trajectories also emerged across subjects because of differences in the weighting of kinematic, energetic and dynamic variables.

Discussion

In this work, we examined the nature of motor planning variables during free-endpoint arm reaching task. Three-dimensional arm movements without a prescribed reach endpoint location were investigated and how speed instructions affected the chosen arm trajectories was measured. The experimental results showed that the reach endpoint (RE) and rotation axis displacements (e3/SE) significantly varied with speed to an extent that depended on individual factors. These idiosyncratic behaviors were accounted for in the framework of optimal control as the outcome of the minimization of a cost weighting kinematic, energetic and dynamic variables. The latter quantities were assumed to represent (a priori) internal values guiding motor decision within the brain and were essentially found to be subject-specific but speed independent. These results are discussed in more details hereafter.

Unrestrained 3D arm trajectories: speed dependence or independence

Our findings revealed significant speed-related changes in both arm trajectories during the free 3D arm movements under consideration, which contrasts with classical conclusions drawn in point-to-point movement studies. Whether the brain controls movement using speed-sensitive or speed-insensitive planning strategies is a long-standing issue in motor control. The term speed-insensitive is used when prominent aspects of the motor strategy (e.g. hand path, time-course of velocity or acceleration) remain invariant in spite of speed differences and/or when simple scaling rules apply to the motor patterns. This question has been extensively investigated for horizontal or vertical planar point-to-point 2D movements ([Flash and Hogan, 1985](#); [Ostry et al., 1987](#); [Gordon et al., 1994](#); [Soechting and Lacquaniti, 1981](#); [Soechting et al., 1995](#); [Atkeson and Hollerbach, 1985](#); [Flanders et al., 1996](#)). In those seminal studies, hand paths were generally considered as straight or slightly curved and velocity profiles bell-shaped regardless of motion speed, as if a scaling law applied to an unique movement pattern. Finer analyzes however revealed that the timing of velocity profiles was significantly affected by the speed at which movements were executed ([Papaxanthis et al., 1998, 2003](#); [Nagasaki, 1989](#)), in agreement with the well-known fact that deceleration duration increases when maximal accuracy and speed are together required, such as in Fitts'-like experiments ([Woodworth, 1899](#); [Elliott et al., 2001](#);

Fitts, 1954; MacKenzie and Iberall, 1994). Even in those such settings, however, the shape of hand paths was widely accepted to be speed-invariant. Further studies extended planar point-to-point reaching paradigms to the 3D case to better tackle the speed-dependence question and lead to the conclusion that, given an initial arm posture and a final target position, neither the final arm posture nor the hand path curvature depended significantly on movement speed (Nishikawa et al., 1999; Zhang and Chaffin, 1999). This lack of significant differences may have been due to the specification of a precise target to reach to, which could have limited the expression or the finding of speed-dependent arm trajectories. Indeed our protocol defined looser task constraints in terms of the final hand position, which may be the reason why the reach endpoint as well as certain joint displacements depended significantly on the motion speed. Dealing with tasks involving undefined reach endpoints is nevertheless ecological and occurs in many tasks. For example catching a ball (e.g. Cesqui et al., 2012) is a task involving an infinity of possible reach endpoints along the ball's trajectory. The existence of differences between constrained and unconstrained tasks was already noticed in Desmurget et al. (1997). The speed dependence found here for discrete movements is also consistent with what Isableu et al. (2009) observed during a cyclical yet comparable arm movement task in which a similar speed-dependent tuning of motor strategy was observed for some subjects. To account for the experimental arm trajectories, we had recourse to inverse optimal control as it makes hypotheses about the nature of the variables possibly relevant to motor planning.

Motor planning variables: kinematic, energetic, dynamic or composite

The above issue about the speed dependence of motor strategies is actually tightly linked with the nature of hypothetical cost functions involved in motor planning, as already noticed in Soechting and Flanders (1998). The former problem actually gains at being rephrased within the normative framework of optimal control as it simplifies both its formulation and analysis. Indeed, analyzing the subjects' behavior in terms of cost functions instead of a bunch of 3D arm trajectories can be seen as a dimensionality reduction since a cost function summarizes the spatiotemporal characteristics of an infinity of joint trajectories at once (see Berniker and Kording, 2015). In the optimal control context, the issue of kinematic versus dynamic motor planning has been the topic of several investigations

(Wolpert et al., 1995a; Flanagan and Rao, 1995; Soechting et al., 1995; Soechting and Flanders, 1998; Vetter et al., 2002; Hermens and Gielen, 2004). Here, solely optimizing an energetic or a dynamic criterion was not adequate for replicating the basic features of arm trajectories: the reach endpoints and the final postures were just too discrepant with the data (see Fig. 3.7). In contrast, optimizing a kinematic cost performed quite well at a first sight. Accordingly, it was found to be the primary cost accounting for the arm displacement of subjects and the dominant humeral rotations. Rotations around the humeral axis (i.e. SE axis) were interpreted in Soechting et al. (1995) as cues of a planning of energetically efficient arm trajectories but the present task shows that strictly rotating around the humeral axis was not energetically optimal (at least when energy expenditure is measured by the absolute work of muscle torques and not as the peak of positive work as in Soechting et al., 1995). The kinematic cost was however not appropriate if one considers the speed-dependence of behaviors. Indeed, such a kinematic cost predicts invariant patterns of joint trajectories when speed varies. Hence, speed does not affect hand path in such models, which was not compatible with the behavior of most participants. From a computational standpoint, kinematic models may be appealing as they do not require new inverse internal model to extract adequate motor commands matching a wide range of velocities. Indeed, taking gravitational and frictional torques apart, the structure of rigid body dynamics is such that movements of different speeds can be generated from a single torque pattern τ despite the non-linearity of the arm dynamics by means of a simple scaling law of the type $\tilde{\tau}(t) = r^2\tau(rt)$ (see Hollerbach and Flash, 1982 for details). More generally, any strategy relying on such a spatiotemporal rescaling of a reference torque pattern (be it initially based upon kinematic, kinetic or any composite optimality criteria) would yield the same hand paths and final postures. Even though experimental evidence was provided for a separation between tonic versus speed-related phasic muscle activity during point-to-point motor tasks (Flanders and Herrmann, 1992; Flanders et al., 1996), the fact that the reach endpoints or other parameters depended significantly upon speed in our data made impossible such a basic scaling principle. The systematic and consistent speed-dependent changes of arm trajectories observed in the present study rather supported the existence of a composite cost underlying the formation of arm trajectories for the range of speeds under consideration. Furthermore, geometric models such as the geodesic model (Biess et al., 2007) would not be able to account for these experimental findings as they hypothesize a decoupling between the geometric and temporal properties of movement, which is at

odds with our experimental findings. Therefore, taken together, our findings revealed the composite nature of the cost function underlying arm movement. These findings extended those found for planar motion in [Berret et al. \(2011a\)](#). Other studies using a different motor task (landing after a vertical jump) reached very similar conclusions about the combination of energetic/dynamic criteria with other factors such as comfort or smoothness ([Zelik and Kuo, 2012](#); [Skinner et al., 2015](#)).

Flexibility of the composite optimality criterion

Within the theory of composite cost functions, there exist intriguing questions pertaining to the degree of flexibility of the combinations. In particular, whether speed affects or not the way elementary costs are weighted was an open question. If results indicate that kinematic, energetic and dynamic costs must be combined to fit the data to the greatest possible extent, the relative relevance of each of these quantities may differ as their order of magnitude also vary with speed. It could be possible that at large speeds, limiting angular jerk because more important than minimizing energy expenditure. In [Berret et al. \(2011a\)](#), arm trajectories starting from several initial postures were studied and a single composite cost was assumed to account for movements starting from all positions at once. However, the study only considered a single movement pace, namely a quick speed. Thus, whether a single combination of costs would also be valid for movements performed at various speeds was uncertain even though, within the composite cost hypothesis, understanding the extent to which the weights depend on external or internal factors seems crucial. The question is also relevant when attempting to predict the pace of natural movements ([Shadmehr, 2010](#); [Shadmehr et al., 2010](#); [Berret and Jean, 2016](#)). In these works, a cost of time was assumed to be combined with trajectory costs (i.e. the subjective costs studied here) and other objective costs. How speed instructions affect such mixtures of costs is not clear especially if the exact nature of the trajectory costs changes with speed instructions. When instructed a subject to move fast or slow, which weights are exactly modified is hard to identify in general. Here we addressed this problem (without considering the cost of time as it does not matter when movement time is taken directly from experimental data as we did here) and assessed whether the weights depended or not on the instructed speed. Our results supported the fact that the speed dependence of arm trajectories of each participant could be accounted for by a unique composite cost (i.e. with invariant

weights). Indeed, no significant gain was found when tuning the weights according to the instructed speed. This is especially if one considers the addition of new fitting parameters when doing so. Following Occam's razor principle, we could not retain the more complex model consisting of adjusting the weights according to movement speed. While we cannot exclude that the weights of objective costs such as accuracy or precision did not change when speed increased because we did not model sensorimotor noise, our conclusions only concern the subjective optimality criterion. Simulations conducted within the stochastic optimal control framework would be required to address such questions (Todorov, 2006), but the numerical tools are not as advanced as in the deterministic settings and therefore treating the stochastic case was not considered. We cannot exclude neither the existence of other subjective costs (there is infinity of movement-related costs and other costs less quantifiable such as discomfort, pain, gracefulness etc.) but the present findings nonetheless argued for a subject-specific composite nature of motor planning variables. It could still be argued that the participants exhibiting the strongest speed dependences of arm trajectories simply suffered from inaccurate sensorimotor control, which would just be emphasized at large speeds. However, the consistency of speed-related fluctuations across trials for these participants tends to disagree with this hypothesis. Moreover, the CNS is known to have good capabilities to predict and anticipate interaction torques (Gribble and Ostry, 1999) and the inertial anisotropy of the human arm (Gordon et al., 1994; van Beers et al., 2004) during motor planning as well as gravity (Berret et al., 2008; Gaveau et al., 2011a, 2014). Therefore, rather than interpreting their behaviors as the realization of inefficient motor control, we instead interpret them as the outcome of efficient motor control, which may be the signature of a composite cost proper to each individual.

Inter-individual differences

Interesting inter-individual differences were pointed out throughout the study, especially with respect to speed instruction. Motivated by applications in neuro-rehabilitation, neuro-prosthetics and related areas, the study of inter-individual differences has developed as a hot topic of research in recent years. Many researchers tried to find whether idiosyncrasy arises from a peripheral or central origin and tried to elaborate on principles that could account for them. In this vein, initial assumptions were related to a different involvement and exploitation of frames of reference (e.g. visual versus kinaesthetic) and to changes

from one frame of reference to another with respect to execution speed (Pozzo et al., 1991; Bernardin et al., 2005; Isableu et al., 2003). Recently, Isableu et al. (2009) provided evidence of individual differences in a task where cyclical 3D arm movements were experimented. These authors showed that different subjects moved preferentially around different rotation axes: some participants always rotated their arm around the geometrical articular axis (termed as “kinematicians”) or around the minimum inertia axis regardless of speed (termed as “dynamicians”) while other switched from the geometrical to the minimum inertia axis when movement speed increased. It was proposed that these rotational axis preferences could originate from prior sensorimotor strategies experienced by the subjects. These strategies indeed allowed subjects to differentially exploit the dynamical arm properties and the passive torques (e.g. interaction or gravity torques) in order to minimize the inertial resistance as well as the muscle torque input to the movement. It is however hard to separate differences due to anthropomorphic or peripheral specificity from those arising from different motor planning principles. The current results thus extend these previous findings for a discrete task and refined them within the context of optimal control. In particular, our results further showed that the subject-specific motor strategies actually correspond to different subjective composite costs. In fact, optimal control simulations take into account the anthropometric characteristics of each participant and if differences between subjects could be explained by such body-related peculiarities then the same composite cost function would have been identified using inverse optimal control. Since different subjects appeared to weight very differently the cost elements, our results rather argue in favor of divergences in the central representation of movement and the subjective values actually attributed to the motor task (smoothness, mechanical energy, muscle torques...). The importance of individual factors when the task constraints are loose, as during such a free-endpoint reaching task, was already pointed out by Cesqui et al. (2012) in a ball catching task. In this task, equally successful yet very different motor solutions were adopted by subjects. We showed that such different solutions were not fully due to musculoskeletal discrepancies across participants but may rather reflect different subjective costs that can operate vicariously. More precisely here our results revealed that the subjects who presented relatively invariant trajectories generally relied upon a kinematic objective or a combination of kinematic and a small amount of energetic objectives regardless of speed (Fig. 3.8), while other participants who presented a change of trajectories often relied upon a combination of kinematic, energetic and dynamic objectives.

Depending on the composite cost chosen, varying the anthropometric characteristics could change the degree of speed-dependence of an individual. On the other hand, for fixed anthropometric characteristics, the relative weights defining the composite cost were critical to explain the degree of speed-dependence of each participant, which proved that inter-individual differences were not only due to anthropometric divergences but also to central factors. These factors may be encoded and traded-off through the cortex-basal ganglia network (e.g. [Scott, 2004](#); [Turner and Desmurget, 2010](#) for reviews) where these variables shaping arm movement trajectories would be valued and might guide motor planning in terms of objective and subjective costs or rewards.

Research limitations

One could wonder whether the reconstruction errors we obtained are small enough to conclude that the composite cost really constitutes a high-level representation of motor planning objectives. It is indeed undeniable that there might still exist a more universal cost accounting better for the present experimental data. Finding such a ubiquitous cost function would be appealing for motor control but what would be its nature and shape is still an open question. Thus far, the existing literature has reported the relevance of several cost functions in the exact same way that neurophysiological studies have reported cortical representation of a large variety of movement-related parameters ranging from kinematic (spatial or nonspatial) to dynamic or muscular. Therefore, assuming composite cost functions is a solution compatible with previous findings that may moreover reconcile prior computational and empirical studies. Within this composite cost hypothesis, knowing which elementary cost should be included may nevertheless be tricky as candidate costs are numerous. The situation is even more complex with regards to the number of DoFs of the system. Precisely, any cost such as the angle jerk is intrinsically composite since different weights could be attributed to different DoFs. In general, researchers have assumed that all those weights are equal to one (including in the present study) for the sake of simplicity but one can easily imagine that such weights actually vary across DoFs. Throughout our analyses, we thus conducted supplementary tests to evaluate whether reconstruction error could be improved by (i) adding other elementary costs or (ii) tuning the weights of the kinematic, energetic and dynamic costs for each DoF separately. To test (i) we added costs such as acceleration, geodesic and muscle torque as in [Berret et al. \(2011a\)](#). In this case,

the best-fitting speed-independent composite cost yielded maximal Cartesian deviations (i.e. E_{Cart} values) of 4.3 ± 2.6 cm, which is not much smaller than when dealing with three costs as we did in our study. Hence the three costs we retained in the current study were quite relevant to account for the present data. This was confirmed when looking at (ii). When we allowed optimization of the weights associated to each DoF separately we found E_{Cart} values of 3.1 ± 2.1 cm. Compared to the 5 cm in our main results, the improvement seems notable even though this approach required 11 variables to be adjusted during the inverse optimal control process (instead of 2 otherwise). This finding suggests that a fine tuning of the weight at each DoF would allow a better replication of the real arm trajectories. However, this approach would drastically complicate the analysis unless one groups the weights according to the underlying type of cost, i.e. kinematic, energetic and dynamic, as we eventually did here. As such, these considerations show that our main conclusions about the compositeness and speed-dependence of optimality criteria would not differ if choosing slightly different modeling approaches.

3.3 Compensation/Exploitation of interaction torque and its links to cost function

Adaptive use of interaction torque during arm reaching movement from the optimal control viewpoint

Van Hoan Vu, Brice Isableu, Bastien Berret

This article is submitted to the Scientific Reports journal

Abstract

The study aimed at investigating the extent to which the brain adaptively exploits or compensates interaction torque (IT) during movement control as a function of velocity and load constraints. Participants performed free end-point reaching movements at slow, neutral and fast speeds and with/without load attached to the forearm. Experimental results indicated that IT overall contributed to net torque (NT) to assist the movement and that such contribution increased with limb inertia and instructed speed. We interpreted these results within the (inverse) optimal control framework, assuming that the empirical arm trajectories derive from the minimization of a certain, possibly composite, cost function. Results indicated that a mix of kinematic, energetic and dynamic costs was necessary to replicate the participants' adaptive behavior at both kinematic and dynamic levels. Furthermore, the larger contribution of IT to NT was associated with an overall decrease of the kinematic cost contribution and an increase of its dynamic/energetic counterparts. Altogether, these results suggest that the adaptive use of IT might be tightly linked to the optimization of a composite cost which implicitly favors more the kinematic or kinetic aspects of movement depending on load and speed.

Introduction

Human movement control is a complex process partly due to the non-linearity induced by the pluri-articulated nature of the skeletal system. Motion in the body structure leads to the emergence of interaction torque (IT) between segments (e.g. action of the forearm onto the upper-arm) but also within a segment (e.g. among the 3 main degrees of freedom of the shoulder joint for the upper-arm in 3D). Such coupled nonlinear dynamics implies that motion at one degree of freedom (DoF) may induce significant motion at the other ones. This property requires the central nervous system (CNS) to rely on effective computational and neural principles for accurately controlling movement even for simple daily living tasks such as putting a cup of tea on your desk while reading those lines. Coping with IT is therefore a critical issue for the CNS and adaptively using it may contribute to motor efficiency by lowering the amount of muscle torque (MT) required to achieve a given task. In contrast, its inadequate use or inefficient exploitation may amplify sensorimotor noise throughout the kinematic chain or lead to greater energy expenditure. Interestingly, a large body of evidence has suggested that the CNS has ability to estimate and anticipate IT via internal models of the limbs' dynamics (e.g. [Ghez and Sainburg, 1995](#)) (but see ([Buhmann and Di Paolo, 2014](#)) for an alternative view based on equilibrium-point theory). In this study, we will rely on the internal model hypothesis and hypothesize that the CNS has some form of knowledge about IT at the motor planning stage. In this view, we may devise two extreme options. On the one hand, the “compensation” hypothesis assumes that IT is canceled itself out during motor planning ([Hollerbach and Flash, 1982](#); [Sainburg et al., 1995, 1999](#); [Bastian et al., 1996](#); [Gribble and Ostry, 1999](#); [Simoneau et al., 2013](#)). On the other hand, the “exploitation” hypothesis assumes the brain can actually utilize IT to generate motion at other DoFs without dedicated muscle effort at those DoFs ([Sainburg and Kalakanis, 2000](#); [Hirashima et al., 2003, 2007](#); [Dounskaia et al., 2002](#); [Dounskaia, 2005](#); [Debicki et al., 2010, 2011](#); [Hore et al., 2011](#); [Asmussen et al., 2014](#)). The solution used by the brain may also lie in-between. Arguably, the extent to which the CNS actually exploits IT should be reflected in the adaptability of arm trajectories with respect to speed and load changes as IT strongly depends on such factors. Hence the purpose of this study was twofold: (i) evaluate whether the CNS adaptively exploits (or systematically compensates) IT during unrestrained 3D arm movements, and (ii) identify normative principles that may account for how the CNS copes with IT during motor planning.

To this aim, we investigated a free 3D arm pointing task and modelled it using optimal control theory. The rationale of our approach was as follows. First, to let emerge motor strategies revealing IT exploitation or compensation strategies, subjects were asked to perform movement without a prescribed reach endpoint. Precisely, we considered 3D arm pointing movements to a planar target. This laboratory task can be thought as similar to pushing a door to open it or throwing a ball to a target (since the ball can be released at any point in space to achieve the task) or the cup of tea example given above: in all these tasks, there is no unique final hand position to achieve the task (Berret et al., 2011b, 2014). It is worth noting that the present task still imposed accuracy constraints forcing participants to spatially control their end-effector along the vertical direction in order to reach the goal (i.e. the plane here) but, importantly, it gave more freedom to the participants than if a target point was assumed instead. Therefore, participants still had to take into account IT during planning or execution to achieve the task just as in classical point-to-point reaching tasks. Considering 3D motion was also critical as the nature of IT strongly differs between 2D and 3D movements (IT only exists between segments in 2D due to parallel rotation axes). Second, to better characterize the role of IT, we varied both the inertia (addition of a load to the forearm) and the speed (slow/fast verbal instructions) as the shape and magnitude of IT critically depends on those factors. We predicted that, if IT is exploited (even partially), the inter/within-segment ITs should contribute more significantly to trajectory formation and torque profiles when inertia and/or motion speed are large. Alternatively, if IT is compensated, such modifications should have no effect on the arm trajectories, except that the MTs should be adjusted to cancel the larger ITs. Third, we aimed at accounting for the empirical pointing strategies via inverse optimal control with composite cost functions (Gielen, 2009; Berret et al., 2011a; Vu et al., 2016). Optimal control theory is an appealing framework to apprehend human motion as it points out possible high-level principles underlying arm movement formation in a concise and normative way (Todorov, 2004; Berniker and Kording, 2015). Here, kinematic costs are typically associated with a “compensation” strategy because they ignore IT during motor planning while energetic and dynamic costs conceivably fall within the “exploitation” category as they take into account IT at the planning stage. To the best of our knowledge, it is the first time that the role of IT on 3D human motion is interpreted from the (inverse) optimal control viewpoint. We hypothesized that any adaptive compensation/exploitation trade-off of IT could be associated to the minimization of composite cost mixing kinematic, dynamic or energetic

quantities.

Materials and Methods

Ten right-handed subjects (5 men) agreed to participate in the study. All of them were healthy and ignorant of the goal of the scientific work. Age, weight and height (mean \pm std) were 27 ± 5 years, 67 ± 10 kg and 168 ± 7.8 cm, respectively. All subjects were made aware of the protocol and written informed consents were obtained before the study. Experimental protocol and procedures were approved by the Univ. Paris-Sud EA 4532 local Ethics Committee and carried out according to the ethical guidelines conforming to the Revised Helsinki Declaration of 2000.

Experimental task

In the present study, we used a “manifold reaching” paradigm quite similar to the experiment described in the work of (Vu et al., 2016). Briefly, participants sat comfortably on a chair and were asked to perform pointing movements with their right (dominant) upper limb to an horizontal planar target (Fig. 3.9). Participants were asked to stop their motion when their index fingertip was onto the target but without striking it. They started from an initial “L-shape” arm configuration where the elbow was approximately flexed at 90 degrees with an upper arm abducted to the horizontal and aligned with the mediolateral direction; this starting posture was realized in practice by asking the participants to put their fingertip at a reference point whose position was adjustable in space. In this way, the initial arm joint configuration was kept similar across participants. Free rotations at the shoulder and elbow joints were allowed while the wrist joint was constrained by a light bar to freeze its motion and simplify subsequent modeling. The trunk was fixed and attached to the chair. The planar target consisted of an horizontal foam-made surface positioned just below the participant’s chest on a table (about 17.5 cm below the shoulder on average). Participants could reach anywhere on the surface without moving the shoulder and the maximal distance they could reach to was limited by their arm’s length and shoulder’s height with respect to the planar target. The size of the foam-made surface was 40 cm in the ML axis and 65 cm in the AP axis and placed to the right hemibody. During movement execution, participants were asked to gaze a reference point placed straight on

the wall in front of them. Importantly, no specific instruction about the reach endpoint was given in this task and the participants were free to choose their preferred final hand position as long as it lay on the planar target. As such, the task was redundant because an infinity of reach endpoints were compatible with task achievement as well as an infinity of final joint configurations. Here the goal of the task was to control the fingertip error along the vertical axis and it mostly involved four degrees of freedom (DoF) of the arm: three at the shoulder joint and one at the elbow joint (the elbow pronation/supination was neglected because of its minor role in a pointing task). Therefore, the set of permissible joint configurations lay on a 3-D manifold (4 joint angles minus 1 equation for the plane constraint).

For the purpose of this study, three speed conditions and two load conditions were investigated. We used a block design for the load. The three speeds, slow, natural and fast and denoted by S, N and F respectively, were randomized across trials to prevent habituation and memorization effects when subjects switched from one speed to another. Load conditions were counterbalanced across subjects. At the beginning of each trial, participants were verbally instructed about the imposed speed by the experimenter (and no feedback was given about their actual speed except if their speed was clearly erroneous). We first recorded a block of 45 trials without load attached to the participant's forearm (no-load condition, 15 trials per speed). In the second block of 45 trials, we attached a load approximately to the center of mass of the forearm (load condition). The load was a thick-walled cylindrical tube whose inner/outer radius was adjustable with respect to the subject's forearm size. The tube's mass was set equal to 0.4, 0.6 or 0.8kg, depending on the weight of the subjects whose values were smaller than 56kg, between 56-65kg or larger than 65kg, respectively. These individual settings were introduced to adjust the arm dynamics modification to the participant's actual weight. Before the experimenter started to record, participants trained for 30 trials familiarize with the pointing task (both no- and with- load conditions). During this process, their performance was visually checked by the experimenter who made sure that the initial arm postures were consistent across trials, that the gaze was directed towards the requested location during movement execution, that speed differences were clearly marked (i.e. S, N and F) and, finally, that subjects stopped their one-shot movements accurately enough on the planar target. Note that adaptation to a load has been previously shown to be very fast in reaching studies (a couple of trials (?)) and hence these training trials were assumed to be enough for the participants to reach a

stable level of performance before the true experimental recordings began. In summary, for each participant, 15 trials were tested per experimental condition (no-load/load, S/N/F speeds), such that 90 trials were recorded and analyzed per participant. In total, 900 trials were therefore analyzed in this study.

Data Recording

The motion kinematics was recorded at a frequency of 500Hz by using a 8-camera optical motion capture system (Vicon Inc. Oxford, UK). A total of 13 plug-in-gait markers were attached to specific anatomical locations on the dominant arm and other parts of the body as follows: seventh cervical vertebrae, 10th thoracic vertebrae, clavicle, sternum, right and left acromion, lateral and medial humeral epicondyles, ulnar and radial styloids, 2nd and 5th metacarpal heads and 1st finger tip. Noise was filtered out from the recorded positions of the markers by using a 2nd-order Butterworth low-pass filter at 10Hz. These 3D positions were then analyzed at kinematic and dynamic levels using a custom-written software in Matlab (Mathworks, Natick, MA), as detailed in the sequel.

Kinematic analysis

Hand kinematics. For each trial, the 3D positions of the fingertip marker were numerically differentiated to obtain the endpoint velocity profile. Based on this velocity profile, the movement duration was estimated as the largest time interval where the velocity is above 5% of its maximal value. Other hand kinematic parameters relevant to the purpose of the present study (e.g. reach endpoint, curvature, vertical accuracy/precision errors) were then calculated, as follows:

- *Index of path curvature (Cur).* The index Cur was computed as $Cur = Dmax \hat{A} \check{D}Disp$ where $Dmax$ is the maximal deviation of the finger from the straight line connecting the initial to the final finger position during the movement and $Disp$ is the length of the latter Euclidean distance.
- *Reach endpoint (RE).* The RE was defined as the 3D coordinates of the fingertip position at the end of the reach, namely the anteroposterior (AP, X axis), mediolateral (ML, Y axis) and vertical (Vert, Z axis) coordinates relative to a frame centered at the shoulder joint. In the present study, the Z-coordinate of the RE was used to

quantify accuracy and precision of the pointing movement (as the target plane was defined by an equation $Z=\text{constant}$). In contrast, the X- and Y- coordinates of the fingertip were freely chosen by the participants, and therefore, were used to assess the reaching strategy selected by the subjects and not pointing errors. When relevant, a normalized RE position along the AP axis (RE_{AP}) was used in the analyses. It was defined as the ratio between the AP coordinate of the RE and its maximum possible value (attained when the subject fully extended the arm, without moving the trunk).

- *Vertical accuracy/precision error calculations* (Za and Zp indexes). The constant error (Za) was defined as the averaged distance from the final fingertip position to its vertical projection on the planar target, while the variable error (Zp) was defined as the standard deviation of reach endpoint positions in the vertical direction across trials, within one experimental condition. The examination of Za and Zp allowed verifying the extent to which subjects stopped their movements in the vicinity of the target plane as required.

Joint kinematics. The joint kinematics (e.g. angular displacements, velocities and accelerations) was estimated based on a method previously described in (Isableu et al., 2009) and (Vu et al., 2016). Local coordinate systems was built from the markers in agreement with the guidelines of the international society of biomechanics (ISB). From the relative orientation of the coordinate systems, rotation matrices and then Euler angles (namely internal/external, elevation/depression, ulnar/radial at shoulder and extension/flexion at elbow) were calculated. At last, the joint speeds and accelerations were evaluated via numerical differentiations.

Dynamic analysis

In order to examine the effect of load and speed on the dynamics of the reaching behavior, a dynamic model of the arm was introduced to allow estimating the muscle, net, interaction and gravity torques. The dynamic model used has also been described in prior works (e.g. Vu et al., 2016).

As it is usual, the arm dynamics was described by the following equation:

$$\boldsymbol{\tau} = \mathcal{M}(\boldsymbol{\theta})\ddot{\boldsymbol{\theta}} + \mathcal{C}(\boldsymbol{\theta}, \dot{\boldsymbol{\theta}}) + \mathcal{G}(\boldsymbol{\theta}) + \mathcal{R}(\boldsymbol{\theta}, \dot{\boldsymbol{\theta}}), \quad (3.9)$$

where τ denotes the muscle torque, \mathcal{M} the inertia matrix (4x4 here), \mathcal{C} the Coriolis/centripetal torque, and \mathcal{G} the gravity torque vector. The term $\mathcal{R}(\boldsymbol{\theta}, \dot{\boldsymbol{\theta}})$ reflects the residual torques created by soft tissues, which affect muscle torque in practice. Here we assumed that \mathcal{R} was small compared to the other torques and we thus ignored it in the present modeling. The vector $\boldsymbol{\theta} = (\theta_1, \dots, \theta_4)^\top$ describes the arm's configuration and time derivatives are indicated with a dot (or multiple dots) throughout the paper.

For the purpose of this article, let us define the following quantities:

$$\begin{aligned}
 \tau_{mus} &= \tau \\
 \tau_{net} &= \text{diag}(\mathcal{M}(\boldsymbol{\theta}))\ddot{\boldsymbol{\theta}} \\
 \tau_{int} &= T_{acc} + T_{vel}, \quad \text{with } T_{acc} = - \left[(\mathcal{M}(\boldsymbol{\theta}) - \text{diag}(\mathcal{M}(\boldsymbol{\theta}))) \ddot{\boldsymbol{\theta}} \right], \quad T_{vel} = -\mathcal{C}(\boldsymbol{\theta}, \dot{\boldsymbol{\theta}}) \\
 \tau_{gra} &= -\mathcal{G}(\boldsymbol{\theta})
 \end{aligned} \tag{3.10}$$

where $\text{diag}(\mathcal{M}(\boldsymbol{\theta}))$ is the diagonal matrix built from the diagonal terms of the mass matrix. Then, equation 3.9 can be compactly written as

$$\tau_{net} = \tau_{mus} + \tau_{int} + \tau_{gra}, \tag{3.11}$$

which is similar to the description given in (Yamasaki et al., 2008) and (Sande de Souza et al., 2009).

To simulate this dynamics in practice, we employed the Featherstone-Newton-Euler algorithm, which is the state-of-the-art of rigid body algorithms (Featherstone and Orin, 2000). Having efficient algorithms is crucial, not for performing inverse dynamics and recovering experimental torque profiles, but for running inverse and direct optimal control simulations as they involve numerous evaluations of the system dynamics.

Direct and Inverse optimal control

We conducted direct and inverse optimal control investigations along the lines of (Berret et al., 2011a) and (Vu et al., 2016). Briefly, this approach involves the definition of a cost function that usually depends on the set of control variables (denoted here by \mathbf{u} , chosen to be the derivative of joint accelerations, i.e. jerk) and the set of controlled variables describing the state of the musculoskeletal system (such as joint angles, velocities and accelerations, denoted by \mathbf{x}). As such, the definition of the considered optimal control problems is as follows:

Direct optimal control (DOC). The direct optimal control problem corresponding to the cost $C(\mathbf{u}, \mathbf{x})$ can be formalized as follows: *Find the optimal control \mathbf{u} and its associated trajectory \mathbf{x} satisfying the dynamical system equation, connecting an initial resting arm posture to a terminal one such that the endpoint lies on the planar target in time T and yielding a minimal value of the cost $C(\mathbf{u}, \mathbf{x})$.*

We examined three cost functions representing the three main classes of existing costs (i.e. kinematic-oriented, energy-oriented and dynamic-oriented respectively, see Table 3.4). Namely, we considered the integral of squared angle jerk (kinematic cost), the work of absolute values of muscle torques (energetic cost) and the integral of squared torque change (dynamic cost). This selection was based on the fact that these three costs were all found relevant in previous arm reaching studies (Wada et al., 2001; Nishii and Murakami, 2002; Berret et al., 2008; Uno et al., 1989; Nakano et al., 1999). We could also have included other optimality criteria based on angle acceleration or muscle torque but the acceleration cost yielded the same joint path as the angle jerk and the muscle torque predicted irrelevant hand path trajectory for the current task (see (Berret et al., 2011a) for more details). For the sake of simplicity and clarity, we thus assumed that the cost function accounting for the experimental trajectories could be a composition of the three elementary costs defined above, as follows:

$$C_{\alpha}(\mathbf{u}, \mathbf{x}) = \sum_{i=1}^3 \alpha_i C_i(\mathbf{u}, \mathbf{x}) \quad (3.12)$$

where $C_i(\mathbf{u}, \mathbf{x})$ ($i = [1, 2, 3]$) are defined precisely in Table 3.4. The vector $\alpha = (\alpha_i)_{1 \leq i \leq 3}$ is referred to as the tuning vector whose elements verify $\alpha_i \geq 0$. The process of searching a best-fitting composite cost is called inverse optimal control and is summarized below (more details can be found in (Berret et al., 2011a; Mombaur et al., 2009; Vu et al., 2016)). Note that only two parameters were actually free in the above IOC problem due to normalization (the solution of $C_{\alpha}(\mathbf{u}, \mathbf{x})$ is the same than $\lambda C_{\alpha}(\mathbf{u}, \mathbf{x})$ for any positive λ).

Criterion	Cost function	References
Kinematic (<i>Angle jerk</i>)	$C_1 = C_{Kine} = \int_0^T \sum_{i=1}^4 \ddot{\theta}_i^2 dt$	(Wada et al., 2001)
Energetic (<i>Absolute work</i>)	$C_2 = C_{Ener} = \int_0^T \sum_{i=1}^4 \dot{\theta}_i \tau_i dt$	(Nishii and Murakami, 2002; Berret et al., 2008)
Dynamic (<i>Torque change</i>)	$C_3 = C_{Dyna} = \int_0^T \sum_{i=1}^4 \dot{\tau}_i^2 dt$	(Uno et al., 1989; Nakano et al., 1999)

Table 3.4. Definition and references for the cost functions used in the current study.

Inverse optimal control (IOC). The inverse optimal control problem is stated here as a bi-level optimization. The lower level simply solves a DOC problem for a given vector α and serves to obtain optimal simulated arm trajectories θ_α^* . The higher level aims at finding the optimal vector $\alpha^* = (\alpha_i^*)_{1 \leq i \leq 3}$ that yields the minimal value of an error function comparing the experimental trajectories θ^{meas} with the optimal simulated ones. This function was denoted by Φ and was defined as $\Phi(\theta_\alpha^*, \theta^{meas}) = \max_t \min_s \|\theta_\alpha^*(t) - \theta^{meas}(s)\|$. It captures the maximum deviation from the simulated joint displacements (which depend on the components of α) to the experimental path in joint space. We will refer to this as E_{Joint} , which can be expressed in degrees.

In practice, we used the Matlab-based software called GPOPS to solve the DOC (lower level). For the higher level and IOC, a derivative-free method called CONDOR was used. For both DOC/IOC processes, the initial/final angle velocities and angle accelerations were set to zeros while the initial arm posture (i.e. four initial examined angles) and the movement duration (T) were imported from the motion capture data.

Cost contribution (in %). We used the formula $\alpha_i C_i / \sum_{j=1}^3 \alpha_j C_j$ to evaluate the contribution of cost i to the total cost (Berret et al., 2011a) (costs are evaluated for the optimal solution). Looking at cost contributions may be useful because elements of the vector α are not always easy to interpret: the cost associated with the largest α_i might play a minor role on trajectory formation depending on the order of magnitude of the other elements of the composite cost. Note that from this definition, the 3 cost contributions sum to 100%.

Interaction torque analysis

Local and global interaction torque indexes

Formulas to assess the contribution (either positive/negative) of IT to NT have been established in previous works but they were mainly designed for 2-DoF planar arms (Sainburg and Kalakanis, 2000; Yamasaki et al., 2008). Here, the 4-DoF arm model required some modifications and extensions of those formulas. A drawback of previous approaches was that they were designed for individual DoFs, making it difficult to get a concise picture of the overall interaction torque contribution for such a system with more DoFs. Here we wanted to compare the 4 interaction torques and evaluate their involvement in the formation of reach strategies. Therefore, we defined two complementary indexes. The first one, called *local IT index* and referred to as IT_j^l allowed analyzing the contribution of

IT to NT at each DoF relatively to the others wherein the subscript j refers to the four DoFs under consideration. The second one, called *global IT index* and referred to as IT^g , allowed revealing the overall contribution of IT to NT. Precisely, the formulas were as follows:

$$IT^g = \sum_{j=1}^4 IT_j^l; \quad (3.13)$$

$$IT_j^l = \frac{s_j \max_t |\tau_{net,j}(t)|}{\sum_{i=1}^4 \max_t |\tau_{net,i}(t)|}; \quad (3.14)$$

$$\text{where, } s_j = \frac{\int_0^T \text{sgn}(\tau_{int,j}(t)\tau_{net,j}(t)) |\tau_{int,j}(t)| dt}{\int_0^T |\tau_{net,j}(t)| dt} \text{ for } j = 1..4 \quad (3.15)$$

where sgn is the standard signum function.

The rationale was twofold: i) contribution of IT to the movement at each DoF was assumed to be revealed by the amount of time during which IT contributed to the corresponding NT modulated by the absolute magnitude of this IT and normalized by the magnitude of the NT and ii) the role of IT at a prominent DoF for the movement under consideration is more important than at other DoFs. In practice, we first adopted the equation proposed by (Sainburg and Kalakanis, 2000) and (Yamasaki et al., 2008) to calculate a sub-index (denoted as s_j , for DoF j), which is given in Eq 3.15. These resulting sub-indexes were then combined with the maximal value of NT at each DoF to yield the local IT index for DoF j (i.e. IT_j^l) as illustrated in Eq 3.14. By taking into account the magnitude of the corresponding NT, the IT_j^l index allowed comparing the contribution of IT to NT between different DoFs. The global interaction torque index (i.e. IT^g) was then defined as a sum of the local IT^l indexes of all 4 DoFs involved into movement as illustrated in Eq 3.13. The resultant value reflected the extent to which the IT overall acted with the NT to assist movements (i.e. globally supporting the motion if the obtained IT^g value was positive) or against the NT to resist movements (i.e. globally opposing the motion if the obtained IT^g value was negative).

Binned interaction torque indexes

In the previous formula, the contribution of IT to NT was computed from the whole movement duration (from the movement onset t_0 to the movement end t_f). However, because IT

depends on speed, these contribution indexes could also depend on the movement phase. In order to evaluate this, we split the whole time window into four consecutive intervals (i.e. 4 bins) and quantified the IT index for each bin separately (using IT^g formula restricted to that bin). Precisely, these four bins were defined from the acceleration profile of fingertip as follows: the 1st interval was specified by the time period starting from t_0 to the instant when the fingertip acceleration obtained its maximal value (denoted by t_{\max}); the 2nd bin was defined from t_{\max} to the time when the fingertip acceleration canceled itself out (crossing the horizontal axis; denoted by t_{zer}); the 3rd interval was estimated from t_{zer} to the instant when the fingertip acceleration reached its minimal value (denoted as t_{\min}); finally, the 4th interval was the remaining part of the movement, measured from t_{\min} to the end of the motion t_f .

T_{acc} versus T_{vel} examination

As noticeable from Eq 3.10, IT is actually composed of two different components (T_{acc} and T_{vel}) whose formulas are based on angular acceleration and velocity variables, respectively. Therefore, it is interesting to assess whether the motor controller exploited separately these two components to assist or resist the movement. To this aim, we relied upon IT^g formula but restricted IT to either its velocity or acceleration component. Precisely, in Eq 3.15, we replaced the total IT torque τ_{int} by its elements (T_{acc} and T_{vel}) to get the respective s_j values before applying Eq 3.14 and Eq 3.13 to obtain the desired indexes.

Comparison between simulated and experimental movement strategies *Cartesian error* (E_{Cart}). In order to evaluate the simulated arm trajectories in Cartesian space, the 3D trajectory of the fingertip was analyzed. More precisely, the Cartesian error was estimated as the maximal deviation from the simulated finger trajectory to its experimental path and denoted by E_{Cart} (this is the Cartesian analog of E_{Joint}).

Absolute IT index error (E_{IT}). In order to evaluate the extent to which the simulated trajectories accounted for IT indexes, the absolute IT index error was computed. It was denoted by E_{IT} and defined as the mean absolute difference between simulated and experimental IT indexes across all speed and load conditions (IT^g). It was computed for each subject separately.

Relative IT index error: load- and speed-related errors ($E_{K_{load}}$ and $E_{K_{speed}}$). To assess the extent to which the simulated results could reproduce the load and speed variations of

IT index, we compared empirical and simulated slopes of linear regressions of IT indexes (IT^g) against the load and speed. For the load condition, the slope K_{load} was computed based on a linear regression of IT^g values against the load variable whose values were taken equal to zero and the real weight of attached load with respect to the no-load/load conditions for every subject. For the speed condition, the slope K_{speed} was calculated separately for each load condition and resulted from linear regressions of IT^g values against the speed variable whose values (corresponding to S, N, F speeds) were imported directly from the recorded data (simply taken as the maximal value of recorded velocity profile) for each subject.

Statistical analyses

Two-way repeated-measures ANOVAs were used to test the effects of load and speed on certain pertinent movement parameters. Moreover, in order to assess the predictive performance of each cost function with respect to the others, one-way repeated-measures ANOVAs were also used when relevant. Post-hoc analyses were conducted with Bonferroni corrections when relevant and a 5% threshold was selected in all cases to reject the null hypotheses. Shapiro-Wilk's statistics was used to evaluate normality for the parameters under investigation. We used SPSS to perform all statistical analyses.

Results

Kinematic analysis

Hand kinematics

The hand kinematics is depicted in Figure 3.10 (top panel) for the participant shown in Figure 3.9. Classical patterns seen in point-to-point reaching movements were observed. The movement was mainly along the AP and vertical directions, with typical sigmoidal patterns, and the velocity was bell-shaped for all speeds. Although the reach endpoint was not imposed in this task, we thus observed quite classical hand kinematic patterns. A quantitative analysis across subjects is given hereafter.

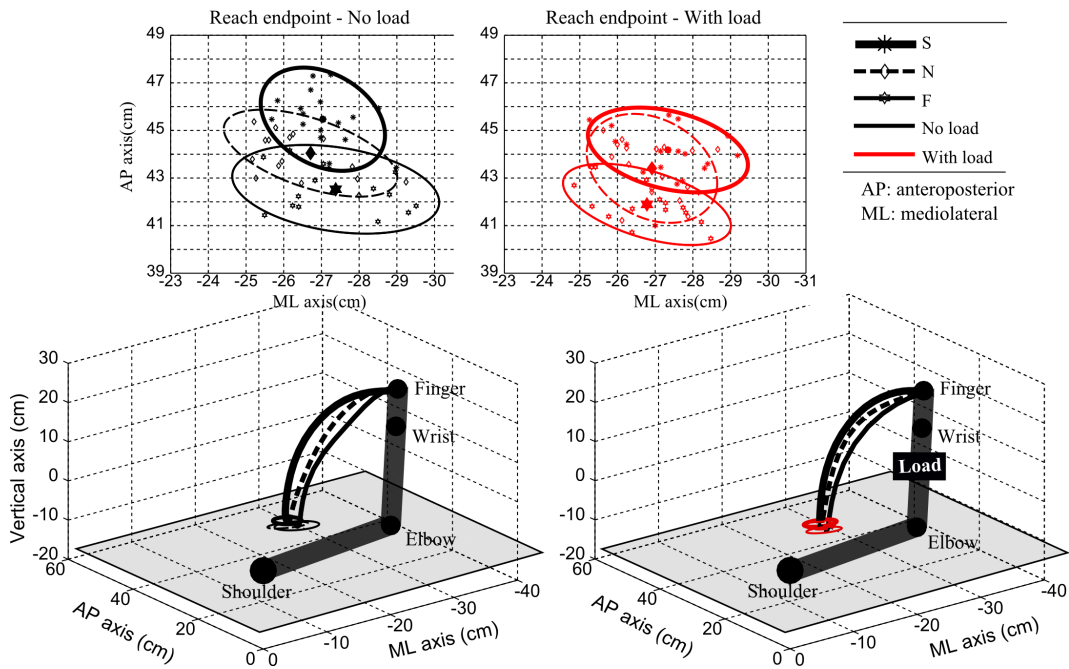


Figure 3.9. Illustration of the experimental paradigm. Fixed initial arm position and horizontal target plane were tested, therefore defining a free reach-endpoint motor task. A 4-DoF model of arm was examined (3 DoFs at the shoulder and 1 DoF at the elbow). Three speed and two load conditions were tested. At the *two bottom panels* displayed the arm posture at the initial time with no load (*left*) and with a load (*right*) approximately attached to the center of mass of the forearm. The average fingertip trajectories of a representative subject were drawn in thick, thin and dotted lines for the three speeds (slow, natural, fast, denoted by S, N, F) respectively. The two *top panels* display the reach endpoint positions across trials for this subject for the three speed condition, and no-load (*left*) and load (*right*) conditions. The 95% confidence ellipses of the reach endpoints are drawn. Note that along the antero-posterior (AP axis), the position of reach endpoint positions tended to get closer to the shoulder position when movement speed increased or when the load was attached to the forearm.

Movement duration (MD). Movement durations for the two experimental blocks (i.e. no-load and with-load), averaged across all subjects, are presented in Table 3.5. For the former block, the values (mean \pm std) corresponding to the three speed conditions (i.e. S, N, F) were respectively 0.85 \pm 0.15, 0.49 \pm 0.07, 0.32 \pm 0.06s. Those values were respectively 0.84 \pm 0.14, 0.52 \pm 0.08, 0.35 \pm 0.07s for the latter block. Two-way repeated measures ANOVAs showed no speed \times load interaction for MD ($p=0.55$). However, significant differences were found across speed conditions ($p<0.001$, $F(2,18)=101.1$, $\eta_p^2=0.91$), but not

between load conditions ($p=0.13$). This result, therefore, implied that the speed-related requirements (i.e. distinguishable within each load condition but consistent between two load conditions) were fulfilled by all subjects during the experiment.

	No load			With load		
	S	N	F	S	N	F
MD (s)	0.85±0.15	0.49±0.07	0.32±0.06	0.84±0.14	0.52±0.08	0.35±0.07
$Sh_{internal/external}$ (°)	11.3±6.6	12.5±6.3	14.1±6.3	11.2±5.5	12.7±5.8	12.2±6.2
$Sh_{elevation/depression}$ (°)	10.3±7.0	11.4±6.3	11.8±6.5	9.9±5.3	10.6±5.2	11.2±5.2
$Sh_{ulnar/radial}$ (°)	96.4±16.1	98.8±15.9	100.5±16.1	97.0±15.1	99.5±14.9	101.7±16.1
$El_{extension/flexion}$ (°)	14.7±8.6	14.6±7.6	14.7±6.9	13.1±8.6	12.4±8.7	12.9±8.2
RE_{AP} (%)	76.3±7.9	74.2±9.3	73.6±9.3	74.4±8.2	72.0±8.9	71.3±9.6
Cur	0.18±0.03	0.17±0.03	0.16±0.03	0.18±0.03	0.17±0.03	0.16±0.04
Za (cm)	0.8±0.7	0.7±0.7	0.6±0.4	0.7±0.6	0.6±0.6	0.6±0.5
Zp (cm)	0.7±0.2	0.8±0.3	0.9±0.5	0.7±0.2	0.8±0.3	0.8±0.3

Table 3.5. Main kinematic movement parameters (mean±std across subjects) for the three speed (S, N, F) and two load (no load, with load) conditions.

Finger accuracy and precision errors (Za and Zp). The finger constant and variable errors along the vertical axis (Za for accuracy and Zp for precision) were averaged across all subjects and displayed in Table 3.5. It is noteworthy that the pointing accuracy along the horizontal axes (AP and ML) were not examined because no prescribed reach endpoint was introduced regarding to the final position of the fingertip on the horizontal plane. Therefore there was no constant error in this plane. Regarding the goal of the task (thus along the vertical axis), Zp values slightly increased while Za values slightly decreased as movement speed increased, regardless of the load condition. However, two-way repeated measures ANOVAs analyses showed no significant load×speed interaction or load/speed variation for Za error ($p_{load \times speed}=0.13$, $p_{load}=0.83$, $p_{speed}=0.46$) and for Zp error ($p_{load \times speed}=0.37$, $p_{load}=0.44$, $p_{speed}=0.08$), thus indicating equal accuracy/precision achievement despite different speed/load movement conditions. In order to evaluate whether the change of speed/load conditions affected the shape of arm trajectories, the following analyses focuses on other relevant and classical kinematic parameters.

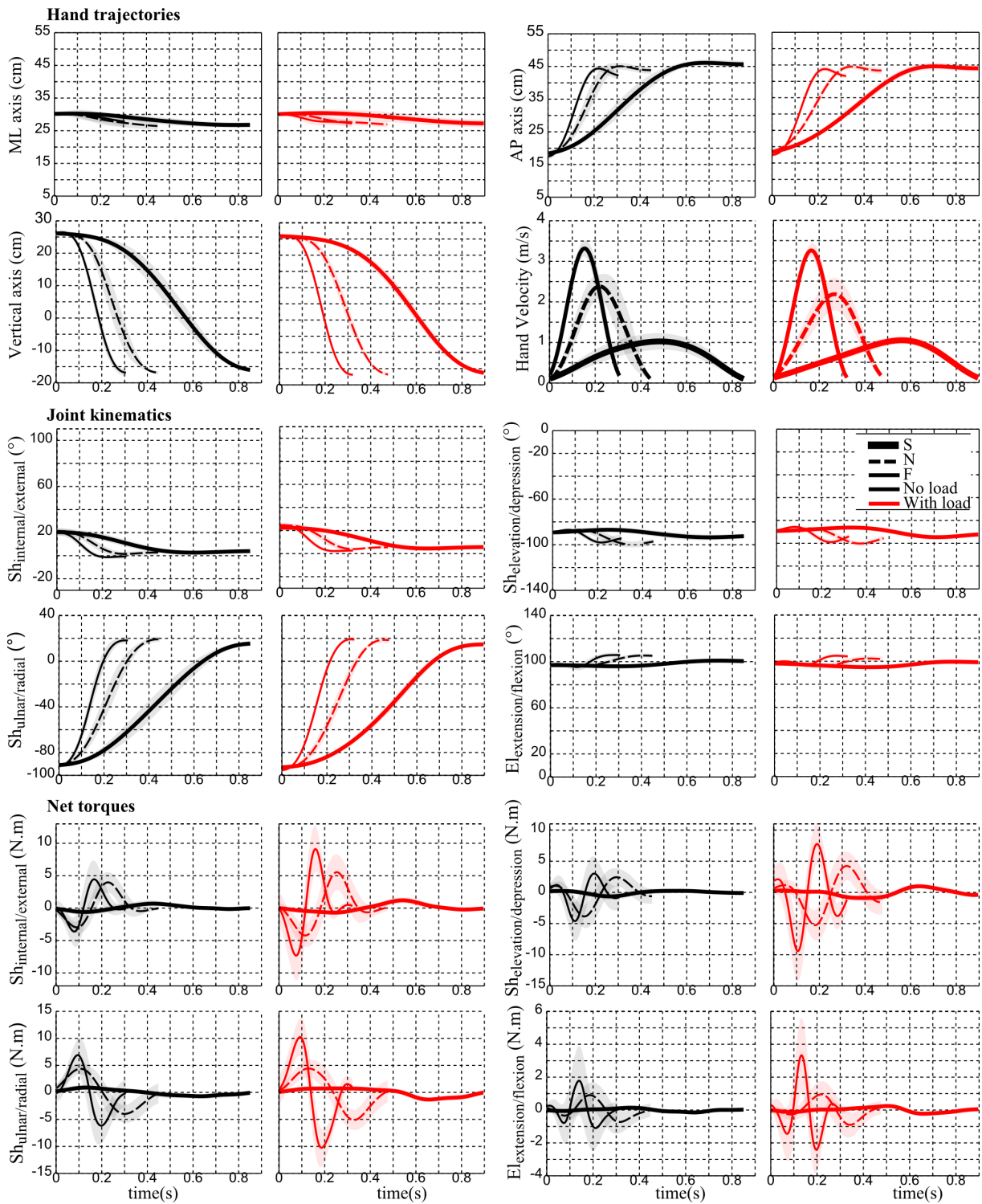


Figure 3.10. Hand, joint and torque profiles for the representative subject of Fig. 3.9. For the hand kinematics, displacements along the AP, ML and vertical axes are depicted as well as the Cartesian hand velocity (average and standard deviation as a shaded area) for the 3 speeds and two load conditions (black is for no-load and red for with-load). For the joint kinematics, the angular displacements for the 4 degrees of freedom are depicted. For the joint torques, we depicted the net torque acting at each degree of freedom.

Reach endpoint analyses. One main variable of the task is the reach endpoint location. We first qualitatively examined the effect of speed and load variations on the reach endpoint position. To this aim, the projection of reach endpoints onto the transversal plane (composed of ML and AP axes) is presented in the top panels of Figure 3.9 for the representative subject. A visual inspection suggests that the distribution of reach endpoints (displayed as 95% confidence ellipses) varies with respect to the different speed and load conditions. Specifically, the subject executed movement trajectories whose endpoint got closer to the shoulder's vertical projection along the AP axis when movement sped up. A similar shift of the reach endpoint toward the shoulder location was observed when adding a load to the forearm. Similar analyses were systematically conducted for all subjects. The normalized reach endpoint index (RE_{AP} , see Materials and Methods for its definition), averaged across all subjects is displayed in Table 3.5. Results showed that the reach endpoint index systematically decreased when movement speed increased and when the load was attached to the arm. This index was $[76.3\pm 7.9\%, 74.2\pm 9.3\%, 73.6\pm 9.3\%]$ for the no-load condition and $[74.4\pm 8.2\%, 72.0\pm 8.9\%, 71.3\pm 9.6\%]$ for the with-load condition, respectively. Two-way repeated measures ANOVAs showed no significant speed \times load interaction ($p=0.83$) but a significant change of RE_{AP} with respect to speed ($p<0.001$, $F(2,18)=12.2$, $\eta_p^2=0.57$) and load ($p<0.05$, $F(1,9)=5.2$, $\eta_p^2=0.36$) changes. This analysis proved that the final hand position, which was freely chosen in this task, changed as a function of speed and load across subjects: subjects tended to point closer to their body when speed or forearm inertia increased.

Curvature index analysis. The averaged curvature indexes are reported in Table 3.5 for the load and speed conditions. For the no-load condition, the index obtained values of 0.18 ± 0.03 , 0.17 ± 0.03 , 0.16 ± 0.03 for the S, N and F speeds respectively. These values were equal to 0.18 ± 0.03 , 0.17 ± 0.03 , 0.16 ± 0.04 respectively for the load condition. Two-way repeated measures ANOVAs revealed no significant speed \times load interaction ($p=0.07$) and no significant effect of load ($p=0.78$) but a significant change of curvature index under speed variations ($p<0.001$, $F(2,18)=13.3$, $\eta_p^2=0.59$). Therefore, hand paths tended to become straighter with speed increments.

Joint kinematics

Like the hand kinematics, the joint kinematics was also illustrated for the representative subject in Figure 3.10 (middle panel). It is visible that the movements were executed mainly

around the shoulder ulnar/radial axis while smaller displacements were observed for the other remaining axes. The magnitude of these angular displacements were analyzed for all subjects and the results are displayed in Table 3.5. Two-way repeated measures ANOVAs showed no significant speed \times load interaction and no significant effect of load and speed for shoulder internal/external, elevation/depression, elbow extension/flexion but a significant change for the shoulder ulnar/radial angle under speed variations ($p < 0.001$, $F(2,18) = 27.8$, $\eta_p^2 = 0.81$). The extent of the rotations around this major axis for the task depended on speed but not load.

In summary, the speed and load dependencies of the reach endpoint and curvature indexes suggested that the CNS may adapt its motor control strategy to best suit the new task constraints. In order to better uncover the possible causes underlying this adaptation, an analysis at the dynamic level is performed hereafter.

Dynamic analysis

Qualitative analysis of torque profiles For the sake of illustration, net torque (NT) profiles are shown in Figure 3.10 for all conditions of speed and load (bottom panels) for the representative subject. The four torque profiles corresponding to the internal/external, elevation/depression, ulnar/radial DoFs of the shoulder and the extension/flexion DoF of the elbow are depicted. Overall, net torque profiles marked clear differences with respect to load or speed variations. The magnitude of net torques typically increased when the load was added or when speed was augmented by a verbal instruction. The patterns were similar to that of an acceleration in most cases, except for the elbow extension/flexion in fast speed. In terms of magnitude, the torques at the elbow joint appeared to be considerably smaller than those produced at the shoulder joint. Within the shoulder joint itself, the torque profiles of the three coupled DoFs were quite complex. Although kinematic analyses showed less involvement of shoulder internal/external and elevation/depression axes in the formation of arm trajectories compared to the shoulder ulnar/radial axis (Tab 3.5), one could however observe quite large torques at the two former axes. Maximum magnitude was about 10 N.m and measured at fast speed (F).

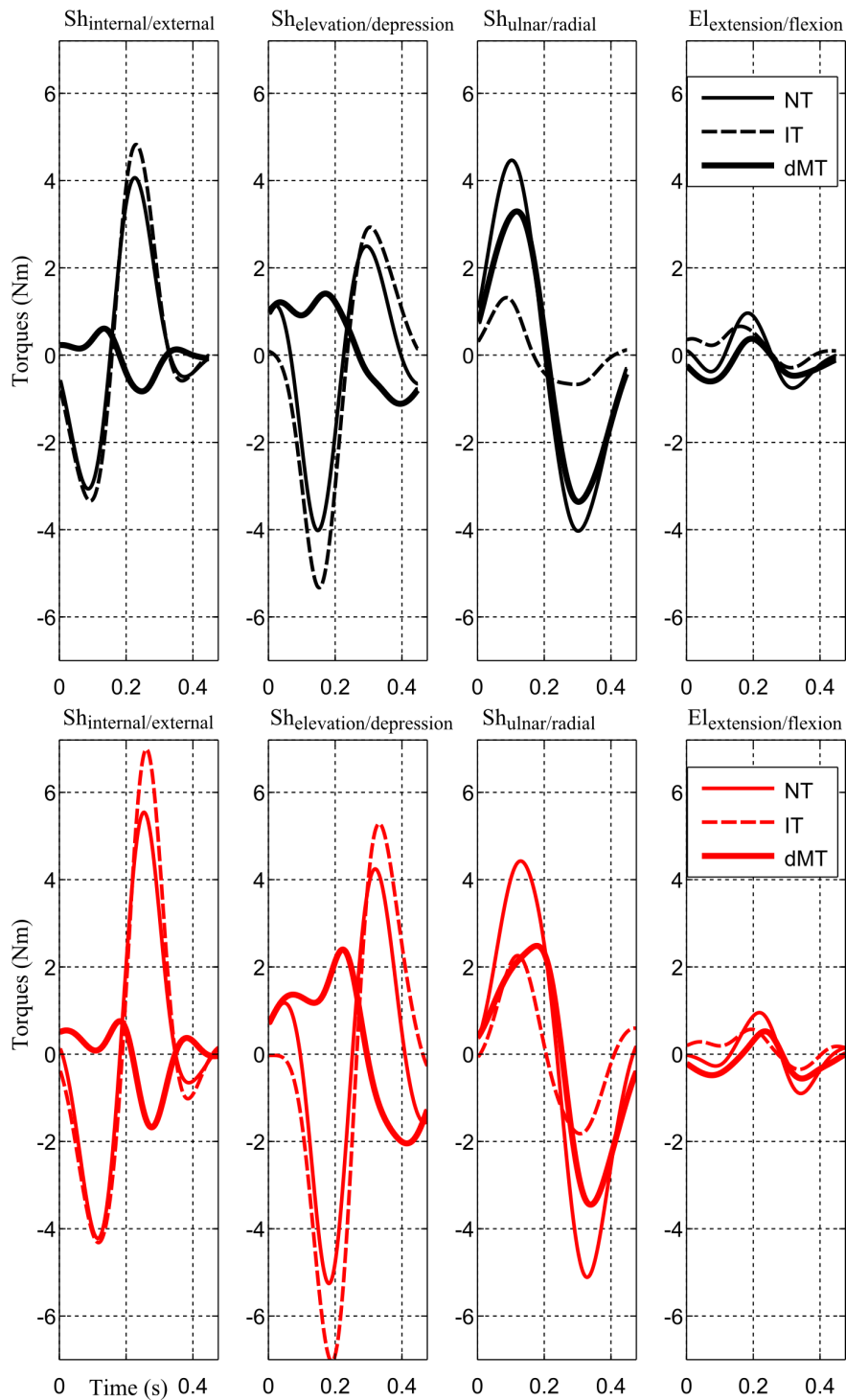


Figure 3.11. Torque profiles (averaged across trials) of the representative subject at N speed for the no-load (*top panel*) and load (*bottom panel*) conditions. From left to right, the four torque profiles are for the shoulder internal/external, elevation/depression, ulnar/radial and elbow extension/flexion DoFs, respectively. The dynamic muscle torque (defined as muscle torque deprived of gravity torque, denoted by dMT), interaction torque (denoted by IT) and net torque (denoted by NT) are plotted.

For a more detailed analysis of the composition of net torques, a focus on normal speed (N) is presented in Figure 3.11 in the two experimental load conditions (no-load/with-load) and for the same representative subject. Other speeds are not illustrated here for clarity but the effect of speed will be treated in the subsequent quantitative and statistical analyses. Specifically, at the prominent axis for the task (i.e. shoulder ulnar/radial), the dynamic muscle torque (defined as muscle torque without the gravity component, denoted as dMT) and the interaction torque (IT) both contributed to the net torque (NT) in the same direction, thus producing quite large NT here. On the contrary, for the other axes (e.g. shoulder internal/external and elevation/depression), the dMT was most of the time opposed to both IT and NT; meanwhile, IT was observed to vary in the same direction with the NT.

A finer examination however revealed few factors that may be responsible for the speed/load-dependent arm kinematics found above. Indeed, in terms of magnitude, while the maximal value of NT at the shoulder ulnar/radial axis in the load condition was pretty similar to that of the no-load condition ($\sim 4\text{Nm}$), the difference in the NT for the two load conditions was much larger at the shoulder internal/external and elevation/depression axes. Interestingly, it is noteworthy that the motion of the internal/external and elevation/depression DoFs of the shoulder joint should have high impacts on the location of the final reach endpoint within the planar target (and maybe curvature too). Therefore, these differences on mean torque profiles, especially at the first two shoulder rotation axes, could possibly account for the speed/load-dependent changes of reach endpoint/curvature observed above.

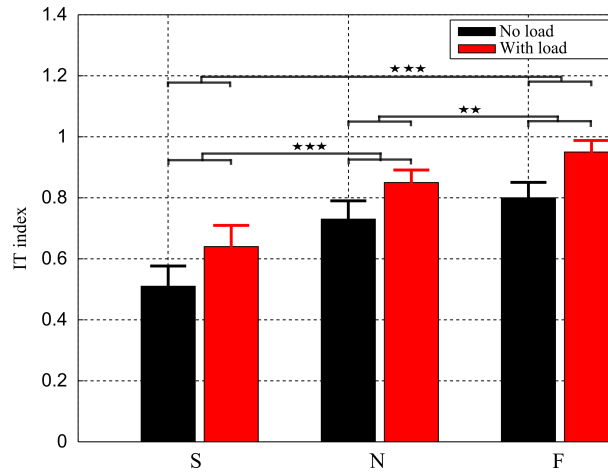


Figure 3.12. Global interaction torque indexes (IT^g), averaged across all subjects, and displayed for the three speed and two load conditions (with standard errors indicated by error bars). It is visible that the IT^g index increased whenever movements sped up or a load was attached to the arm. In addition, its values were always positive, thus indicating that the IT positively contributed to the NT to some extent. Note that horizontal bars with stars indicate the results of post-hoc analysis for the speed condition. One, two, three stars stand for $p < 0.05$, $p < 0.01$ and $p < 0.001$ respectively.

Interestingly, note that the magnitude of IT increased clearly with the addition of the load (as expected) and that it reached quite large compared to the other torques (dMT, NT). Moreover, IT appeared to vary systematically in the same direction than NT (i.e. assisting the motion), thereby explaining what dMT were relatively small in general. Therefore, from these plots, it seems possible that the CNS may take into account the presence of IT to facilitate and assist movement. In order to clarify this hypothesis, we next quantitatively examined the impact of IT on NT in terms of IT^g and IT^l indexes (see Materials and Methods for their definitions), which are indexes designed to assess the degree of contribution of IT to NT.

Torque profile quantitative analyses

Global interaction torque index (IT^g). The IT^g indexes, averaged across all subjects for both speed/load experimental conditions, are shown in Figure 3.12. In terms of load effect, it is visible that the IT^g indexes were larger in the load condition than in the no-load condition, regardless of motion speed. Precisely, the IT^g indexes shifted from $[0.51 \pm 0.21$,

0.73±0.19, 0.80±0.16] for the no-load condition to [0.64±0.22, 0.85±0.13, 0.95±0.12] for the load condition with respect to S, N, F speeds, respectively. In terms of speed effect, the IT^g indexes of both load conditions increased whenever the movement was sped up. Two-way repeated measures ANOVAs on IT^g yielded no significant speed×load interaction ($p=0.56$) but significant effects of load ($p<0.001$, $F(1,9)=89.1$, $\eta_p^2=0.90$) and speed ($p<0.001$, $F(2,18)=41.2$, $\eta_p^2=0.86$), indicating that IT were exploited to a greater extent whenever the load and the movement speed were increased. Moreover, it is noteworthy that IT^g values were always positive (>0.5) while they could theoretically be negative as well. Altogether, these results implied that in general IT assisted the movement and that, importantly, this contribution of IT to the movement was strengthened with load or speed augmentations (which increase overall IT magnitudes).

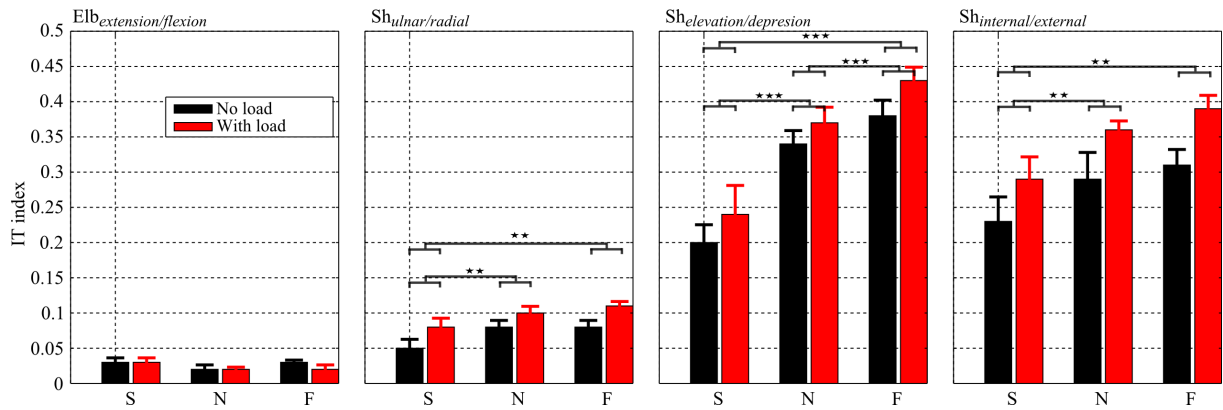


Figure 3.13. Local interaction torque indexes (IT^l), averaged across all the subjects, displayed for the three speed and two load conditions. From left to right: IT^l of elbow extension/flexion, shoulder ulnar/radial, elevation/depression, internal/external, respectively. Noticeably, compared with shoulder-related DoFs, the IT^l indexes at the elbow extension/flexion were considerably smaller. Between the three DoFs at the shoulder, the IT^l indexes of shoulder ulnar/radial were smaller than the others. Statistical analyses showed significant effects of speed/load on the IT^l index for these three DoFs, as indicated by horizontal bars

Interaction torque contribution characteristics *Spatial investigation: local interaction torque indexes (IT^l).* In order to better understand the mechanism the CNS may rely on to adaptively use IT at different DoFs, we investigated the local IT contribution

index (IT^l) for every rotation axis involved in the limb's movement. The averaged IT^l indexes for both load and speed conditions are given in Figure 3.13. Like IT^g index, we observed that the IT^l index was also speed and load dependent. Indeed, for most DoFs (except the elbow extension/flexion axis), two-way repeated measures ANOVAs on IT^l indexes showed no significant speed \times load interaction but a significant increase of IT^l ($p_{uln/rad} < 0.01$, $F_{uln/rad}(1,9) = 19.2$, $\eta_p^2 = 0.68$; $p_{ele/dep} < 0.001$, $F_{ele/dep}(1,9) = 20.2$, $\eta_p^2 = 0.69$; $p_{int/ext} < 0.001$, $F_{int/ext}(1,9) = 41.4$, $\eta_p^2 = 0.82$) when the load was attached to the arm or when the movement sped up ($p_{uln/rad} < 0.001$, $F_{uln/rad}(2,18) = 11.6$, $\eta_p^2 = 0.56$; $p_{ele/dep} < 0.001$, $F_{ele/dep}(2,18) = 30.7$, $\eta_p^2 = 0.77$; $p_{int/ext} < 0.001$, $F_{int/ext}(2,18) = 14.9$, $\eta_p^2 = 0.62$). Finer analysis showed that IT was utilized to assist movement at several DoFs but to different extents. Indeed, for the two load conditions, the IT indexes of elbow extension/flexion axis were always smaller than those of shoulder-related ones. Between the three coupled rotation axes of the shoulder joint, the IT indexes of shoulder internal/external and elevation/depression axes were considerably larger than those of shoulder ulnar/radial axis irrespective of speed/load conditions. Given that these three axes belong to a same joint, these results revealed the complexity of IT contribution.

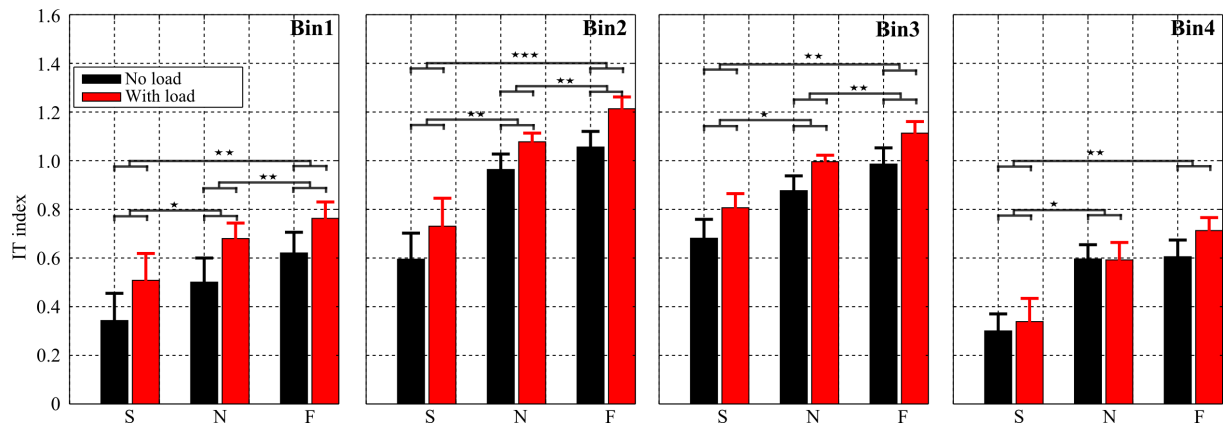


Figure 3.14. Bin analysis of interaction torque exploitation. From left to right: average interaction torque indexes (across subjects) for bin1, bin2, bin3 and bin4 respectively. Note that these four bins were defined by dividing movement duration into a series of 4 intervals based on the acceleration profile (see Methods). Note that IT index values were smaller for bins 1 and 4, while it was larger for middle bins (2 and 3). For each bin, statistical significance of post-hoc tests is reported.

Temporal investigation: interaction torque index analysis across bins. The binned global IT indexes, averaged across all subjects, are illustrated in Figure 3.14. It is visible that the pattern of IT indexes over the four bins for the two load conditions remains relatively consistent across all movement speed conditions. At normal speed (N) for example, the IT indexes of four bins clearly changed in a manner that is reminiscent of the bell shape of the hand velocity profile. Indeed, when the subjects started or terminated motion (bin1 or bin4), the IT index obtained the relatively small values of $[0.50 \pm 0.31, 0.59 \pm 0.18]$ for the no-load condition and of $[0.68 \pm 0.20, 0.59 \pm 0.22]$ for the load condition. Around the peak of velocity (i.e. bin2 or bin3), the IT index increased considerably and reached $[0.96 \pm 0.2, 0.87 \pm 0.19]$ for the no-load and $[1.07 \pm 0.11, 0.99 \pm 0.08]$ for the load conditions respectively. This may not be a surprise given that IT magnitude depends on speed and accelerations, which are greater during the course of a reaching movement than near the initiation or termination phases. A main effect of speed on IT index was also present for each of the four bins. Two-way repeated measures ANOVAs on IT index showed no significant speed \times load interaction but a significant effect of speed for all bins ($p_{bin1} < 0.001$, $F_{bin1}(2,18) = 13.1$, $\eta_p^2 = 0.59$; $p_{bin2} < 0.001$, $F_{bin2}(2,18) = 20.1$, $\eta_p^2 = 0.69$; $p_{bin3} < 0.001$, $F_{bin3}(2,18) = 12.2$, $\eta_p^2 = 0.57$ and $p_{bin4} < 0.001$, $F_{bin4}(2,18) = 11.1$, $\eta_p^2 = 0.55$). In terms of load effect, the binned IT indexes were generally consistent with the above results. Indeed, the IT indexes in the load condition were always significantly larger than those in the no-load condition for the first three bins ($p_{bin1} < 0.001$, $F_{bin1}(1,9) = 39.6$, $\eta_p^2 = 0.81$; $p_{bin2} < 0.01$, $F_{bin2}(1,9) = 18.2$, $\eta_p^2 = 0.66$; $p_{bin3} < 0.01$, $F_{bin3}(1,9) = 13.6$, $\eta_p^2 = 0.60$) but no significant difference was found for the fourth bin ($p_{bin4} = 0.13$).

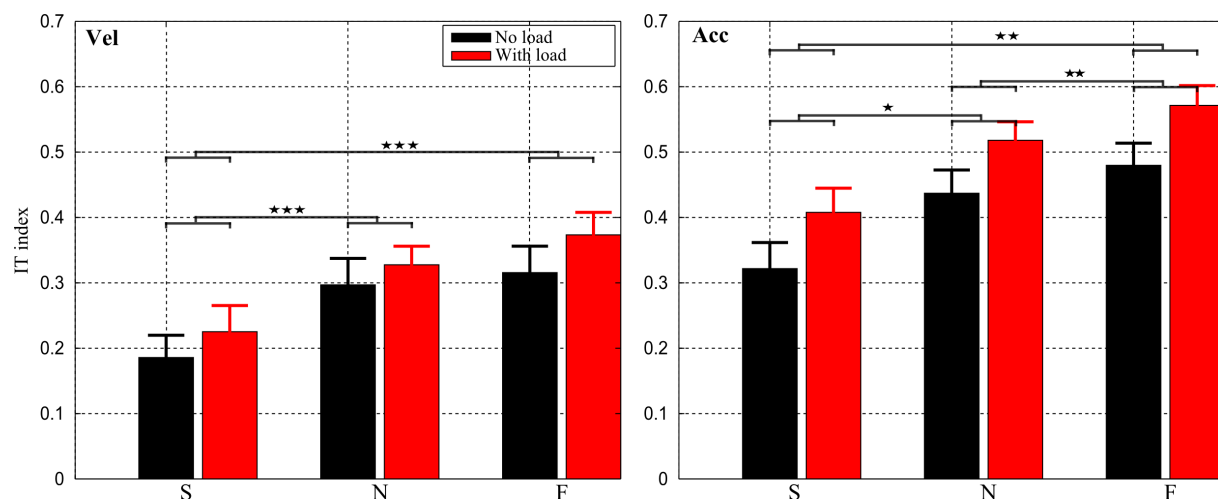


Figure 3.15. Component analysis of interaction torque exploitation. The IT indexes, averaged across subjects, are displayed for the three speed and two load conditions for the two components of IT. *Left*: velocity-related component (IT_{vel}); *Right*: acceleration-related component (IT_{acc}). It is visible that IT_{acc} was always greater than IT_{vel} . Statistical analyses showed significant effects of speed and load on the IT index for both IT components.

Nature of interaction torque: velocity- versus acceleration-based IT index. The averaged IT indexes across all subjects taken separately for the two interaction torque components (T_{acc} and T_{vel}) are reported in Figure 3.15 (see the Materials and Methods section for their definitions). Overall, the IT indexes of the two torque components were quite similar, suggesting that IT originating from velocities and accelerations are both used during the movement. Indeed, both IT indexes increased whenever movement speed increased. In terms of load effect, we also observed an upward shift of IT index for both T_{acc} and T_{vel} . Two-way repeated measures ANOVAs showed no significant speed \times load interaction ($p_{T_{acc}} = 0.85$, $p_{T_{vel}} = 0.48$) but significant main effects of speed/load conditions for both T_{acc} ($p_{speed} < 0.001$, $F_{speed}(2,18) = 14.9$, $\eta_p^2 = 0.62$; $p_{load} < 0.001$, $F_{load}(1,9) = 95.4$, $\eta_p^2 = 0.91$) and T_{vel} ($p_{speed} < 0.001$, $F_{speed}(2,18) = 34.3$, $\eta_p^2 = 0.79$; $p_{load} < 0.001$, $F_{load}(1,9) = 21.9$, $\eta_p^2 = 0.71$). Finer analysis revealed that the IT indexes of T_{acc} were always larger than those of T_{vel} regardless of speed/load conditions but their difference remained approximately constant with respect to the change of speed/load. Nonetheless, it is remarkable that the IT indexes of both T_{acc} and T_{vel} were always positive, thereby implying that in all cases both T_{acc} and T_{vel} contributed positively to NT and that, overall, IT assisted the movement.

In summary, the above empirical results revealed a significant effect of speed and load on both the kinematics and dynamics of the motor behaviors during the free 3D arm pointing movements we considered here. This effect seems to originate from the unequal influence of IT on NT when speed or/and load are modified. Next, to interpret and propose principles to explain the above kinematic and kinetic adaption of reach strategies to load and speed variations, inverse optimal control simulation results are presented. Inverse optimal control is dedicated to automatically characterize the cost with respect to which empirical trajectories are optimal. In other words, this is done to characterize the best-fitting composite cost for the experimental motion data under investigation.

Optimal control results

Arm kinematics predicted by composite and elementary costs

We applied direct optimal control (DOC) separately to the three elementary cost functions under consideration (see Table 3.4) for all subjects to check whether each of them could account for the experimental observations. These simulated optimal trajectories were used to compute errors in terms of angular displacements (E_{Joint}) and Cartesian displacements (E_{Cart}), which were then used as reference values for comparisons with the performance of the composite cost obtained from the inverse optimal control (IOC) procedure, as illustrated in Figure 3.16. The Cartesian error E_{Cart} of the composite and kinematic costs were equal to $5.5\pm 3.2\text{cm}$ and $6.2\pm 3.4\text{cm}$ respectively. These errors were clearly smaller than those of the dynamic cost ($E_{Cart}= 11.4\pm 5.3\text{cm}$) and even much smaller than those of the energetic cost ($E_{Cart}= 15.5\pm 4.7\text{cm}$). Repeated measures one-way ANOVAs showed significant differences between the composite/kinematic costs and the dynamic/energetic costs ($p<0.001$, $F(3,177)=79.6$, $\eta_p^2=0.57$) but no significant difference between the kinematic and composite cost ($p=1.0$) when pooling all experimental conditions together. Similar conclusions were reached for the joint space errors (E_{Joint}). Like the Cartesian errors, the angular errors (E_{Joint}) of the composite and kinematic costs were quite small compared to those of the dynamic/energetic costs. Repeated measures one-way ANOVAs for E_{Joint} errors also showed significant differences between the composite/kinematic costs and the dynamic/energetic costs ($p<0.001$, $F(3,177)=125.8$, $\eta_p^2=0.68$) but the difference between the kinematic and composite cost was not significant ($p=1.0$). Altogether, one can conclude that both composite and kinematic costs performed better than the dynamic/energetic

costs at replicating the main kinematic features of the recorded data. Therefore, pure energetic and dynamic costs can be ruled out as they are clearly unable to predict accurately some basic features of the task (e.g. hand path), and the composite and kinematic costs appear as the only candidates to account for the experimental trajectories at this point. In order to distinguish between these two costs, we further examined their performances in dynamic space. In particular, we investigated whether the IT index and its speed/load dependencies were replicated by such models.

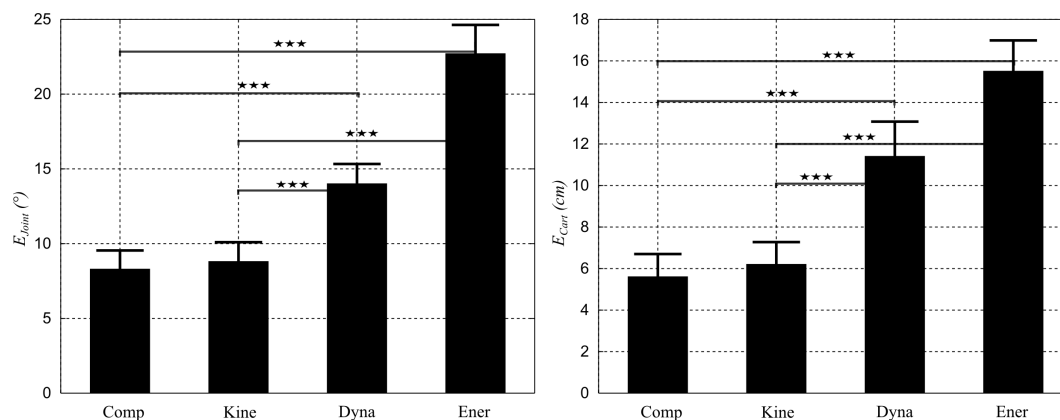


Figure 3.16. Reconstruction errors in joint space (E_{Joint} , *left panel*) and Cartesian space (E_{Cart} , *right panel*) for the best-fitting composite cost and each of the three cost elements taken separately. Error values were averaged across speeds, loads and then across subjects (with standard errors indicated by error bars). Noticeably, in terms of both joint and Cartesian errors, the composite (Comp) and kinematic (Kine) costs performed better than the dynamic (Dyna) and energetic (Ener) costs.

Arm dynamics predicted by composite and kinematic costs

For the sake of illustration, the dynamic strategies predicted by the identified composite and kinematic costs at normal speed (N) are shown in Figure 3.17 in the no-load condition for the representative subject. It is visible that the two costs predicted quite different torque profiles if one considers the interplay between torques. Indeed, for the kinematic cost, large magnitudes of dMTs were required mainly to cancel out the perturbations caused by ITs, especially at the first two DoFs (i.e. shoulder internal/external and shoulder elevation/depression, about 3Nm). Moreover, it happened that IT was opposed to NT,

especially for the 2nd DoF. On the other hand, for the composite cost, smaller dMTs were required to perform the task and, clearly, this was achieved by letting IT contribute to NT on certain time periods. To assess the consistency of this observation, we further quantified their performance in terms of IT index as presented below.

We first calculated the absolute reconstruction error of IT index (E_{IT}) for both composite and kinematic costs. Their E_{IT} value was averaged across speeds, loads and then across subjects and displayed in the right panel of Figure 3.18. Importantly, the composite cost predicted the IT index much better than the kinematic costs. Indeed, the (mean \pm std) E_{IT} values of the composite cost were equal to 0.18 ± 0.16 , nearly eight times smaller than those of the kinematic cost ($E_{IT}=1.49\pm 0.53$). Given that the empirical IT indexes (IT^g) always obtained positive values larger than 0.5, the predicted IT index of the kinematic cost was considerably discrepant from the recorded data. Indeed, the kinematic cost exhibited such large E_{IT} errors because it often produced trajectories whose IT indexes were negative (opposite to the real ones) irrespective of speed/load conditions. Repeated measures one-way ANOVAs for E_{IT} showed significant difference between the composite cost and the kinematic cost ($p<0.001$, $F(1,59)=420$, $\eta_p^2=0.87$).

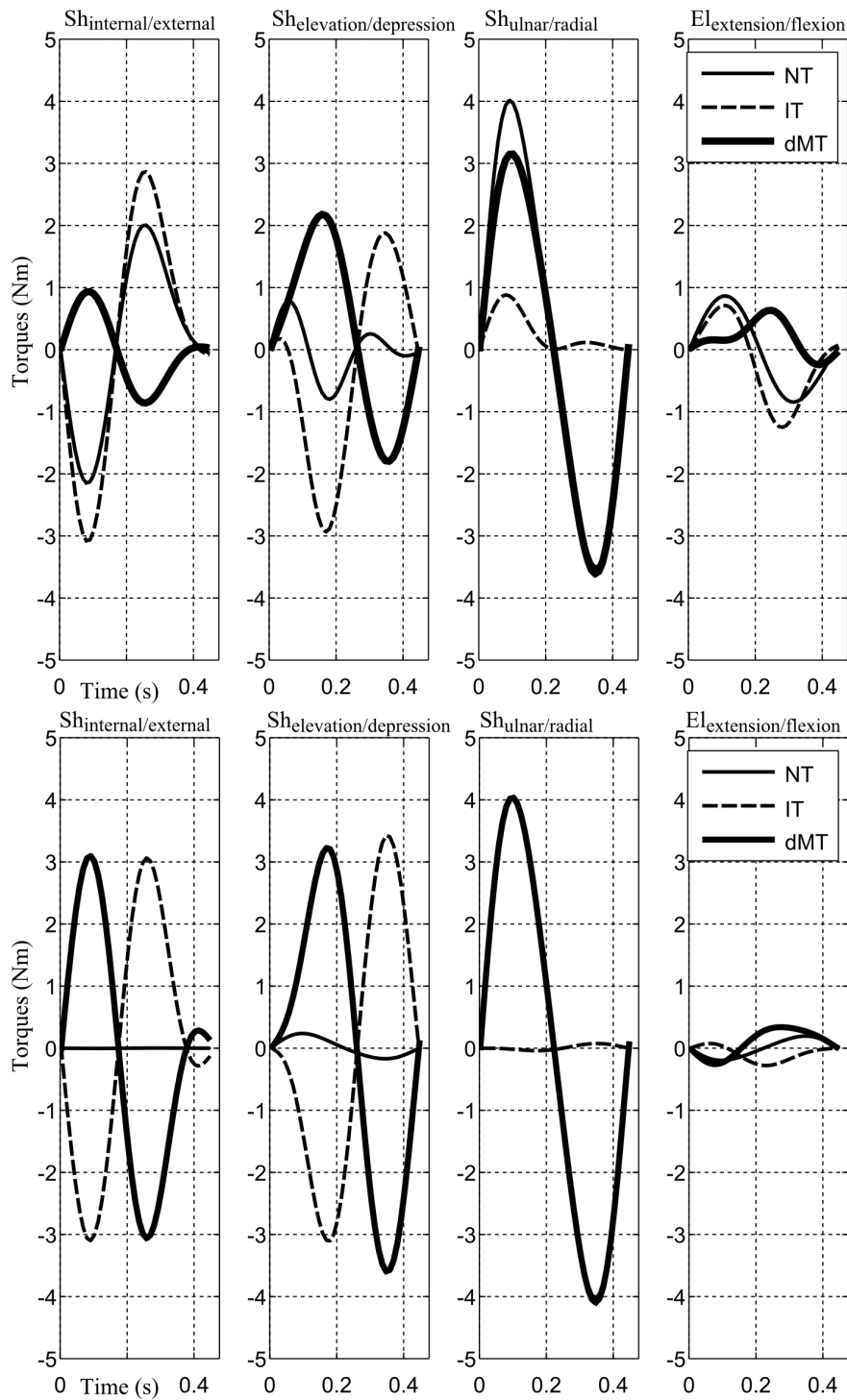


Figure 3.17. Torque profiles predicted by the identified composite cost (*top panels*) and the kinematic cost (*bottom panels*) for a representative subject at N speed and in no load condition. It is visible that the composite cost tends to let ITs contribute to NTs in order to get smaller dMTs while it is the opposite for the kinematic cost.

Furthermore, we tested if the composite cost better reproduced the speed/load dependencies of IT indexes than the kinematic cost. To this aim, the prediction of slope obtained from a linear regression of IT index against speed/load variables was investigated. The left and middle panels of Figure 3.18 show the errors $E_{K_{speed}}$ and $E_{K_{load}}$. In terms of speed effect, it is visible that the optimization of a composite cost predicted the speed-dependent change of IT indexes better than the kinematic cost. Indeed, the $E_{K_{speed}}$ error was 0.13 ± 0.09 for the composite cost, which was nearly twice smaller than for the kinematic cost ($E_{K_{speed}} = 0.25 \pm 0.15$). Repeated measures one-way ANOVAs for $E_{K_{speed}}$ showed significant difference between the composite and kinematic costs ($p < 0.01$, $F(1,19) = 8.8$, $\eta_p^2 = 0.32$). In terms of load effect, the difference between the composite and kinematic cost was even larger. Compared with the composite cost, the kinematic cost replicated quite poorly load-dependent variations ($E_{K_{load}} = 0.61 \pm 0.38$, i.e. nearly seven times larger than the error for the composite cost). Again, repeated measures one-way ANOVAs for $E_{K_{load}}$ revealed that the composite and kinematic costs differed significantly ($p < 0.001$, $F(1,9) = 20.7$, $\eta_p^2 = 0.67$). Overall, our results therefore revealed that the composite cost could capture reasonably well both the adaptive kinematic and dynamic characteristics of the reach strategies while the kinematic cost clearly failed to explain the reach strategies in torque space.

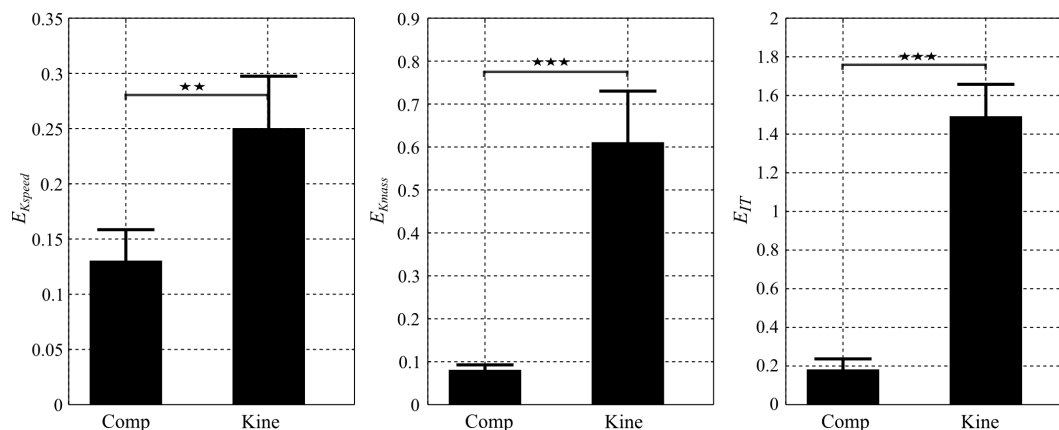


Figure 3.18. Reconstruction errors for some relevant parameters ($E_{IT}, E_{Kspeed}, E_{Kmass}$) for the composite and kinematic costs. Error values were averaged across speeds, loads and then across subjects for E_{IT} while averaged only across subjects for E_{Kspeed}/E_{Kmass} . Noticeably, in terms of E_{IT} and E_{Kspeed}/E_{Kmass} errors, the composite cost performed much better than the kinematic cost, yielding to a conclusion that only composite cost could predict relatively well the IT index and its speed/mass dependencies as observed in the experimental movement.

Cost contribution evaluation

In order to assess how each elementary cost contributed to the total (composite) cost according to speed and load changes, we estimated the influence of each of the kinematic, dynamic and energetic components (see Materials and Methods) and the results are reported in Figure 3.19. Here, we display only results of the kinematic and dynamic costs since the three cost contributions sum to 100% by definition. Overall, the contribution of the kinematic cost was largely dominant. Specifically, the average contribution (across speed and load conditions and subjects) of the kinematic cost was about $67 \pm 14\%$ while those of energetic and dynamic elements were $16 \pm 11\%$ and $17 \pm 18\%$ respectively. This result thus confirmed the important role played by the kinematic cost during the motor planning process, which is consistent with its role for replicating the kinematics of the arm pointing movements.

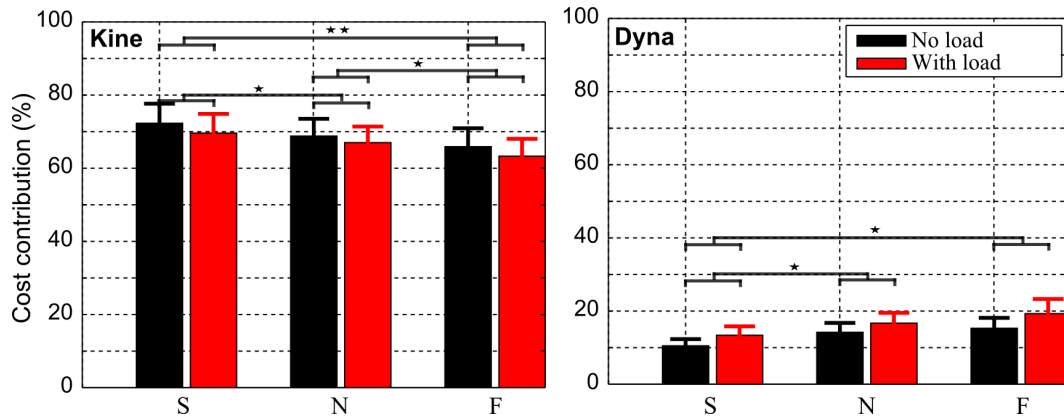


Figure 3.19. Cost contribution analyses. The contribution of elementary cost to the composite cost, averaged across all the subjects, is reported for the three speed and two load conditions. *Left*: cost contribution of kinematic cost; *Right*: cost contribution of dynamic cost. It is visible that the contribution of kinematic cost tended to decrease while those of dynamic cost increased with respect to the increase of movement speed and load.

Further analyses showed that the contribution of each cost with respect to the composite cost varied whenever movements sped up or a load was attached to the forearm (even if the combination weights were fixed). Particularly, the kinematic contribution tended to decrease while the energetic and dynamic contributions increased. Indeed, when the speed increased from slow to natural and then to fast, the kinematic contribution reduced on average by [4%, 7%] while the energetic and dynamic contribution increased amount of [0.5%, 1%] and [3.5%, 6%] respectively. Two-way repeated measures ANOVAs yielded no significant speed \times load interaction ($p_{kine} = 0.73$; $p_{ener} = 0.09$; $p_{dyna} = 0.39$) but a significant effect of load ($p_{kine} < 0.05$, $F_{kine}(1,9) = 5.9$, $\eta_p^2 = 0.39$; $p_{ener} < 0.05$, $F_{ener}(1,9) = 6.8$, $\eta_p^2 = 0.43$; $p_{dyna} < 0.01$, $F_{dyna}(1,9) = 13.9$, $\eta_p^2 = 0.60$) and speed ($p_{kine} < 0.001$, $F_{kine}(2,18) = 12.6$, $\eta_p^2 = 0.58$; $p_{ener} < 0.05$, $F_{ener}(2,18) = 2.9$, $\eta_p^2 = 0.25$; $p_{dyna} < 0.01$, $F_{dyna}(2,18) = 9.3$, $\eta_p^2 = 0.51$) on the contribution values for all variables.

In summary, these results show that the CNS may largely rely upon a kinematic cost to plan motion kinematics but that dynamic/energetic cost elements are crucial to account for the kinetics of the reach strategies and their adaptation to speed and load variations. This interpretation is confirmed by a reduction of the kinematic cost contribution which is gradually replaced by a larger contribution of its dynamic and energetic counterparts as

speed and/or load increase.

Discussion

In the current work, we examined the extent to which the brain adaptively exploits or compensates the interaction torque (IT) to assist or resist human arm movements and analyzed where this could originate from. To this aim, a free 3D arm pointing task (without predefined reach endpoint) was investigated while varying both limb inertia and movement speed, two factors that are known to influence IT. The experimental results showed that IT partly contributed to net torque (NT) thereby assisting the movement and that such contribution increased with limb inertia and movement speed. This finding might either be due to a lack of explicit compensation for IT or be a purposive goal of the CNS in order to exploit IT whenever it is sensible. This question was tackled by assuming that the observed trajectories were optimal with respect to a certain optimality criterion, and results showed that the present empirical observations were overall compatible with a composite cost trading-off kinematic, energetic and dynamic variables and not by any of these costs taken individually. Moreover, the increment of IT-to-NT contribution index was associated with a decreased contribution of the kinematic cost to the composite cost. This may shed new light on the origin of the adaptive use of IT, which might be related to the optimization of a trade-off between motion smoothness (i.e. kinematic) and effort (i.e. energetic/dynamic) that inherently reshapes the kinematic and kinetic aspects of a movement depending on speed/load constraints. These results are discussed in details hereafter.

Load and speed dependent use of interaction torque

Both load and speed was varied in this study in order to clarify the role of IT in motion planning. Indeed, IT critically depends on limb's inertia and speed characteristics. So if IT is an integral part of motion planning, some relevant motion parameters should vary significantly with respect to load/speed variations during the considered free pointing task. In the literature, several studies varied loads to examine the extent to which the brain tunes motor planning according to inertial properties. This was done in a series of works which have shown that motion kinematic parameters such as movement paths, endpoint variability and normalized velocity profiles were load-independent ([Atkeson and Hollerbach, 1985](#);

Bock, 1990; Papaxanthis et al., 1998; Hatzitaki and McKinley, 2001; Bagesteiro and Sainburg, 2003). These findings thus argued for a load compensation strategy since no effect of load on the arm trajectories was observed. However, this compensation strategy was questioned by other studies (Pagano and Turvey, 1995; Riley and Turvey, 2001; Bernardin et al., 2005) showing that the kinaesthetic perception of limb's position was significantly affected by rotational inertia variables such as the minimum inertia principal axis. Therefore, the brain seems to take into account not only the load but also the specific distribution of the masses involved in rotational movements and might therefore use it during motor control. This latter idea found support in recent studies which showed significant effects of the racket polar moment of inertia on the limb movement strategy when examining tennis serve (Rogowski et al., 2009, 2014). However, these studies were either limited to the analysis of the kinematic aspect of motor tasks or only concentrated on analyzing the effect of load on muscle torque (MT) while the effect of load on IT was not thoroughly examined, especially regarding to the contribution of IT to other torques (e.g. NT or MT). In the present work, using a quantitative approach to estimate the contribution of IT to NT allowed us to establish a more direct link between the limb inertia and the selected motor command defining the muscle patterns driving the arm. Interestingly, our results revealed that the brain purposely let IT increasingly contribute to NT to assist the movement when the limb inertia was increased via the addition of a load on the forearm.

Similar to the load effect, our results showed a significant effect of speed regarding the role of IT in the control of free arm pointing. Quantitative analyses showed that IT contributed more to NT such that IT assisted the movement more when the movement sped up. This finding was interesting given that IT magnitude is also known to increase drastically with speed, which was already shown to lead to IT utilization strategies in throwing tasks (Debicki et al., 2010, 2011; Hore et al., 2005, 2011; Hirashima et al., 2003, 2007). Further examination of IT at different phases of the movement (Fig. 3.14) showed that the contribution of IT to the movement was the highest around the peak of velocity. This finding was coherent with the work of (Asmussen et al., 2014) where the effect of IT was proved to vary with different temporal phases of the movement during a catching task. Additionally, the IT indexes related to accelerations (T_{acc}) and velocities (T_{vel}) both increased with respect to the movement speed. This finding actually confirms the work of (Hollerbach and Flash, 1982) which showed that the IT velocity terms have the same order of magnitude than the IT acceleration terms for a large range of movement speeds.

We next addressed the question of what principles or rules account for such an adaptive speed/load dependent use of IT. Namely, is it due to a lack of explicit compensation for IT or a goal purposely planned by the CNS in order to exploit IT? In the subsequent paragraph, we discuss why the brain could both compensate for and exploit IT, and why discriminating between compensation and exploitation of IT is sometimes a challenging task.

Compensation or exploitation of interaction torques, or both?

In the literature, the role of IT (being compensated or exploited) has long been debated and our study may help to disentangle some controversial interpretations. The compensation of IT has been proposed to account for the invariant aspects of certain movement kinematic parameters such as straight hand paths and bell-shaped speed profiles and extensively investigated in several studies of multi-joint limb movement focusing on planar point-to-point reaching tasks (Hollerbach and Flash, 1982; Sainburg et al., 1995, 1999; Bastian et al., 1996; Buhrmann and Di Paolo, 2014; Gribble and Ostry, 1999). These studies argued that the explicit compensation of IT could remove the non-linearity and noise-related errors caused by IT in control signals, thereby contributing to stabilize and smooth out the movement. This hypothesis is actually compatible with the kinematic-based motor planning principles such as the well-known minimum jerk (Atkeson and Hollerbach, 1985) as it allows using a simple “scaling law” to accommodate various movement speeds (Hollerbach and Flash, 1982). The common aspect of these studies is that the experimental setup was designed for planar motion involving quite a small number of DoFs (usually 2), and usually constrained the arm motion (e.g. via a manipulandum) and imposed a specific predefined reference point as a target, which may have affected their control strategies (Desmurget et al., 1997). In some studies, the setup could even lead subjects to freeze themselves the motion at specific DoFs. This was the case in the work of (Sainburg et al., 1995) where the same elbow excursion was always required whereas shoulder excursion could vary, or by the work of (Gribble and Ostry, 1999) where the experimental setup allowed accomplishing the task by only rotating around 1 DoF while keeping the motion state at another DoF either stationary or unchanged. As such, these protocols might have induced an IT compensation strategy in the sense that it was somewhat necessary to guarantee the task requirements. Nonetheless, it demonstrated clearly that the brain has the ability to

estimate and accurately compensate for IT when relevant for the task.

On the other hand, when examining more complex movement tasks (usually involving more than 3 DoFs) and without predefined final configuration of the limb (e.g. overthrowing task (Hirashima et al., 2003, 2007; Debicki et al., 2010, 2011; Timmann et al., 2008)), some authors have rather argued for the exploitation of IT to assist the movement. Interestingly, this latter idea allowed to explain many experimental observations. For instance, (Timmann et al., 2008) showed that the inability to exploit the passive inter-segmental interaction forces was associated with the poor ability to throw fast balls in cerebellar and unskilled subject. In a cyclical arm rotation task, (Isableu et al., 2009) showed that different rotation axes were chosen by different subjects, which was interpreted as different levels of IT exploitation depending on individual sensorimotor characteristics (more visual or proprioceptive). These findings were actually generalized into the hierarchical control hypothesis (Hirashima et al., 2003, 2007) or the leading joint hypothesis Dounskaia, 2005 that stressed the role of shoulder as a fundamental motion generator at other joints, via inter-segmental interaction acting at distal joints. Common to all these studies was the optimization of performance, which was a clear task objective (e.g. throw a ball at maximal speed will require a subject to effectively coordinate torques to gain more acceleration), and the freedom offered by the motor task (relatively weak spatial constraints).

The above discussion emphasizes a possible link between the role of IT and the requirements of the task. It suggests that (i) the brain can compensate or exploit IT depending on the characteristics of the task and (ii) compensation or exploitation may not be a mere property of the motor controller; instead, it could be the consequences of higher processes within the brain that are related to the subjective and objective goals of the movement. Therefore, if the compensation versus exploitation debate seems to have a task-dependent origin, difficulties also arose because the answer could only be about a “partial exploitation” or “partial compensation” in general. Indeed, what is not full compensation can be seen as partial exploitation and vice-versa. In most existing studies which supported the compensation of IT (Hollerbach and Flash, 1982; Sainburg et al., 1995, 1999; Bastian et al., 1996; Buhrmann and Di Paolo, 2014; Gribble and Ostry, 1999), subjects failed to perfectly counterbalance the effect of IT. It was then argued that this was due to the lack of explicit compensation of IT, or to a partial compensation of IT (Gribble and Ostry, 1999). In fact, there was still a small contribution of IT to NT. Similarly, in studies supporting IT exploitation, IT was never observed to contribute completely to NT, meaning that a

part of IT was actually canceled out by MT. In other words, the joints (often distal) were not entirely moved by IT, likely because such perfect exploitation would have driven the system to states incompatible with the task achievement or have yielded to undesired arm kinematics (e.g. more jerky trajectories). Therefore, it seems tricky to conclude whether the brain plans to partially compensate or partially exploit IT, but what is undeniable is that the brain elaborates motor commands such that IT contributes to NT whenever it is possible and relevant for the task. We discuss below how this relative exploitation versus compensation strategies may arise during motor planning.

Motor planning: a trade-off between kinematic and kinetic factors

The above issue about IT compensation/exploitation is in fact strongly related to the nature of hypothetical cost functions underlying motor planning. At a theoretical level, it is clear that the optimization of a kinematic cost would produce maximally smooth movements that account for the case of a full compensation of IT. In contrast, the optimization of dynamic or energetic costs would minimize the magnitude or the work of MT which will result in IT exploitation, to the greatest possible extent. In other words, this will improve the efficiency of the motor controller with respect to motion effort. Therefore, the question of whether the brain exploits or compensates IT during movement planning can be reappraised in optimal control theory by comparing between kinematic versus dynamic or energetic cost functions. Indeed, kinematic cost functions cannot exploit IT while cost functions involving torque-related variables can exploit IT. In this vein, assessing whether human movement is planned in terms of kinematic or dynamic/energetic variables has been tested in several studies ([Wolpert et al., 1995a](#); [Flanagan and Rao, 1995](#); [Soechting et al., 1995](#); [Soechting and Flanders, 1998](#); [Vetter et al., 2002](#); [Hermens and Gielen, 2004](#)). Here, optimizing only energetic or dynamic criteria lead to discrepant arm trajectories in terms of joint and Cartesian displacements, in which case it made no sense to further investigate what happened in torque space. In contrast, maximizing smoothness in joint space (angular jerk, i.e. kinematic cost) was remarkably efficient to fit the angular and Cartesian displacements but it failed to describe accurately the movement in torque space. The only model that could explain both kinematic and kinetic aspects of the reach strategies, and their speed/load dependences, was the composite optimality criterion mixing variables of different nature. This composite cost idea was already advanced and investigated differently in

previous studies (Gielen, 2009; Berret et al., 2011a; Vu et al., 2016).

Interestingly, the effectiveness of a composite cost mixing these criteria to replicate the experimental data may help to understand why the reach strategies planned by the brain were as observed, in particular for what concerns ITs. For instance, one could wonder why the brain did not let IT drive the movement more extensively (e.g. at the 1st and 2nd DoF of the shoulder joint). Indeed, less MT would be required at these DoFs, which may be dynamically more efficient. However, in this case the arm trajectory would have been very different from the empirical one, possibly quite jerky, and the existence of large IT might even be harmful for the anatomical arm structure. One could also wonder why the brain did not try to cancel out all ITs to gain movement smoothness and stability but also to simplify motor planning. In that case, the brain should totally compensate or even “overcompensate” for ITs, that is, having both NT and MT opposed to IT at a given DoF. However, the big disadvantage would be that large muscle torques are required to do so. Therefore, although motor planning could be simplified by neglecting IT effects and subsequently canceling them out during motor execution, the dynamic efficiency of the movement would simply be non-optimal. Reconciling all the advantages and disadvantages of these two extreme strategies, the empirical and simulation results indicated that the brain may choose an mixed motor planning principle combining both kinematic and kinetic variables whose relative contributions to the control strategy may be differentially revealed by the task demands. This composite cost may automatically yield the adaptive IT compensation/exploitation trade-offs described in the present study, although it required the introduction of two additional free parameters for each subject to capture the adaptive use of IT (see below).

Limitations

At this point, it worth stressing some limitations of the present work. First, the superiority of the composite cost over the kinematic cost requires 2 additional parameters for each participant. Therefore, it is questionable whether the improvement in the fitting is large enough to justify these additional tuning parameters. To clarify this point, we computed Akaike information criterion (AIC) according to the formula $AIC = n \log(RSS/n) + 2k$ where n is the number of samples, RSS is the residual sum of squares for the predicted variable and k is the number of parameters plus one (?). An optimal control model predicts

a whole movement and, therefore, many parameters can be extracted and used to compare simulated and experimental trajectories. Here we used a kinematic measure (RE index) and a dynamic measure (IT index) to assess the two models. AIC for the kinematic and composite cost models were respectively 27.0 ± 3.9 and 26.6 ± 3.1 for the joint space error. This means that there was no need for a composite cost function to account for the experimental joint kinematics. At this level of analysis, using a composite cost was likely overfitting. Yet, when looking at the predictions in dynamic space (via IT index), AIC were 6.7 ± 1.0 and -15.2 ± 2.5 for the kinematic and composite costs respectively. At this level of analysis, using a composite cost with adjustable parameters became well justified. These considerations emphasize a key question in motor control: what metric or parameters should we use to compare simulated and experimental data in general? If researchers would probably agree that the kinematics should first be predicted before the dynamics, it is conceivable that a good model should explain motion in both spaces at once.

Second, one should also stress that our formalism might overestimate the role of the kinematic cost in motor planning. Indeed, we used deterministic optimal control in which a feedforward motor plan is completely established before movement is executed. This complete planning of the trajectory is not strictly required by the optimal feedback control (OFC) formalism that assumes a feedback control law whose characteristics moreover depend on the signal-dependent noise present in the nervous system (Todorov and Jordan, 2002). In a similar task with redundant targets, we have shown in an earlier study that OFC was especially useful to account for intertrial variability via the minimum intervention principle (Berret et al., 2011b) (which should explain ellipses in Fig. 3.9). However, when looking at average behaviors, a deterministic modelling was overall consistent with such models (Berret et al., 2011a). Signal-dependent noise may nevertheless reshape the mean optimal trajectories to some extent. This could affect the kinematic model that requires large MT in this deterministic setting. With signal-dependent noise and a variance cost on the endpoint it is conceivable that such large MT would be penalized as they would increase motor variability. But variability increases with “effort” as noise is multiplicative, which is related to the size of motor command (e.g. torque change in our modeling). Therefore, a kinematic and variance cost would be reminiscent of the composite cost investigated in the present deterministic framework.

GENERAL DISCUSSION

4.1 Conclusions

4.1.1 Speed and load dependence of arm trajectories

The research described in the present dissertation aims at identifying the planning principles during the 3D non-constraint limb movements under different conditions of speed or load. To achieve this goal, we studied a free reach endpoint task starting from a L-shaped arm posture toward an horizontal plane at slow (S), natural (N) and fast (F) speeds and with or without load attached to the forearm.

For the speed effect, our experimental results showed that the subjects exhibited different motor strategies depending on the instructed speeds. These results supported certain findings (Fitts, 1954; Papaxanthis et al., 1998; MacKenzie and Iberall, 1994; Elliott et al., 2001; Isableu et al., 2003, 2009) while diverging from the other ones (Flash and Hogan, 1985; Ostry et al., 1987; Gordon et al., 1994; Soechting and Lacquaniti, 1981; Soechting et al., 1995; Flanders et al., 1996). More specifically, in the latter studies, researchers found that several prominent aspects of motor strategies such as the hand path, the final hand variability or the final arm posture were globally independent with respect to speed variations. However, in the former studies, researchers revealed certain evidence of speed dependence of the arm movements. What caused these different conclusions? Interestingly, one could observe that in most of the studies showing no effect of speed, the motor tasks were mainly designed to be executable in either vertical or horizontal plane and usually assigned a single spot for the target. As such, the tasks were generally considered as 2D point-to-point movements involving motion of few DoFs (normally 2 or 3 DoFs) in the joint space while the target position was specified by two coordinates in the Cartesian space. Consequently, certain features of the motor strategy were possibly induced by the sensorimotor transformations which causally limited the variability of the motor command. On the contrary, when the task constraints were reduced, the arm trajectories was reported to be changed according to the speed of movement. This was exemplified by the work of Isableu et al. (2009) who studied a cyclic arm rotation involving a 3D free arm motion and found clear evidence for a switch of rotation axes from a geometric to an inertia-related one when the movement speed increased from S to F. In the present studies, we extended this motor task to the case of discrete movement in a paradigm which did not prompt any specific endpoint to reach to. As such, the experimental setup offered the external task redundancy which provided the subjects with freedom to decide the “where to go” and

the “how to go there” by themselves and allowed the motor controller exhibiting various characteristics to the greatest possible extent. Consequently, our studies revealed quite interesting speed-dependent variations of the motor command, for example in terms of interaction torque contributions which were apparent on the hand paths. Thus it suggested a tangible link between speed-dependence of arm trajectories and the constraint at the level of the motor task: the looser the constraint of the task, the more visible the speed-dependence of hand paths.

Similarly to the speed effect, our studies showed significant effect of load on motor commands in a way that led to significant hand path modifications. Specifically, we observed different motor strategies (e.g. final reach endpoint, coordination of torques) with respect to different conditions of load. This load-dependent finding was in contrast with the results of some studies (Atkeson and Hollerbach, 1985; Bock, 1990; Papaxanthis et al., 1998; Hatzitaki and McKinley, 2001; Bagesteiro and Sainburg, 2003) while supporting other studies (Pagano and Turvey, 1995; Riley and Turvey, 2001; Bernardin et al., 2005; Rogowski et al., 2009, 2014). Indeed, in the former studies, researchers argued for the load-independence of arm trajectories where the disturbance introduced by the load was supposedly compensated. However, this argument has been questioned by the latter studies which have shown the significant influence of attached load on the limb trajectories (in motion state) or limb kinaesthetic perception (in stationary state). In the present work, using a quantitative approach to estimate the effect of load, especially at dynamic level, our results revealed that the brain purposefully modified its sensorimotor controller to assist the movement when the limb inertia increased via the addition of a load.

Therefore, these results suggest that interesting findings can be found by considering tasks in which the constraints imposed by the experimenter are reduced. This is by the way a situation that occurs in daily life as most motor tasks do not impose where to go, how to get there and with what pace and so on. Letting participants to make such motor decisions allows to get useful insights about the properties of the motor command triggered after movement planning.

4.1.2 Inter-individual differences

In the present dissertation, our results also provided interesting evidence of inter-individual differences. When examining the effect of speed, for instance, analyses showed that differ-

ent subjects exhibited various degrees of speed-dependence of their motor strategy (small dependence for some subjects vs strong dependence for the others). Indeed, inter-individual differences have been emerging as a hot topic of research and intensively studied by researchers in recent years. In this vein, it could be listed here the work of some researchers such as Pozzo et al. (1991); Bernardin et al. (2005); Isableu et al. (2003). However, in these studies, inter-individual differences were mostly examined at the kinematic level (the lowest level of motor control) and thus they lacked an explicit explanation for such differences. In the work of Isableu et al. (2009) where the dynamic analyses (a higher-level of motor control) were conducted, the authors found that there existed a relevant link between the inter-individual differences and the coordination of the interaction torque, the joint muscle torque, the gravitational torque with respect to the net torque. Yet, it could not point out which principle may be internally used to control such coordination. In the present studies, we try to interpret the inter-individual difference issue at the neural level of motor control. We hypothesize that the motor planning may be tightly linked with the optimization of composite of certain kinematic-, energetic- or dynamic-oriented variables and that some subjects should rely more heavily on kinematics (kinematicians) while others should rely more heavily on dynamics cost functions (dynamicians) (Isableu et al., 2009, 2010). Interestingly, our results showed that the inter-individual differences between subjects were not fully due to their anthropometric differences but rather reflected the different strategies that the subjects may use to weight each variable differently inside the composite cost. According to this view, depending on the chosen composite cost, varying the anthropometric characteristics could change the degree of speed-dependence of an individual. On the other hand, for fixed anthropometric characteristics, the relative weights defining the composite cost were critical to explain the degree of speed-dependence of each participant. Thus, if two subjects have similar anthropometric parameters, it is still possible that one subject is speed-sensitive while another is speed-insensitive if their brain weighted the combination of cost (kinematic, energy, dynamic) differently during the motor planning processes.

Finer analyses of the contribution of each element to the composite cost (measured in percent) allowed interpreting more clearly the origin of the inter-individual differences. The results showed that the contributions of kinematic and energetic/dynamic costs are unequal and subject-dependent. Indeed, the subjects who showed the speed-insensitive kinematics tended to use more kinematic variables but less energetic/dynamic variables during the motor planning than the others who showed the speed-sensitive kinematics

regardless of movement conditions of speed/load. Thus it would be coherent to expect that there must exist a relevant link between the cost contribution (its absolute values) and the kinematical parameter of interest (e.g. RE, e3). However, the linear regression results over the subjects participated in our first experiment (Section 3.2) revealed that no or quite weak significance was obtained between these indexes (showed on the left panels of Figure 4.1). Nonetheless, when examining the cost contribution changes with respect to speed variation, this means, the relative changes (defined as subtraction) of these indexes were used corresponding to the shift of speed from S to N, S to F and N to F, an interesting result was gained (showed on the right panels of Figure 4.1). Particularly, we obtained a significant linear regression across all subjects. These results implied that at a specific pace of movement (e.g. S), different subjects may plan different contributions for different costs depending on their anthropometric characteristics and/or their preferential motor control strategies but when the movement speed changed from S to F, there existed a certain rule governing over all subjects, that is, the brain purposefully adjusted the contribution of elementary cost by increasing the contribution of energetic/dynamic elements while decreasing the contribution of kinematic ones.

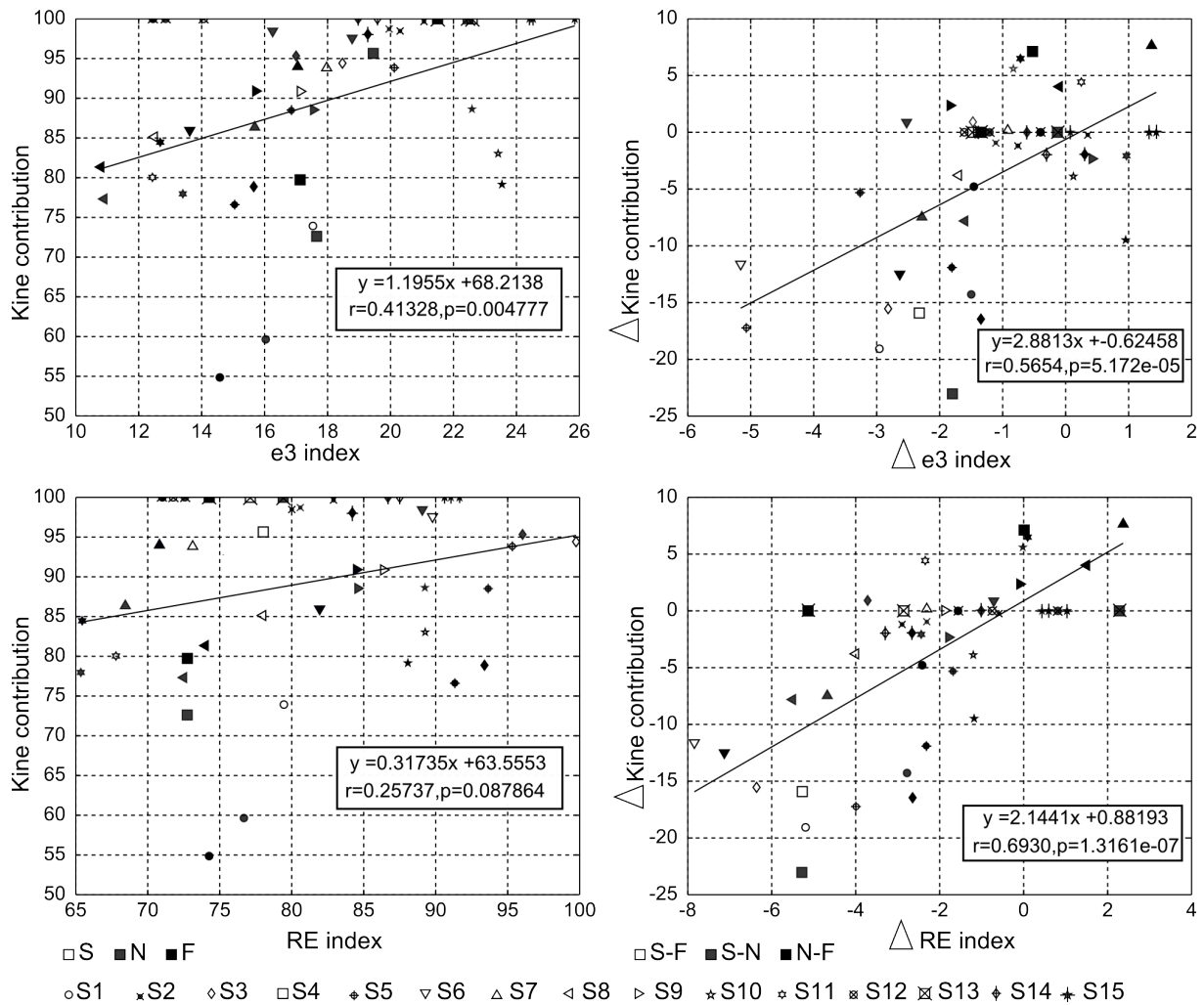


Figure 4.1. Linear correlation analysis between kinematic cost contributions and each examined movement parameter (e3 and RE) for 15 subjects participated in our 1st experiment. *On the left panels* are absolute values. *On the right panels* are relative values (i.e. changes of the values when comparing different speeds) and emphasized by the symbol Δ . It is visible that the linear correlation results are considerably improved as the relative values is examined, indicating a quite strong link between the e3/RE indexes and the kinematic contribution: with the increased kinematic contribution, the e3 and RE indexes increase.

4.1.3 Compensation versus exploitation of passive source of movement

Our results shed new light on the controversy regarding the idea of whether the brain should exploit or compensate for interaction torque (IT). Indeed, this issue has been a long-standing debate between researchers. Some researchers argued for the compensation of IT in favor of smooth and stabilized movement (Hollerbach and Flash, 1982; Sainburg et al., 1995, 1999; Bastian et al., 1996; Gribble and Ostry, 1999) while others argued for the exploitation of IT to assist the movement (Sainburg and Kalakanis, 2000; Hirashima et al., 2003, 2007; Dounskaia et al., 2002; Dounskaia, 2005; Debicki et al., 2010, 2011; Hore et al., 2011; Asmussen et al., 2014; Wang and Dounskaia, 2015; Dounskaia and Shimansky, 2016). In order to reconcile these different ideas, we proposed two hypotheses, which are: (i) the brain could have ability to both compensate and exploit IT and (ii) compensation or exploitation of IT might be task-dependent. If such hypotheses are correct, on which principles the brain might rely to establish such a trade-off between compensation and exploitation of IT?

In section 3.4, we found evidence to confirm these hypotheses. Indeed, trying to distinguish the compensation from the exploitation of IT is not necessary because it is natural that what is not compensation is exploitation. In fact, in the earlier studies, whatever the brain compensated or exploited the IT, we have never observed a complete compensation of IT or a total 100% exploitation of IT. Therefore, it is relatively hard to definitely conclude whether the brain plans to partially compensate or partially exploit IT but it is undeniable that the brain purposefully let IT increasingly contribute to the net torque to assist movement when possible and relevant for the task. Therefore, we come back to the question raised above: which variables/rules drive the integration of IT into the motor command?

Using the optimal control approach to simulate the recorded motor commands, our results show that the compensation and exploitation issue could be tightly linked to a trade-off between smoothness and effort of movement. This trade-off is in turn specified by a combination of elementary variables (kinematic, energetic/dynamic) possibly encoded inside the brain during the motor planning process. This mechanism could be explained more clearly as follows: For the tasks which supported the compensation of IT, a kinematic variable would be dominant at the motor planning level while the presence of

energetic/dynamic variables would be more negligible. Consequently, the optimization of kinematic cost would produce a smooth and stabilized movement by mostly canceling out the dynamical effects of IT. On the contrary, for other tasks (e.g. throwing ball) where the exploitation of IT was put forward, a kinematic variable could still highly contribute to the motor planning process to obtain a smooth/natural movement but the participation of energetic/dynamic variables could be significantly increased. This increase of the weight of energetic/dynamic elements would let the brain use IT as much as possible to assist the movement and produce economic arm trajectories.

Here a more general question is emerging: should the brain treat the other passive torques (defined as all other torques involving into movement except net torque, e.g. gravity torque) in the same way as with IT? It is not easy to obtain a clear answer. In fact, like IT, the possibility to compensate for the gravity torque is quite well-known among the robotic community wherein the gravity torque is usually compensated in order to simplify the control algorithm. However, it is more complex in the studies of human motor control as different researchers argue for opposite ideas: some researchers support the compensation hypothesis while others for the exploitation hypothesis of GT. Indeed, the former idea has been dominant for a long time as it permits cancelling out the impact of GT on arm trajectories and using a "scaling law" to produce the same movements at various speeds (Atkeson and Hollerbach, 1985; Bock, 1990; Papaxanthis et al., 1998; Hatzitaki and McKinley, 2001; Bagesteiro and Sainburg, 2003). However, this idea is recently questioned by other researchers who have found evidence that the brain exploits GT to assist movement to a certain extent (Pagano and Turvey, 1995; Riley and Turvey, 2001; Bernardin et al., 2005). Particularly, in Gaveau and Papaxanthis (2011), the authors uncovered that during a vertical pointing task (the effect of GT is the most relevant in a vertical plane), the GT was integrated into the motor planning which led to different arm kinematics for upward and downward movements. In Gaveau et al. (2014), the author further revealed that the CNS optimizes gravity mechanical effects on the moving limbs depending on the direction of movement and magnitude of GT. Moreover, this gravity effect is only accounted for by a composite of the minimum absolute work and jerk costs (Berret et al., 2008). Here, the similarity of the results obtained for IT and GT thus suggests that the brain possibly takes into account all the passive torques and tries to exploit them to assist the movement whenever this exploitation is relevant for the task. Exploiting the forces coming from the body motion itself or from the environment would then be a global

objective of the motor system as it would allow to reduce the overall effort associated with movements. Such considerations to generate economic yet smooth movements could originate from evolution and development during life. Although the gain may be small for a single movement, the savings accumulated over time could be significant and would constitute a key characteristics of human sensorimotor control.

4.1.4 Necessity of composite cost

According to which cost function (variables) human trajectories are optimal is a long-standing issue in motor neuroscience. In this vein, some researchers argued for the kinematic-oriented motor planning where the non-linearities of the motion dynamics were just compensated for or suppressed by the brain to preserve limb's stability (Hollerbach and Flash, 1982; Atkeson and Hollerbach, 1985; Bastian et al., 1996; Sainburg et al., 1995, 1999; Gribble and Ostry, 1999). On the contrary, other researchers argued for the energy/dynamic-based motor planning where the mechanical limb properties were taken into account and exploited to the greatest extent possible (Dounskaia et al., 2002; Debicki et al., 2010, 2011; Hore et al., 2005, 2011; Berret et al., 2008; Wada et al., 2001; Uno et al., 1989; Nakano et al., 1999). To reconcile all these controversial findings, the idea of composite cost functions relying upon kinematic, energetic and dynamic variables emerged as a possible avenue. However, it was only until 2011 that the evidence for the existence of composite cost was first found. By examining a 2D vertical reaching-to-plane task from different initial positions at a relatively fast space, Berret et al. (2011a) has shown that only combination of angle jerk and absolute work costs could account for recorded arm reaching trajectories. Yet, it remained unclear whether these results would extend to 3D motion?

Interestingly, our results provided answers to the above question, confirming that the 3D recorded arm trajectory was an outcome of optimization of a cost possibly weighting kinematic, energetic and dynamic variables. Here, questions about the flexibility of composite cost under different conditions of movement speed subsequently emerged. For instance, is an unique composite cost sufficient to account for the arm trajectories at different speed? Or must the brain modify the weight of each element inside the composite cost when the movement speed changes? If so, which principle might the brain use to tune the composition of the cost? In this vein, our results indicated that an unique cost was possible to explain movements executed at different speed for each subject and that the subjective

cost was not necessarily modified according to speed constraints.

More importantly, our results prove that the idea of composite cost might be a new solution to reconcile many controversial conclusions in the earlier studies. Actually, motor planning has been shown to be a complex process and seems to be task-dependent such that researchers could obtain contradictory results. In the literature, such controversies could be observed quite often, involved all aspects of arm movements from the lowest to highest level analyses of motor control. For instance, if one focuses on the effect of speed on arm movement, one can find a conclusion of speed dependence in some researches (Flash and Hogan, 1985; Ostry et al., 1987; Gordon et al., 1994; Soechting and Lacquaniti, 1981; Soechting et al., 1995; Flanders et al., 1996) and the opposite idea in the other (Woodworth, 1899; Fitts, 1954; Papaxanthis et al., 1998; MacKenzie and Iberall, 1994; Elliott et al., 2001; Isableu et al., 2009; Vu et al., 2016). Again, if one focuses on torque pattern at a dynamic level, one can find some studies arguing for the compensation of certain torques of interest (e.g. IT, gravity torque (Hollerbach and Flash, 1982; Sainburg et al., 1995, 1999; Bastian et al., 1996; Gribble and Ostry, 1999; Papaxanthis et al., 1998)) but also other studies arguing for the exploitation of these torques (Sainburg and Kalakanis, 2000; Hirashima et al., 2007; Dounskaia et al., 2002; Dounskaia, 2005; Debicki et al., 2010, 2011; Wang and Dounskaia, 2015; Dounskaia and Shimansky, 2016). The interesting thing is that all these studies reached their conclusion using specific tasks and methods. This means that the brain seems to possess all these alternative planning strategies, but depending on the circumstance of the motor task, authors would observe certain characteristics and not the other. Thus, the resulting question is of how can we explain for such different behaviors in a common and generic framework?

Interestingly, in terms of cost function, optimizing separately single cost could allow to account for certain characteristics of movement but is not sufficient to reconcile the controversial aspects of movement. For instance, the speed-independence, the compensation of IT and possibly of GT could be accounted for by the kinematic-oriented planning while the opposite behaviors (i.e. speed-dependence, exploitation of IT, GT) could be accounted for by the energetic/dynamic-oriented planning or simply lead energetic/dynamic cost to emerge (they could be only a consequence). Indeed, the same kind of results were obtained in the present studies across participants. Actually, in section 3.2, the results showed that kinematic cost could account for trajectories executed by the speed-insensitive subjects but failed for the speed-sensitive subjects. On the other hand, the energetic/dynamic

costs predicted better the speed-dependent modification of motor trajectories but the simulated trajectories were too far from the real ones to be plausible optimality criteria. Similar results were observed in section 3.3 where we examined nature of the motor command in torque space. Again, the kinematic cost could only replicate well the trajectories of hand paths but totally failed to predict what really happens in terms of coordination of torques. On the contrary, the dynamic cost predicted quite well the coordination of torques but could not reconstruct the real trajectories. Thus, none of the single cost could both extreme behaviors observed in motor control studies. However, in terms of the composite cost where the weighting factors are mostly subject-dependent, we have been able to explain both speed-dependent and speed-independent characteristics observed among different subjects. We were also able to show that IT exploitation was linked to a trade-off between kinematic and energetic/dynamic costs. Thus, the idea of composite cost may be a useful means to reconcile prior conflicting studies which attempted to uncover the principles underlying arm movement planning.

4.2 Limitations

4.2.1 Technological limitations

The fact that the markers of motion capture system attached on the subject's body could move with the skin might prevent us from reconstructing exactly the displacement of joints. Indeed, in an ideal case, the extraction of the marker position should reflect explicitly the rotation of the joint. However, in practice, it is rare to achieve the ideal case because of the slide of skin effect where we attached the marker on. Such effect of skin's slide might be small at each joint motion evaluation but can accumulate to cause a large effect to the end-effector in the Cartesian space.

Besides the impact of marker's position, our studies were also affected by the number of camera. Indeed, we used 8 cameras to track 12 markers attached at different position on the trunk and the right upper limb of subjects. Statistical analyses showed that we had to reject in total about 10 % of data because the cameras lost data of certain markers at certain moments during the limb movement.

4.2.2 BSIP estimation

The estimation of BSIP is quite crucial in the present studies, especially in the computation of the rotation axes (e3) and in the analyses of inverse dynamics. Here, we used a regression methods based on the scaling functions proposed by [Dumas et al. \(2007\)](#). Although this method is easy to apply, it has a few downsides since the BSIP are not individualized very precisely and are scaled for specific ethnic populations.

4.2.3 Simulation limitations

In the present dissertation, we use a numerical optimal control methodology to simulate the motor commands. Although this method allows us to explain many empirical observations, it still has some limitations.

In general, it is not easy to implement an optimal control program as it requires researchers to have multidisciplinary knowledge. Actually, an optimal control program consists of two main parts, which are the optimal control calculation and the kinematic/dynamic estimation of the system under consideration. For the former part, there are different softwares to approximate the continuous-time optimal control problem as sparse nonlinear programming problem. Here, we used a Matlab-based software called GPOPS as it is relatively user-friendly and more importantly it allows us inheriting certain works of other researchers in our group. However, the slow running speed of Matlab caused quite a lot of troubles in the current studies because Matlab was quite time-consuming in the kinematic/dynamic calculation of limb model of large DoFs (4 DoFs in our cases). Indeed, if we calculated necessary torques for the simulation process directly in Matlab, the optimal control program might take hours to find out the optimal solution corresponding to the minimization of a specific cost function. In case of inverse optimal control where we inferred the cost based on the recorded data, it even took more time, up to days/weeks, to gain its final solution. Obviously, such program was inefficient and quite hard to debug and parametrized. In order to solve this problem, we calculated the kinematic/dynamic processes outside of Matlab environment based on the classical Newton-Euler method by compiling a mex-file that allowed us to carry out all computations in C programming language. This step considerably improved the speed of the inverse optimal control program but it was still not fast enough. Fortunately, the problem was finally made tractable in terms of running speed when we used the Featherstone-based method. Briefly, this method

is based on Newton-Euler methodology but its computation is carried out in space of 6 dimensions at one instead of 3 conventional dimensions. However, it required some efforts to understand and adapt this method to our specific model and to use it with mex files. Overall, this shows that several difficulties may arise when modeling high-dimensional systems and that development efforts must be done to make those methods usable in practice. It is thus important to have access to state-of-the-art methods and toolboxes to run such simulations. But with the development of robotics, increasingly more software packages are proposed and this time-consuming step is going to be simplified in coming years.

Secondly, due to the limit of time, in the present studies, only effect of subjective cost was examined. Although the results showed the important part of subjective costs to explain for the observed motor strategies, it was impossible to reject the role of other factors associated with the objective of the motor task which is usually related to the goal of task such as minimizing the time of movement or maximizing the speed/acceleration of hand at the moment of ball release in a ball -throwing task. The examination of such objective costs is especially crucial as a lot of evidence showed task-dependent characteristics of motor planning. Furthermore, the existing fitting error between the recorded motion and the simulated one could reflect the fact that only modelling subjective cost is not enough to fully account for the real arm trajectories of subjects. This means that besides subjective cost there must be contribution of other cost to the motor planning. Finding out these costs will allow us to have a deeper understanding of principle that the brain might use to plan motion. In particular, when instructed a subject to adapt his/her speed, we introduce a new task constraint. While a natural movement pace can emerge from subjective criteria, urging someone to move fast or slow may introduce additional objective costs that we should or could take into account (move slow may mean to penalize large velocities in an objective cost).

4.3 Perspectives

This project aimed at identifying and simulating 3D multi-joint non-constrained movements of the upper limb. In the present studies, our results may be pretty task-dependent as only one type of arm motion was examined, although we varied speed and load conditions to better decipher the principles guiding motor planning. However, similar tools and analyses could be extended to:

- Other studies, especially to the existing behavioral studies, describing motor control characteristics without an explicit explanation of what may happen at the motor planning level. The application of optimal control to such studies will provide researchers with a better insight of what internally happen within the brain.
- The examination of the role of objective costs with respect to the subjective costs. This might be an interesting work which can reveal a potential trade-off between the objective and subjective costs during the motor planning process.
- Assessing the role of vision (gaze) in the achievement of movement as it is undeniable that vision plays an important role in sensorimotor control. By associating a cost function with vision (via a final cost related to gaze direction for example), an analysis of cost contribution may allow us to quantify the contribution of vision to movement planning in tasks where no final hand location is imposed to the subject (such as when putting an object on a table, the object could be placed in plenty of locations).
- Finding the biological evidence for the existence of composite cost via the electromyography(EMG) or the electroencephalography (EEG) will strengthen the validity of the result found in the current thesis.

Finally, porting these findings and methods to other fields and populations (e.g. in athletic subjects, in patients with altered or with motorized prosthetic devices) could be interesting to optimize performance in sport, imagine better rehabilitation protocols and develop biological control loops that are compatible with human motion when a subject and an artificial device of moving together toward a common goal.

LIST OF TABLES

2.1	Anatomical landmarks	26
2.2	Trunk coordinate definition	28
2.3	Humerus coordinate definition	28
2.4	Forearm coordinate definition	28
2.5	Hand coordinate definition	28
2.6	The segment coordinate system based on the marker set and the order of rotational axes	34
2.7	Scaling factors for the weight of each segment of upper limb (Dumas et al., 2007)	39
2.8	Scaling factors for the position of the CoM of each segment in percent of each segment's length, measured experimentally (Dumas et al., 2007)	39
2.9	Scaling factors for the inertia tensor (Dumas et al., 2007)	40
2.10	Denavit-Hartenberg parameters associated with each DOF of the model	44
3.1	Cost functions considered in this article. Their overall class (kinematic, energetic or dynamic), the chosen representative element of each class with its classical name, the mathematical definition of the cost and the references which proposed them.	74
3.2	Experimental movement parameters (mean±std across subjects).	79
3.3	Correlation analyses for RE and e3 indexes for all the participants. Correlation coefficients R, statistical significance p and slopes of linear regression (K) for two examined parameters (RE, e3) with respect to the peak of velocity (in m/s) are reported for each of the 15 subjects. Correlation coefficients significantly different from 0 are emphasized in bold.	84
3.4	Definition and references for the cost functions used in the current study.	112

3.5 Main kinematic movement parameters (mean \pm std across subjects) for the
three speed (S, N, F) and two load (no load, with load) conditions. 118

LIST OF FIGURES

2.1	The sensorimotor loop can be divided into three stages. These three are represented in the CNS as the inverse model, the forward dynamic model and the forward sensory model, respectively Wolpert and Ghahramani (2000) . . .	10
2.2	Internal sensorimotor integration model proposed by Wolpert et al. (1995b) .	12
2.3	Experimental evidence for the existence of the internal inverse models. Panel A shows the trajectories without the perturbations; Panel B shows the initial perturbations that cause large movement variations; Panel C shows the trajectories with the perturbations after learning sessions and panel D shows the after effects of the trajectories when the perturbations are removed (Shadmehr and Mussa-Ivaldi, 1994).	13
2.4	Anatomical model of the human upper body (Hansen, 2013).	26
2.5	Body landmarks of the thorax, clavicle, scapula and humerus (Wu et al., 2005).	27
2.6	The segment coordinate model and the joint model of the upper right limb .	30
2.7	A motion capture system composing of eight cameras (Hansen, 2013).	32
2.8	A set of marker used in the current work for the upper body (Hansen, 2013).	32
2.9	Illustration of Devavit-Hartenbeg principle	41
2.10	Coordinate systems of the upper arm based on D-H description	43
2.11	Characterization of Link i for Newton-Euler formulation(Bruno Siciliano, 2009)	46
2.12	Algorithm of Newton-Euler method(Bruno Siciliano, 2009)	48

3.1	Illustration of the experimental paradigm. Fixed initial arm position and horizontal target plane were tested, thereby defining a free reach-endpoint motor task. The reach endpoint was one prominent movement parameter. Two other relevant movement parameters (rotation axis displacements, SE and e3) are depicted. Gaze direction was controlled during the movement as indicated by the arrow. Note that any possible path leading to any location onto the surface was possible regarding task achievement. The task was thus redundant (3 free joint angles for most endpoint locations) and 3D as the arm could freely move in 3D space without any constraint, except that of reaching the target plane at various instructed speeds (slow, normal and fast, denoted by S, N and F respectively).	68
3.2	Reach endpoint positions of two subjects (S5 and S14) for the three different speeds (S, N and F). The 95% confidence ellipses of reach endpoints in the S, N and F speed conditions are drawn in thick, thin and dotted lines, respectively. Note that along the antero-posterior (AP) axis, the distributions of finger positions of S14 remain relatively constant regardless of movement speed while those of S5 tend to decrease when movement speed increases.	81
3.3	Dependence of RE and e3 indexes on movement speed for the two subjects S5 (<i>left</i>) and S14 (<i>right</i>). For each examined index, linear correlation and regression lines (thin black lines) were computed based on all recorded data (each dot of the graphs corresponds to a single trial). For S14, RE and e3 indexes appear to be nearly independent of speed variations while those of S5 decrease clearly when movement speed increases.	82

-
- 3.4 Movement parameters predicted by each elementary cost (kinematic, energetic and dynamic) during the plane-reaching task at three different speeds (S, N and F). *Left.* Movement paths of the fingertip start from the same position (black circle) but end at different reach endpoints on the target surface. *Right.* Variation of RE and e3 indexes with respect to speed. The kinematic cost generated speed-invariant trajectories (constant movement path as well as RE and e3 indexes), whereas the dynamic and energetic costs generated relatively small and large speed-dependent trajectories respectively. RE and e3 indexes varied accordingly for the two latter costs. These two costs exhibited some degree of speed dependence because they both involved dynamic variables such as muscle torques and the musculoskeletal dynamics was highly nonlinear. 86
- 3.5 Reconstruction errors in joint space (E_{Joint}) and Cartesian space (E_{Cart}) for the best-fitting speed-dependent composite cost (SDComp) and speed-independent composite cost (SIComp) as well as each of the three cost elements taken separately, for the different speeds (S, N and F). Error values were averaged across subjects (with standard errors indicated by error bars). Noticeably, in terms of both joint and Cartesian errors, the composite costs (SDComp and SIComp) performed better than each elementary cost taken alone (Kine, Ener and Dyna). Horizontal bars with stars indicate the results of post-hoc analysis. One, two and three stars stand for $p < 0.05$, $p < 0.01$ and $p < 0.001$ respectively. 88
- 3.6 Simulated finger paths predicted from the best-fitting composite cost (SIComp) and average experimental finger paths for subject S5. *Left.* 3D finger paths for the three speeds for experimental (plain traces) and simulated (dotted lines) data. *Right.* The zoomed-in projections of finger paths on the sagittal plane (*top*) and the transverse plane (*bottom*) for the last part of the movement, in order to emphasize differences. In general, fitting errors mainly arose from the discrepancy of trajectories along the ML axis while along the AP axis (main axis of interest here), the simulated trajectories better matched the recorded ones and clearly exhibited a speed dependence. 89
-

3.7 Reconstruction errors for some relevant movement parameters (E_{e3} , E_{RE} , $E_{\bar{K}_{e3}}$, $E_{\bar{K}_{RE}}$) for the SDComp, SIComp costs and the three cost elements taken separately. Error values were first averaged across speeds and then across subjects (with standard errors indicated by error bars). Visual inspection reveals that in terms of both E_{RE} and E_{e3} the dynamic cost performs quite poorly compared to the other costs. In terms of $E_{\bar{K}_{RE}}$ and $E_{\bar{K}_{e3}}$, the energy cost overestimates the speed dependence of RE and e3 parameters. Overall, the kinematic cost performs relatively well but the composite costs perform significantly better than the latter. Importantly, the kinematic cost is also unable to account for any speed-dependence as it predicts constant movement parameters for all speeds. Finally, no significant difference was found between the SDComp and SIComp. 90

3.8 3D plots of K_{RE} , K_{e3} and E_{Joint} for the two typical subjects S5 (*left*) and S14 (*right*) as a function of the weights of the composite cost $C(\alpha)$. In these graphs, α_1 and α_2 were varied to visualize how the speed dependence as well as the error minimized during inverse optimal control varied according to the chosen weights. Remind that $C(\alpha) = C_{Kine} + \alpha_1 C_{Ener} + \alpha_2 C_{Dyna}$. The squares indicated on each 3D plot show the position of the best-fitting speed-independent composite cost (SIComp) found during inverse optimal control. S5 and S14 have different anthropometric characteristics. Interestingly, by choosing appropriate α_1 and α_2 weights, subjects could exhibit different degree of speed dependence (almost zero K_{RE}/K_{e3} or negative K_{RE}/K_{e3}). For example, S14 could have been speed dependent if he/she chose a different cost combination (but this was not uncovered here because his/her trajectories were not compatible with such a cost function. 93

-
- 3.9 Illustration of the experimental paradigm. Fixed initial arm position and horizontal target plane were tested, therefore defining a free reach-endpoint motor task. A 4-DoF model of arm was examined (3 DoFs at the shoulder and 1 DoF at the elbow). Three speed and two load conditions were tested. At the *two bottom panels* displayed the arm posture at the initial time with no load (*left*) and with a load (*right*) approximately attached to the center of mass of the forearm. The average fingertip trajectories of a representative subject were drawn in thick, thin and dotted lines for the three speeds (slow, natural, fast, denoted by S, N, F) respectively. The two *top panels* display the reach endpoint positions across trials for this subject for the three speed condition, and no-load (*left*) and load (*right*) conditions. The 95% confidence ellipses of the reach endpoints are drawn. Note that along the antero-posterior (AP axis), the position of reach endpoint positions tended to get closer to the shoulder position when movement speed increased or when the load was attached to the forearm. 117
- 3.10 Hand, joint and torque profiles for the representative subject of Fig. 3.9. For the hand kinematics, displacements along the AP, ML and vertical axes are depicted as well as the Cartesian hand velocity (average and standard deviation as a shaded area) for the 3 speeds and two load conditions (black is for no-load and red for with-load). For the joint kinematics, the angular displacements for the 4 degrees of freedom are depicted. For the joint torques, we depicted the net torque acting at each degree of freedom. 119
- 3.11 Torque profiles (averaged across trials) of the representative subject at N speed for the no-load (*top panel*) and load (*bottom panel*) conditions. From left to right, the four torque profiles are for the shoulder internal/external, elevation/depression, ulnar/radial and elbow extension/flexion DoFs, respectively. The dynamic muscle torque (defined as muscle torque deprived of gravity torque, denoted by dMT), interaction torque (denoted by IT) and net torque (denoted by NT) are plotted. 122
-

- 3.12 Global interaction torque indexes (IT^g), averaged across all subjects, and displayed for the three speed and two load conditions (with standard errors indicated by error bars). It is visible that the IT^g index increased whenever movements sped up or a load was attached to the arm. In addition, its values were always positive, thus indicating that the IT positively contributed to the NT to some extent. Note that horizontal bars with stars indicate the results of post-hoc analysis for the speed condition. One, two, three stars stand for $p < 0.05$, $p < 0.01$ and $p < 0.001$ respectively. 124
- 3.13 Local interaction torque indexes (IT^l), averaged across all the subjects, displayed for the three speed and two load conditions. From left to right: IT^l of elbow extension/flexion, shoulder ulnar/radial, elevation/depression, internal/external, respectively. Noticeably, compared with shoulder-related DoFs, the IT^l indexes at the elbow extension/flexion were considerably smaller. Between the three DoFs at the shoulder, the IT^l indexes of shoulder ulnar/radial were smaller than the others. Statistical analyses showed significant effects of speed/load on the IT^l index for these three DoFs, as indicated by horizontal bars 125
- 3.14 Bin analysis of interaction torque exploitation. From left to right: average interaction torque indexes (across subjects) for bin1, bin2, bin3 and bin4 respectively. Note that these four bins were defined by dividing movement duration into a series of 4 intervals based on the acceleration profile (see Methods). Note that IT index values were smaller for bins 1 and 4, while it was larger for middle bins (2 and 3). For each bin, statistical significance of post-hoc tests is reported. 126
- 3.15 Component analysis of interaction torque exploitation. The IT indexes, averaged across subjects, are displayed for the three speed and two load conditions for the two components of IT. *Left*: velocity-related component (IT_{vel}); *Right*: acceleration-related component (IT_{acc}). It is visible that IT_{acc} was always greater than IT_{vel} . Statistical analyses showed significant effects of speed and load on the IT index for both IT components. 128

-
- 3.16 Reconstruction errors in joint space (E_{Joint} , *left panel*) and Cartesian space (E_{Cart} , *right panel*) for the best-fitting composite cost and each of the three cost elements taken separately. Error values were averaged across speeds, loads and then across subjects (with standard errors indicated by error bars). Noticeably, in terms of both joint and Cartesian errors, the composite (Comp) and kinematic (Kine) costs performed better than the dynamic (Dyna) and energetic (Ener) costs. 130
- 3.17 Torque profiles predicted by the identified composite cost (*top panels*) and the kinematic cost (*bottom panels*) for a representative subject at N speed and in no load condition. It is visible that the composite cost tends to let ITs contribute to NTs in order to get smaller dMTs while it is the opposite for the kinematic cost. 132
- 3.18 Reconstruction errors for some relevant parameters ($E_{IT}, E_{Kspeed}, E_{Kmass}$) for the composite and kinematic costs. Error values were averaged across speeds, loads and then across subjects for E_{IT} while averaged only across subjects for E_{Kspeed}/E_{Kmass} . Noticeably, in terms of E_{IT} and E_{Kspeed}/E_{Kmass} errors, the composite cost performed much better than the kinematic cost, yielding to a conclusion that only composite cost could predict relatively well the IT index and its speed/mass dependencies as observed in the experimental movement. 134
- 3.19 Cost contribution analyses. The contribution of elementary cost to the composite cost, averaged across all the subjects, is reported for the three speed and two load conditions. *Left*: cost contribution of kinematic cost; *Right*: cost contribution of dynamic cost. It is visible that the contribution of kinematic cost tended to decreased while those of dynamic cost increased with respect to the increase of movement speed and load. 135
-

- 4.1 Linear correlation analysis between kinematic cost contributions and each examined movement parameter (e3 and RE) for 15 subjects participated in our 1st experiment. *On the left panels* are absolute values. *On the right panels* are relative values (i.e. changes of the values when comparing different speeds) and emphasized by the symbol Δ . It is visible that the linear correlation results are considerably improved as the relative values is examined, indicating a quite strong link between the e3/RE indexes and the kinematic contribution: with the increased kinematic contribution, the e3 and RE indexes increase. . . . 148

BIBLIOGRAPHY

- Asfour T, Dillmann R (2003) Human-like motion of a humanoid robot arm based on a closed-form solution of the inverse kinematics problem In *Intelligent Robots and Systems, 2003. (IROS 2003). Proceedings. 2003 IEEE/RSJ International Conference on*, Vol. 2, pp. 1407–1412.
- Asmussen MJ, Przysucha EP, Dounskaia N (2014) Intersegmental dynamics shape joint coordination during catching in typically developing children but not in children with developmental coordination disorder. *J Neurophysiol* 111:1417–1428.
- Atkeson CG, Hollerbach JM (1985) Kinematic features of unrestrained vertical arm movements. *J Neurosci* 5:2318–2330.
- Bagesteiro LB, Sainburg RL (2003) Nondominant arm advantages in load compensation during rapid elbow joint movements. *Journal of Neurophysiology* 90:1503–1513.
- Bastian AJ, Martin TA, Keating JG, Thach WT (1996) Cerebellar ataxia: abnormal control of interaction torques across multiple joints. *J Neurophysiol* 76:492–509.
- Bellman RE (1957) *Dynamic Programming* Princeton, NJ.
- Ben-Itzhak S, Karniel A (2008) Minimum acceleration criterion with constraints implies bang-bang control as an underlying principle for optimal trajectories of arm reaching movements. *Neural Comput* 20(3):779–812.
- Benoit DL, Ramsey DK, Lamontagne M, Xu L, Wretenberg P, Renström P (2006) Effect of skin movement artifact on knee kinematics during gait and cutting motions measured in vivo. *Gait Posture* 24:152–164.
- Bernardin D, Isableu B, Fourcade P, Bardy BG (2005) Differential exploitation of the inertia tensor in multi-joint arm reaching. *Exp Brain Res* 167:487–495.

- Berniker M, Kording KP (2015) Deep networks for motor control functions. *Front Comput Neurosci* 9:32.
- Berret B, Darlot C, Jean F, Pozzo T, Papaxanthis C, Gauthier JP (2008) The inactivation principle: mathematical solutions minimizing the absolute work and biological implications for the planning of arm movements. *PLoS Comput Biol* 4:e1000194.
- Berret B, Jean F (2016) Why don't we move slower? the value of time in the neural control of action. *J Neurosci* in press.
- Berret B, Bisio A, Jacono M, Pozzo T (2014) Reach endpoint formation during the visuo-motor planning of free arm pointing. *Eur J Neurosci* 40:3491–3503.
- Berret B, Chiovetto E, Nori F, Pozzo T (2011a) Evidence for composite cost functions in arm movement planning: an inverse optimal control approach. *PLoS Comput Biol* 7:e1002183.
- Berret B, Chiovetto E, Nori F, Pozzo T (2011b) Manifold reaching paradigm: how do we handle target redundancy? *J Neurophysiol* 106:2086–2102.
- Berret B, Ivaldi S, Nori F, Sandini G (2011c) Stochastic optimal control with variable impedance manipulators in presence of uncertainties and delayed feedback In *Proc. IEEE/RSJ Int Intelligent Robots and Systems (IROS) Conf*, pp. 4354–4359.
- Berthoz (1991) Reference frames for the perception and control of movement. *Brain and space (Paillard J, ed)*, pp 81–110. Oxford, U K: Oxford University Press. .
- Biess A, Liebermann DG, Flash T (2007) A computational model for redundant human three-dimensional pointing movements: integration of independent spatial and temporal motor plans simplifies movement dynamics. *J Neurosci* 27:13045–13064.
- Bock O (1990) Load compensation in human goal-directed arm movements. *Behav Brain Res* 41:167–177.
- Bruno Siciliano LS LVGO (2009) *Robotics: Model, Planning and Control* Springer.
- Buhrmann T, Di Paolo EA (2014) Spinal circuits can accommodate interaction torques during multijoint limb movements. *Front Comput Neurosci* 8:144.
-

- Cappozzo A, Catani F, Leardini A, Benedetti MG, Croce UD (1996) Position and orientation in space of bones during movement: experimental artefacts. *Clin Biomech (Bristol, Avon)* 11:90–100.
- Ceseracciu E, Sawacha Z, Fantozzi S, Cortesi M, Gatta G, Corazza S, Cobelli C (2011) Markerless analysis of front crawl swimming. *J Biomech* 44:2236–2242.
- Cesqui B, d’Avella A, Portone A, Lacquaniti F (2012) Catching a ball at the right time and place: individual factors matter. *PLoS One* 7:e31770.
- Chandler WK, Schneider MF, Rakowski RF, Adrian RH (1975) Charge movements in skeletal muscle. *Philos Trans R Soc Lond B Biol Sci* 270:501–505.
- Cheng CK, Chen HH, Chen CS, Chen CL, Chen CY (2000) Segment inertial properties of chinese adults determined from magnetic resonance imaging. *Clin Biomech (Bristol, Avon)* 15:559–566.
- Chung PYM, Ng GYF (2012) Comparison between an accelerometer and a three-dimensional motion analysis system for the detection of movement. *Physiotherapy* 98:256–259.
- Darling WG, Hondzinski JM (1999) Kinesthetic perceptions of earth- and body-fixed axes. *Exp Brain Res* 126:417–430.
- Debicki DB, Gribble PL, Watts S, Hore J (2011) Wrist muscle activation, interaction torque and mechanical properties in unskilled throws of different speeds. *Exp Brain Res* 208:115–125.
- Debicki DB, Watts S, Gribble PL, Hore J (2010) A novel shoulder-elbow mechanism for increasing speed in a multijoint arm movement. *Exp Brain Res* 203:601–613.
- Dempster WT (1955) Space requirement of the seated operator. *Ohio: Aerospace Medical Research Laboratories*. .
- Desmurget M, Jordan M, Prablanc C, Jeannerod M (1997) Constrained and unconstrained movements involve different control strategies. *J Neurophysiol* 77:1644–1650.
- Dounskaia N (2005) The internal model and the leading joint hypothesis: implications for control of multi-joint movements. *Exp Brain Res* 166:1–16.
-

- Dounskaia N, Shimansky Y (2016) Strategy of arm movement control is determined by minimization of neural effort for joint coordination. *Exp Brain Res* 234:1335–1350.
- Dounskaia NV, Ketcham CJ, Stelmach GE (2002) Influence of biomechanical constraints on horizontal arm movements. *Motor Control* 6:366–387.
- Dumas R, Chèze L, Verriest JP (2007) Adjustments to mcconville et al. and young et al. body segment inertial parameters. *J Biomech* 40:543–553.
- Elliott D, Helsen WF, Chua R (2001) A century later: Woodworth’s (1899) two-component model of goal-directed aiming. *Psychol Bull* 127:342–357.
- et al LC (2011) A low cost wearable optical-based goniometer for human joint monitoring. *Frontiers of mechanical engineering*. 6, 13-22. .
- Featherstone R, Orin D (2000) Robot dynamics: equations and algorithms In *Robotics and Automation, 2000. Proceedings. ICRA '00. IEEE International Conference on*, Vol. 1, pp. 826–834.
- Fitts PM (1954) The information capacity of the human motor system in controlling the amplitude of movement. *J Exp Psychol* 47:381–391.
- Flanagan JR, Rao AK (1995) Trajectory adaptation to a nonlinear visuomotor transformation: evidence of motion planning in visually perceived space. *J Neurophysiol* 74:2174–2178.
- Flanders M, Herrmann U (1992) Two components of muscle activation: scaling with the speed of arm movement. *J Neurophysiol* 67:931–943.
- Flanders M, Pellegrini JJ, Geisler SD (1996) Basic features of phasic activation for reaching in vertical planes. *Exp Brain Res* 110:67–79.
- Flash T, Hogan N (1985) The coordination of arm movements: an experimentally confirmed mathematical model. *J Neurosci* 5:1688–1703.
- Galloway JC, Koshland GF (2002) General coordination of shoulder, elbow and wrist dynamics during multijoint arm movements. *Exp Brain Res* 142:163–180.

- Ganley KJ, Powers CM (2004) Determination of lower extremity anthropometric parameters using dual energy x-ray absorptiometry: the influence on net joint moments during gait. *Clin Biomech (Bristol, Avon)* 19:50–56.
- Gauthier JP, Berret B, Jean F (2010) A biomechanical inactivation principle. *Proceedings of the Steklov Institute of Mathematics* 268:93–116.
- Gaveau J, Paizis C, Berret B, Pozzo T, Papaxanthis C (2011a) Sensorimotor adaptation of point-to-point arm movements after space-flight: the role of the internal representation of gravity force in trajectory planning. *J Neurophysiol* .
- Gaveau J, Paizis C, Berret B, Pozzo T, Papaxanthis C (2011b) Sensorimotor adaptation of point-to-point arm movements after spaceflight: the role of internal representation of gravity force in trajectory planning. *J Neurophysiol* 106:620–629.
- Gaveau J, Papaxanthis C (2011) The temporal structure of vertical arm movements. *PLoS One* 6:e22045.
- Gaveau J, Berret B, Demougeot L, Fadiga L, Pozzo T, Papaxanthis C (2014) Energy-related optimal control accounts for gravitational load: comparing shoulder, elbow, and wrist rotations. *J Neurophysiol* 111:4–16.
- Georgopoulos AP, Kalaska JF, Caminiti R, Massey JT (1982) On the relations between the direction of two-dimensional arm movements and cell discharge in primate motor cortex. *J Neurosci* 2:1527–1537.
- Ghez C, Sainburg R (1995) Proprioceptive control of interjoint coordination. *Can J Physiol Pharmacol* 73:273–284.
- Gielen S (2009) *Progress in Motor Control. A Multidisciplinary Perspective*, chapter Review of Models for the Generation of Multi-Joint Movements in 3-D, pp. 523–550 Springer US.
- Gordon J, Ghilardi MF, Cooper SE, Ghez C (1994) Accuracy of planar reaching movements. ii. systematic extent errors resulting from inertial anisotropy. *Exp Brain Res* 99:112–130.

- Gottlieb GL, Corcos DM, Agarwal GC (1989a) Organizing principles for single-joint movements. i. a speed-insensitive strategy. *J Neurophysiol* 62:342–357.
- Gottlieb GL, Corcos DM, Agarwal GC (1989b) Strategies for the control of voluntary movements with one mechanical degree of freedom. *Behavioral and Brain Sciences* 12:189–250.
- Gottlieb GL, Corcos DM, Jaric S, Agarwal GC (1988) Practice improves even the simplest movements. *Exp Brain Res* 73:436–440.
- Gribble PL, Ostry DJ (1999) Compensation for interaction torques during single- and multijoint limb movement. *J Neurophysiol* 82:2310–2326.
- Gribble PL, Ostry DJ, Sanguineti V, Laboissière R (1998) Are complex control signals required for human arm movement? *J Neurophysiol* 79:1409–1424.
- Guigon E, Baraduc P, Desmurget M (2007) Computational motor control: redundancy and invariance. *J Neurophysiol* 97:331–347.
- Hanavan Jr. EP (1964) A mathematical model of the human body. *Amrl-Tr-64-102. Amrl Tr: 1-149.* .
- Hansen C (2013) Role of the minimal inertia axis in the kinaesthetic control of unconstrained 3d movements Master’s thesis, University Paris-Sud.
- Hatzitaki V, McKinley P (2001) Effect of single-limb inertial loading on bilateral reaching: interlimb interactions. *Exp Brain Res* 140:34–45.
- Hermens F, Gielen S (2004) Posture-based or trajectory-based movement planning: a comparison of direct and indirect pointing movements. *Exp Brain Res* 159:340–348.
- Hirashima M, Kudo K, Watarai K, Ohtsuki T (2007) Control of 3d limb dynamics in unconstrained overarm throws of different speeds performed by skilled baseball players. *J Neurophysiol* 97:680–691.
- Hirashima M, Kudo K, Ohtsuki T (2003) Utilization and compensation of interaction torques during ball-throwing movements. *J Neurophysiol* 89:1784–1796.
- Hollerbach MJ, Flash T (1982) Dynamic interactions between limb segments during planar arm movement. *Biol Cybern* 44:67–77.
-

- Hore J, Debicki DB, Watts S (2005) Braking of elbow extension in fast overarm throws made by skilled and unskilled subjects. *Exp Brain Res* 164:365–375.
- Hore J, Debicki DB, Gribble PL, Watts S (2011) Deliberate utilization of interaction torques brakes elbow extension in a fast throwing motion. *Exp Brain Res* 211:63–72.
- Isableu B, Ohlmann T, Cremieux J, Vuillerme N, Amblard B, Gresty MA (2010) Individual differences in the ability to identify, select and use appropriate frames of reference for perceptuo-motor control. *Neuroscience* 169:1199–1215.
- Isableu B, Rezzoug N, Mallet G, Bernardin D, Gorce P, Pagano CC (2009) Velocity-dependent changes of rotational axes in the non-visual control of unconstrained 3d arm motions. *Neuroscience* 164:1632–1647.
- Isableu B, Ohlmann T, Crémieux J, Amblard B (2003) Differential approach to strategies of segmental stabilisation in postural control. *Exp Brain Res* 150:208–221.
- Isableu B, Vuillerme N (2006) Differential integration of kinaesthetic signals to postural control. *Exp Brain Res* 174:763–768.
- J P (1991) Motor and representational framing in space. *Brain and space (Paillard J, ed)*, pp 163–182. Oxford, U K: Oxford University Press .
- JF Soechting FL (1981) Invariant characteristics of a pointing movement in man. *The Journal of Neuroscience* .
- Johannes Schrder-Schetelig PM FW (2010) Using efference copy and a forward internal model for adaptive biped walking. *Auton Robot* .
- Kalaska JF, Cohen DA, Hyde ML, Prud’homme M (1989) A comparison of movement direction-related versus load direction-related activity in primate motor cortex, using a two-dimensional reaching task. *J Neurosci* 9:2080–2102.
- Kawato M, Furukawa K, Suzuki R (1987) A hierarchical neural-network model for control and learning of voluntary movement. *Biol Cybern* 57:169–185.
- Knill DC, Bondada A, Chhabra M (2011) Flexible, task-dependent use of sensory feedback to control hand movements. *J Neurosci* 31:1219–1237.
-

- Lee JK, Park EJ (2011) 3d spinal motion analysis during staircase walking using an ambulatory inertial and magnetic sensing system. *Med Biol Eng Comput* 49:755–764.
- MacKenzie C, Iberall T (1994) *The Grasping Hand* Advances in psychology. North-Holland.
- Maletsky LP, Sun J, Morton NA (2007) Accuracy of an optical active-marker system to track the relative motion of rigid bodies. *J Biomech* 40:682–685.
- Malmström EM, Karlberg M, Melander A, Magnusson M (2003) Zebris versus myrin: a comparative study between a three-dimensional ultrasound movement analysis and an inclinometer/compass method: intradevice reliability, concurrent validity, intertester comparison, intratester reliability, and intraindividual variability. *Spine (Phila Pa 1976)* 28:E433–E440.
- McConville JT, Clauser CE, Churchill TD, Cuzzi J, Kaleps I (1980) Anthropometric relationships of body and body segment moments of inertia Technical report, DTIC Document.
- Mombaur K, Truong A, Laumond JP (2009) From human to humanoid locomotion - an inverse optimal control approach. *Autonomous Robots* .
- Morasso P (1981) Spatial control of arm movements. *Exp Brain Res* 42:223–227.
- Mungiole M, Martin PE (1990) Estimating segment inertial properties: comparison of magnetic resonance imaging with existing methods. *J Biomech* 23:1039–1046.
- Mussa-Ivaldi FA (1988) Do neurons in the motor cortex encode movement direction? an alternative hypothesis. *Neurosci Lett* 91:106–111.
- Nagasaki H (1989) Asymmetric velocity and acceleration profiles of human arm movements. *Exp Brain Res* 74:319–326.
- Nakano E, Imamizu H, Osu R, Uno Y, Gomi H, Yoshioka T, Kawato M (1999) Quantitative examinations of internal representations for arm trajectory planning: minimum commanded torque change model. *J Neurophysiol* 81:2140–2155.
- Nelson WL (1983) Physical principles for economies of skilled movements. *Biol Cybern* 46:135–147.
-

- Nishii J, Murakami T (2002) Energetic optimality of arm trajectory In *Proc of Int Conf on Biomechanics of Man*, pp. 30–33.
- Nishikawa KC, Murray ST, Flanders M (1999) Do arm postures vary with the speed of reaching? *J Neurophysiol* 81:2582–2586.
- Ostry DJ, Cooke JD, Munhall KG (1987) Velocity curves of human arm and speech movements. *Exp Brain Res* 68:37–46.
- Pagano CC, Turvey MT (1995) The inertia tensor as a basis for the perception of limb orientation. *J Exp Psychol Hum Percept Perform* 21:1070–1087.
- Pai DK (2010) Muscle mass in musculoskeletal models. *J Biomech* 43:2093–2098.
- Paolo Viviani TF (1995) Minimum-jerk, two-thirds power law, and isochrony: Converging approaches to movement planning. *Journal of Experimental Psychology: Human Perception and Performance* .
- Papaxanthis C, Pozzo T, Popov KE, McIntyre J (1998) Hand trajectories of vertical arm movements in one-g and zero-g environments. evidence for a central representation of gravitational force. *Exp Brain Res* 120:496–502.
- Papaxanthis C, Pozzo T, Schieppati M (2003) Trajectories of arm pointing movements on the sagittal plane vary with both direction and speed. *Exp Brain Res* 148:498–503.
- Papaxanthis C, Pozzo T, Stapley P (1998) Effects of movement direction upon kinematic characteristics of vertical arm pointing movements in man. *Neurosci Lett* 253:103–106.
- Pearsall DJ, Costigan PA (1999) The effect of segment parameter error on gait analysis results. *Gait Posture* 9:173–183.
- Pigeon P, Bortolami SB, DiZio P, Lackner JR (2003) Coordinated turn-and-reach movements. i. anticipatory compensation for self-generated coriolis and interaction torques. *J Neurophysiol* 89:276–289.
- Pozzo T, Berthoz A, Lefort L, Vitte E (1991) Head stabilization during various locomotor tasks in humans. ii. patients with bilateral peripheral vestibular deficits. *Exp Brain Res* 85:208–217.

- Rao AV, Benson DA, Darby CL, Patterson MA, Francolin C, Sanders I, Huntington GT (2010) Algorithm 902: Gpops, a matlab software for solving multiple-phase optimal control problems using the gauss pseudospectral method. *ACM Transactions on Mathematical Software* 37:1–39.
- Rao G, Amarantini D, Berton E, Favier D (2006) Influence of body segments' parameters estimation models on inverse dynamics solutions during gait. *J Biomech* 39:1531–1536.
- Reinschmidt C, van den Bogert AJ, Nigg BM, Lundberg A, Murphy N (1997) Effect of skin movement on the analysis of skeletal knee joint motion during running. *J Biomech* 30:729–732.
- Richards L (1999) The measurement of human motion: A comparison of commercially available systems. *Human Movement Science* 18, 589-602. .
- Riley MA, Turvey MT (2001) Inertial constraints on limb proprioception are independent of visual calibration. *J Exp Psychol Hum Percept Perform* 27:438–455.
- Rogowski I, Creveaux T, Chèze L, Macé P, Dumas R (2014) Effects of the racket polar moment of inertia on dominant upper limb joint moments during tennis serve. *PLoS One* 9:e104785.
- Rogowski I, Creveaux T, Faucon A, Rota S, Champely S, Guillot A, Hautier C (2009) Relationship between muscle coordination and racket mass during forehand drive in tennis. *European journal of applied physiology* 107:289–298.
- Sainburg RL, Ghez C, Kalakanis D (1999) Intersegmental dynamics are controlled by sequential anticipatory, error correction, and postural mechanisms. *J Neurophysiol* 81:1045–1056.
- Sainburg RL, Ghilardi MF, Poizner H, Ghez C (1995) Control of limb dynamics in normal subjects and patients without proprioception. *J Neurophysiol* 73:820–835.
- Sainburg RL, Kalakanis D (2000) Differences in control of limb dynamics during dominant and nondominant arm reaching. *J Neurophysiol* 83:2661–2675.
- Sande de Souza LAP, Dionísio VC, Lerena MAM, Marconi NF, Almeida GL (2009) The linear co-variance between joint muscle torques is not a generalized principle. *J Electromyogr Kinesiol* 19:e171–e179.

- Schneider K, Zernicke RF, Schmidt RA, Hart TJ (1989) Changes in limb dynamics during the practice of rapid arm movements. *J Biomech* 22:805–817.
- Scott SH (2004) Optimal feedback control and the neural basis of volitional motor control. *Nat Rev Neurosci* 5:532–546.
- Senk M, Chèze L (2006) Rotation sequence as an important factor in shoulder kinematics. *Clin Biomech (Bristol, Avon)* 21 Suppl 1:S3–S8.
- Shadmehr R, Mussa-Ivaldi FA (1994) Adaptive representation of dynamics during learning of a motor task. *J Neurosci* 14:3208–3224.
- Shadmehr R (2010) Control of movements and temporal discounting of reward. *Curr Opin Neurobiol* 20:726–730.
- Shadmehr R, Orban de Xivry JJ, Xu-Wilson M, Shih TY (2010) Temporal discounting of reward and the cost of time in motor control. *J Neurosci* 30:10507–10516.
- Simoneau M, Guillaud É, Blouin J (2013) Effects of underestimating the kinematics of trunk rotation on simultaneous reaching movements: predictions of a biomechanical model. *J Neuroeng Rehabil* 10:54.
- Skinner NE, Zelik KE, Kuo AD (2015) Subjective valuation of cushioning in a human drop landing task as quantified by trade-offs in mechanical work. *J Biomech* 48:1887–1892.
- Soechting JF, Buneo CA, Herrmann U, Flanders M (1995) Moving effortlessly in three dimensions: does donders' law apply to arm movement? *J Neurosci* 15:6271–6280.
- Soechting JF, Flanders M (1998) *Movement planning: kinematics, dynamics, both or neither?* Vision and Action, edited by Harris LR, Jenkin M. Cambridge, UK: Cambridge Univ. Press.
- Soechting JF, Lacquaniti F (1981) Invariant characteristics of a pointing movement in man. *J Neurosci* 1:710–720.
- Timmann D, Lee P, Watts S, Hore J (2008) Kinematics of arm joint rotations in cerebellar and unskilled subjects associated with the inability to throw fast. *Cerebellum* 7:366–378.
- Todorov E (2004) Optimality principles in sensorimotor control. *Nat Neurosci* 7:907–915.
-

- Todorov E (2006) *Optimal control theory*, chapter 12, pp. 269–298 Bayesian Brain: Probabilistic Approaches to Neural Coding, Doya K (ed).
- Todorov E, Jordan MI (2002) Optimal feedback control as a theory of motor coordination. *Nat Neurosci* 5:1226–1235.
- Turner RS, Desmurget M (2010) Basal ganglia contributions to motor control: a vigorous tutor. *Curr Opin Neurobiol* 20:704–716.
- Uno Y, Kawato M, Suzuki R (1989) Formation and control of optimal trajectory in human multijoint arm movement. minimum torque-change model. *Biol Cybern* 61:89–101.
- van Beers RJ, Haggard P, Wolpert DM (2004) The role of execution noise in movement variability. *J Neurophysiol* 91:1050–1063.
- Venture G, Ayusawa K, Nakamura Y (2009a) Identification of human mass properties from motion. *IFAC Proceedings Volumes* 42:988–993.
- Venture G, Ayusawa K, Nakamura Y (2009b) A numerical method for choosing motions with optimal excitation properties for identification of biped dynamics—an application to human In *Robotics and Automation, 2009. ICRA'09. IEEE International Conference on*, pp. 1226–1231. IEEE.
- Vetter P, Flash T, Wolpert DM (2002) Planning movements in a simple redundant task. *Curr Biol* 12:488–491.
- Vũ VH, Isableu B, Berret B (2016) On the nature of motor planning variables during arm pointing movement: Compositeness and speed dependence. *Neuroscience* .
- Wada Y, Kaneko Y, Nakano E, Osu R, Kawato M (2001) Quantitative examinations for multi joint arm trajectory planning—using a robust calculation algorithm of the minimum commanded torque change trajectory. *Neural Netw* 14:381–393.
- Wang W, Dounskaia N (2015) Influence of workspace constraints on directional preferences of 3d arm movements. *Exp Brain Res* 233:2141–2153.
- Windolf M, Götzen N, Morlock M (2008) Systematic accuracy and precision analysis of video motion capturing systems—exemplified on the vicon-460 system. *J Biomech* 41:2776–2780.
-

- Wolpert DM, Ghahramani Z (2000) Computational principles of movement neuroscience. *Nat Neurosci* 3 Suppl:1212–1217.
- Wolpert DM, Ghahramani Z, Jordan MI (1995a) Are arm trajectories planned in kinematic or dynamic coordinates? an adaptation study. *Exp Brain Res* 103:460–470.
- Wolpert DM, Ghahramani Z, Jordan MI (1995b) An internal model for sensorimotor integration. *Science* 269:1880–1882.
- Woodworth R (1899) *The Accuracy of Voluntary Movement* Columbia University contributions to philosophy, psychology and education. Columbia University.
- Wu G, van der Helm FCT, Veeger HEJD, Makhsous M, Van Roy P, Anglin C, Nagels J, Karduna AR, McQuade K, Wang X, Werner FW, Buchholz B, ISoB (2005) Isb recommendation on definitions of joint coordinate systems of various joints for the reporting of human joint motion—part ii: shoulder, elbow, wrist and hand. *J Biomech* 38:981–992.
- Yamasaki H, Tagami Y, Fujisawa H, Hoshi F, Nagasaki H (2008) Interaction torque contributes to planar reaching at slow speed. *Biomed Eng Online* 7:27.
- Young JW, Chandler RF, Snow CC, Robinette KM, Zehner GF, Lofberg MS (1983) Anthropometric and mass distribution characteristics of the adult female Technical report.
- Zelik KE, Kuo AD (2012) Mechanical work as an indirect measure of subjective costs influencing human movement. *PLoS One* 7:e31143.
- Zhang X, Chaffin DB (1999) The effects of speed variation on joint kinematics during multisegment reaching movements. *Human Movement Science* 18:741–757.